Holographic Effective Theories for Strongly Coupled Physics

by

Hsien-Hang Shieh

BSc. Simon Fraser University, 2002
M.Sc., The University of British Columbia, 2004

A THESIS SUBMITTED IN PARTIAL FULFILLMENT OF
THE REQUIREMENTS FOR THE DEGREE OF

DOCTOR OF PHILOSOPHY

in

The Faculty of Graduate Studies

(Physics)

THE UNIVERSITY OF BRITISH COLUMBIA

(Vancouver)

August 2009

Abstract

In this thesis we summarize three of our work using the gauge/gravity dualities to build effective theories for strongly coupled phenomena. First, we study the thermodynamics of large N pure 2+1 dimensional Yang-Mills theory on a small spatial S^2. By studying the effective action for the Polyakov loop order parameter, we show analytically that the theory has a second order deconfinement transition. Our results together with extrapolation of lattice QCD results imply a critical radius in the phase diagram where the deconfinement transition switches from second order to first order. We show that the point at the critical radius and temperature can be either a tricritical point with universal behavior or a triple point separating three distinct phases. Second, we study a model of holographic QCD at zero temperature and finite chemical potential. We find that as the baryon chemical potential is increased, the system transitions to a nuclear matter phase characterized by a condensate of instantons on the probe D-branes in the string theory dual. The electrostatic interactions between the instantons cause the condensate to expand towards the UV with increasing chemical potential, giving a holographic version of the expansion of the Fermi surface. We also find possible explanation of the "chiral density wave" instability in large N QCD. We argue that the model can be used to make semi-quantitative predictions of the binding energy per nucleon for nuclear matter in QCD. Third, we consider an Abelian Higgs model placed in an AdS black hole background. Such model has been shown to exhibit superconductor like transitions. In the superconducting phase the system shows infinite DC conductivity. This suggests the possibility of turning on a time independent supercurrent. In this paper we study such supercurrent solutions and the associated phase diagram. We find a critical point in the phase diagram where the second order superconducting transition becomes first order. Supercurrent solutions are well studied in condensed matter systems. We find some qualitative agreement with known results.

Table of Contents

List of Figures

Acknowledgements

I would like to thank my supervisors Dr. M. Van Raamsdonk and Dr. D. Witt for their patience constant support and guidance. I would also like to thank my friends and colleagues P. Basu, J.Y. He, H. Ling, A. Mukherjee, K. Papadodimas, G. van Anders and J. Wu. This work cannot be completed without valuable inputs from Ian Affleck, Ofer Aharony, Michael Douglas, Marcel Franz, Adrian Giuseppe, Gary Horowitz, Igor Klebanov, Joseph Marsano, Del Maestro, David Mateos, Shiraz Minwalla, Herbert Neuberger, Roman Petryk, Krishna Rajagopal, Moshe Rozali, Eran Sela, Gordon Semenoff, Steve Shenker, Spenta Wadia, Wen-Yu Wen, Eric Zhitnitsky and the String Theory Group at UBC.

Chapter 1

Introduction and Overview

One of the most exciting developments in string theory in the last decade is that it provides systematic ways of constructing dualities between string theories in certain gravitational backgrounds and gauge theories [1]. In some cases the duality is realized in a way that can be interpretated as examples of the holography principle which states there exists a dual description of gravitaional theories as some field theories in lower dimensional spacetimes. A common feature of known examples of such duality is that it relates strongly coupled physics on one side to regimes in the dual theory where analytic methods are applicable. Besides extending analytic control, the duality relations give new insights to the mechanism behind strongly coupled physics such as phase transitions in gauge theories and the resolution of singularities in gravity.

As mentioned earlier string theory gives us a backdrop where the gauge/gravity duality can be consistently realized. Let us begin by reviewing the objects in string theory [2]. String theory can be viewed as a natural extension of the quantum mechanics for particles to a quantum description of one-dimensional objects– fundamental strings which have no substructures. The fundamental strings can be either closed with the topology of the circle or open where additional degrees of freedom can be associated to its ends. It is realized that an interacting open string theory is not consistent without the closed strings as the string ends can join. It can be used to describe particle physics when we look at a length scale which is much larger than the length of the strings. Perturbatively, each vibrational and spin mode of a free string can be viewed as a different species of particle with a different mass and spin. It has the advantage of being UV finite and it comes with only two parameters: α'which characterizes the length of a fundamental string and g_s which gives the strength of the string coupling. As the string moves in the space-time it sweeps out a two-dimensional world sheet instead of a world line as in the particle case. The perturbative expansion of string theory in g_s is an expansion in the string world sheet genus. This takes the place of the loop expansion in Feynman diagrams for particles. We will show in a later section that this genus expansion matches onto a particular arrangement of the perturbative expansion of a gauge theory. Unfortunately, a theory that describes multiple strings and their interactions, that is, a string field theory has not been written down. However, one can consider for each string mode a quantum field theory describing the interactions within a selected subset of the particle spectrum contained in a string theory.

String theory was first invented to be an effective theory for the strong interaction and was successful in modeling the spectrum of hadrons. However it was discovered that a relativistic quantum string theory is only mathematically consistent in certain critical dimensions.

It should be noted that there are consistent string theories in any number of dimensions. These noncritical string theories contain additional fields other than the ones that describe the embeddings of the fundamental strings in space-time. Noncritical string theories are interesting and can sometimes be more tractable. They have been used to study the emergence of spacetimes and the general structure of string theories and dualities between them. The critical dimension is 26 for bosonic string theories and 10 for the supersymmetric string theories. We will focus on the critical superstring theories from now on as the bosonic string theory contains a tachyon. It turns out that the lowest energy excitations, the massless modes of closed superstrings have exactly the matter content of the 10 dimensional supersymmetric gravity theories which includes the metric, the antisymmetric tensor and other matter fields such as the dilaton and the Ramond-Ramond form fields– higher dimensional versions of electromagnetic field strength. By requiring the theory to maintain the superconformal symmetries at the quantum level the massless modes are also required to satisfy the equations of motion of the supergravity theories. This suggests that superstring theory is described by supergravity at low energies and is a candidate for a consistent quantum gravity theory.

So far we have been discussing the perturbative spectrum of free strings. String theory also contains solitonic excitations known as the Dirichlet D_p branes. They are realized geometrically as hypersurfaces extended in p spatial dimensions. In terms of the fundamental strings they are where the ends of an open string are confined to move on. The D branes describe the collective excitations of the open strings ending on them and they can also interact with the closed strings. For example, ends of an open string can join and then move off the branes. This suggests that they are charged under the closed string fields. In particular, they can carry the charges of the metric and the Ramond-Ramond fields in the 10 dimensional supergravity theory. At low energies and if we are interested in the physics at the length scale much larger than the string scale, the presence of the D branes can be accounted for by treating them as sources of mass and charges for the supergravity fields. Such supergravity solutions have been found before the discovery of D branes and they are known as the black p branes. On the other hand, the physics of D branes can be described by the dynamics of the open strings ending on them and closed strings scattering from the branes. At leading order in α' the low energy effective descriptions of the brane bound open strings turns out to be Yang Mills type of field theories. Therefore we have two very different low-energy descriptions of D branes and in the following section we will describe a particular limiting procedure which allows us to establish a map between degrees of freedoms close to the branes from the two effective descriptions. This is the basis for the gauge/gravity duality.

Here we will review the construction of such duality in its earliest and probably most studied example: the AdS/CFT correspondence. In particular, we will focus on the correspondence between a conformal field theory, the $\mathcal{N} = 4$ super Yang-Mills theory, and the quantum gravity theory (string theory) on $AdS_5 \times S^5$. The correspondence is found to be a weak-strong coupling duality. It connects the strongly coupled regime of the gauge field

theory to the weakly coupled sector of the gravitaional theory and vice versa. This makes the correspondence difficult to check but all the more significant. The behavior of gauge field theories in their strongly coupled regime has been a long standing problem. With the help of the AdS/CFT correspondence, we are able to gain understanding of strongly coupled gauge theory by studying weakly coupled gravity where all interactions are under control.

The AdS/CFT correspondence is conjectured to be valid beyond the gravity limit. That is, the boundary field theory will encode all the information of the bulk, including all orders of corrections in the string tension α', and string coupling constant g_s. This conjecture has passed many checks through calculations involving gauge theory operators whose behaviors are protected by symmetry all the way to the strongly coupled limit and compared with the corresponding supergravity calculations.

An interesting aspect of the AdS/CFT correspondence is how the boundary field theory detects topology change in the bulk. Here by topology change we mean those with the boundary of the spacetimes left invariant. In the present case, we will consider two topologically distinct spacetimes that are asymptotically AdS. They are the pure AdS spacetime and the AdS-Schwarzschild black hole. It has been shown that there exists a thermal phase transition between the two spacetimes in the bulk gravitational theory[24]. On the field theory side this is translated into the deconfinement phase transtion of the Yang-Mills theory[3]. Lets start with a more detailed description of the AdS/CFT correpondence.

1.1 AdS/CFT Correpondence: Motivation

Consider pure SU(N) Yang-Mills theory with Lagrangian:

$$L = \frac{1}{g^2} Tr[F^{\mu\nu} F_{\mu\nu}] \tag{1.1}$$

where $F_{\mu\nu} = \partial_\mu A_\nu - \partial_\nu A_\mu - i[A_\mu, A_\nu]$ with $A^\mu_{ij}(x)$ being traceless Hermitian matrices living in the adjoint representation of SU(N), and $\mu, \nu = 1..d$, $i, j.. = 1..N$ are the space-time and SU(N) index, respectively. The traces are to ensure SU(N) gauge invariance of the action. The Feymann diagrams of the above theory can be represented with the double line notation due to 't Hooft [4]. We see from fig(1.1). each propagtor contributes a factor of g^2 while all the vertices carry a factor of $1/g^2$. Due to the trace on the vertices we need to identify the gauge index on the same single line, and there is a sum over $i = 1..N$ for each closed single loop. As a result, we get a factor of N from each closed single line loop in a diagram. To summarize, each Feymann diagram will have a prefactor:

$$(g^2)^{\text{no. of propagators}-\text{no. of vertices}} N^{\text{no. of closed single lines}} \tag{1.2}$$

It turns out the double line diagrams have a natural geometrical representaion. We can draw an arbitrary double line graph on a two dimensional boundaryless orientable manifold– a Riemann surface, with appropriate number of holes and cycles (topology). The Feymann

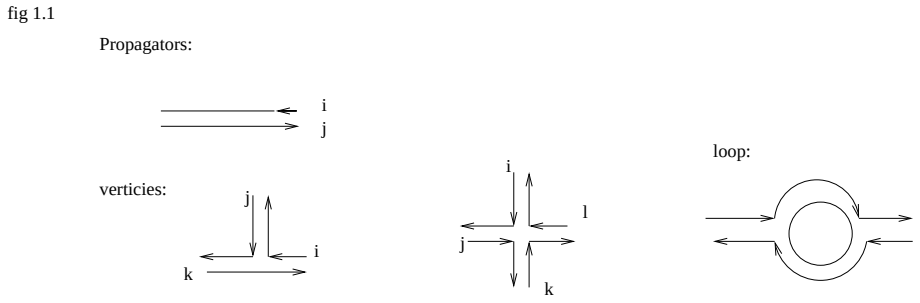

Figure 1.1: Double line representation of SU(N) gauge theory

diagrams give a triangulation of the corrsponding Riemann surface. The power counting in (1.2) can now be rearranged into:

$$(1.2) = N^E (Ng^2)^{\text{no. of propagators–no. of vertices}} \tag{1.3}$$

where E is the Euler number of the Riemann surface E = no. of faces − no. of edges + no. of vertices $= 2 - 2h$ where h is the genus of the correponding surface fig(1.2). (the faces and edges refer to those in the triangulation) If we take the 't Hooft limit: $N \to \infty$, $g^2 N = \lambda$, the 't Hooft coupling, fixed, the Feymann diagram expansion is now seen as a genus expansion of the Riemann surfaces. Note due to the Hermiticity of the matrices, we need to include only orientable surfaces in the expansion. If we introduce additional matter fields transforming in the fundamentals of SU(N) into the theory, we will need to consider Riemann surfaces with boundary, as the fundamentals are represented by single lines in the double line notation. The partition function of the theory now has the form:

$$log(Z) = \sum_E N^E f_E(g^2 N) \tag{1.4}$$

At large N, we can focus on contributions from the planar diagrams (those can be drawn on a two sphere or a plane). Heuristically, if we consider diagrams with more and more loops and vertices (higher order in $O(\lambda)$), we would be filling up the Riemann surfaces with little triangles and the partition function is seen to approximate the summing of the world sheet configurations as in string perturbation theory. Let us make this more quantitative by looking at the duality between $AdS_5 \times S^5$ and $\mathcal{N} = 4$ super Yang-Mills on $R^{1,3}$.

The duality between type IIB string theory on $AdS_5 \times S^5$ and gauge theory can be understood as a result of matching two equivalent descriptions of a stack of N $D3$ branes in the appropriate limit. On the one hand, a stack of $D3$'s in 10 dimensional Minkowski space can be discribed by the excitation of open strings ending on the branes, the closed string modes that propogate in the bulk off the branes, and their interactions. In this picture, strings are propagating in flat space with Dirichlet boundary conditions for the open strings

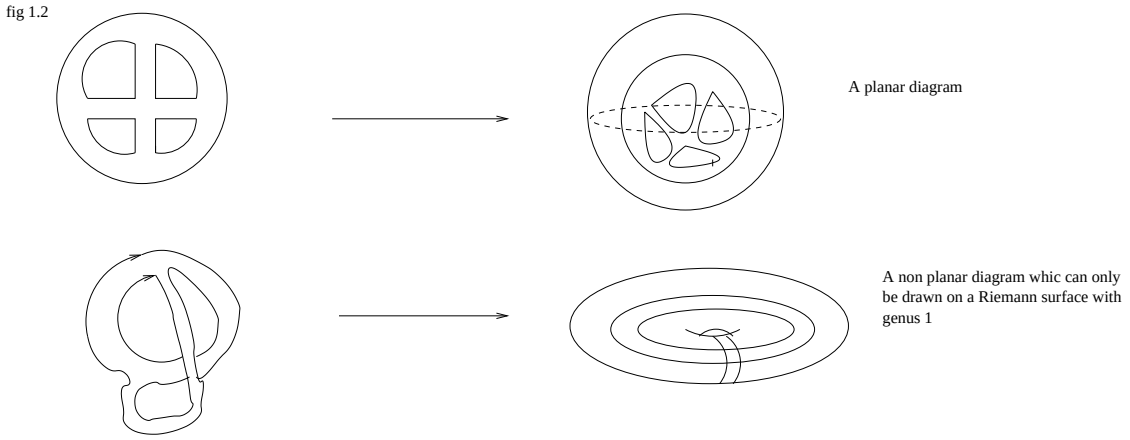

Figure 1.2: Double line diagrams on Riemann surfaces

at the loaction of the branes. At low energy, we can focus on the massless sectors of the string theory spectrum. This configuration can be described by an effective action with all the massive excitations integrated out.

$$S_{eff} = S_{brane} + S_{closedstring} + S_{int} \tag{1.5}$$

The closed string dynamics can be captured by the 10 dimensional supergravity action while the open strings are described by the $\mathcal{N} = 4$ super Yang-Mills at leading order in α'. It can be shown that if we only keep the leading order terms in α', the closed and open string sectors decouple. The low energy physics of the N closely positioned $D3$ branes is just that of free 10 dimensional supergravity plus a super Yang-Mills theory living on the four dimensional world volume of the $D3$ branes.

On the other hand, from calculation of gravitons scattering off the $D3$ branes and the Ramond-Ramond charges they carry, it can be deduced that the presence of the stack of N $D3$ branes will generate a geometry which at large distances from the branes becomes an extremal black 3-brane solution of 10d supergravity carrying N units of Ramond-Ramond charge[5].

$$\begin{aligned} ds^2 &= f^{-1/2}[-dt^2 + dx^2 + dy^2 + dz^2] + f^{1/2}[dr^2 + r^2 d\Omega_5^2] \\ F_5 &= (1 + *)dtdxdydzdf^{-1} \\ f &= 1 + \frac{R^4}{r^4}, R^4 = 4\pi g_s \alpha'^2 N \end{aligned} \tag{1.6}$$

for coincident branes. The horizon of the black three brane is at $r = 0$. An excitation with energy E near the horizon will become $E' = \lim_{r=0} f^{-1/4} E$ as viewed by an observer at $r = \infty$ ($f(r)$ approaches unity) due to the Tolman red shift factor. Therefore from the

point of view of observers at infinity, all of the physics happening near the horizon of the $D3$ branes are redshifted to low energy. To these observers, the low energy physics in the background generated by the stack of $D3$ branes also contain two pieces: the first is the red shifted version of the near horizon behavior; the second is the low energy supergravity modes propagating in the bulk. In the low energy limit we are interested in, the two pieces also decouple. This can be seen as in this limit the bulk low energy modes would have wavelength much larger than the scale set by the curvature of the black three brane. These modes are completely delocalized compared to a length scale that is "near" horizon. We now have two equivalent descriptions of the low energy physics in a background generated by a stack of N $D3$ branes. In both versions there is a piece which is just the low energy 10 dimensional supergravity modes. Since in both cases the supergravity modes decouple, we are then prompted to identify the other part from the two descriptions. We will relate the near horizon physics of (1.6) to the $\mathcal{N} = 4$ super Yang-Mills theory living on the world volume of the $D3$ branes. As the gravity modes decouple from the physics on the brane in the low energy limit, it is safe to assume the world volume of the $D3$'s to be the 1+3 Minkowski spacetime. Note that because of the red shift, the low energy excitations from the near horizon region as observed at infinity can in principle include modes with arbitarily high energy as measured by a near horizon observer. The duality is conjectured to exetend beyond the supergravity limit and include higher string modes.

The near horizon geometry of (1.6) is the $AdS_5 \times S^5$ as can be checked by taking $r << R$, and approximate $f^{1/2}$ by R^2/r^2:

$$ds^2 = \frac{r^2}{R^2}[-dt^2 + dx^2 + dy^2 + dz^2] + \frac{R^2}{r^2}dr^2 + d\Omega_5^2 \tag{1.7}$$

In (1.7), the AdS part of the metric is written in the Poincare coordinate, which, however, only covers part of the AdS spacetime. It is easy to see by taking the limit $r \to \infty$ that the metric (1.7) becomes conformal to the flat Minkowski space $R^{1,3}$ (the radius of the internal five sphere shrinks to zero). To an observer living on the boundary of the AdS spacetime, the duality can be stated as:

The type IIB string theory on $AdS_5 \times S^5$ is dual to the $\mathcal{N} = 4$ SU(N) super Yang-Mills on the conformal boundary $R^{1,3}$ of $AdS_5 \times S^5$.

1.2 AdS/CFT Correpondence: The Duality

In this section we will introduce the mapping between the Hilbert spaces of the boundary field theory and the bulk string theory. First we will look at the parameters in the two theories and see how to map them to each other[6]. In the field theory, we have the Yang-Mills coupling g_{YM} and N from the gauge group SU(N) (and the theta angle which does not play an impotant role in the discussion to come). On the string theory side, there is

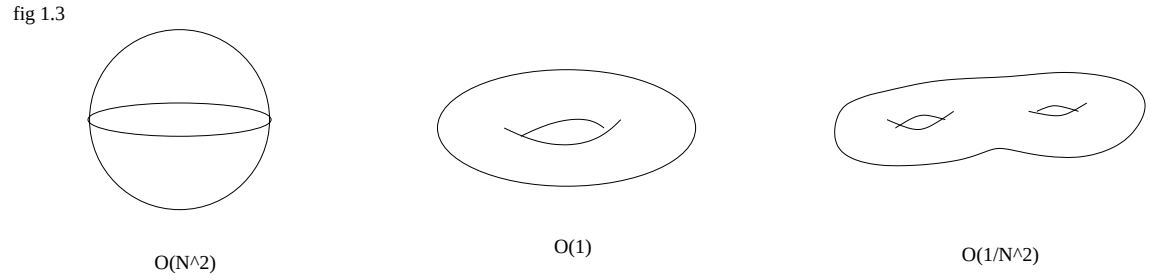

Figure 1.3: Large N expansion versus genus expansion

the string coupling g_s, the funadamental string length $l_s^2 = \alpha'$ and from the background, the radius of $AdS_5 \times S^5$, R, and the R-R five form charge $N = R^4/(4\pi g_s \alpha'^2)$. From calculations of how D_p-branes couple to Ramond-Ramond $(p+1)$-form potential, we can calculate the relationship between the Yang-Mills coupling and the D_p-brane tension $\tau_p \propto 1/g_s(\alpha')^{-\frac{p+1}{2}}$ [2]. It gives us the following relation:

$$g_{YM,p}^2 \propto \tau_p^{-1}\alpha'^{-2} = g_s\alpha'^{(p-3)/2} \tag{1.8}$$

For $p = 3$, we see $g_{YM}^2 = g_s$. If we use units in which $R = 1$, we find

$$\alpha' \sim 1/(g_s N)^{1/2} \sim 1/(g_{YM}^2 N)^{1/2} = 1/(\lambda)^{1/2} \tag{1.9}$$

, and the 10 dimensional Newton's constant

$$G_{10} \propto \alpha'^4 g_s^2 \sim \frac{1}{N^2} \tag{1.10}$$

The relationship (1.9) gives evidence for our heuristic identification of the large N 't Hooft expansion and the string world sheet genus expansion in fig(1.3). The parameter α' is inversely proprotional to the 't Hooft coupling λ of the Yang-Mills theory. This indicates that in order to perform perturbative canculations on the field theory side, we need to turn on the stringy (α') corrections to the gravity computations. On the other hand, in order for the supergravity description in the bulk to be valid, we need the scale set by the curvature of the spacetime to be much larger than the string scale, that is:

$$1 << (\frac{R}{l_s})^4 \sim g_{YM}^2 N = \lambda \tag{1.11}$$

This says the dual field theory will give comparable result to the bulk supergravity calculation only if we include all the loop corrections (at the planar level). We have reached the conclusion that the AdS/CFT correspondence is a strong/weak coupling duality. As mentioned before, this makes the duality hard to check, but it also gives us a new avenue to the nonperturbative behaviors of gauge theories. Notice also, there are two limiting procedures

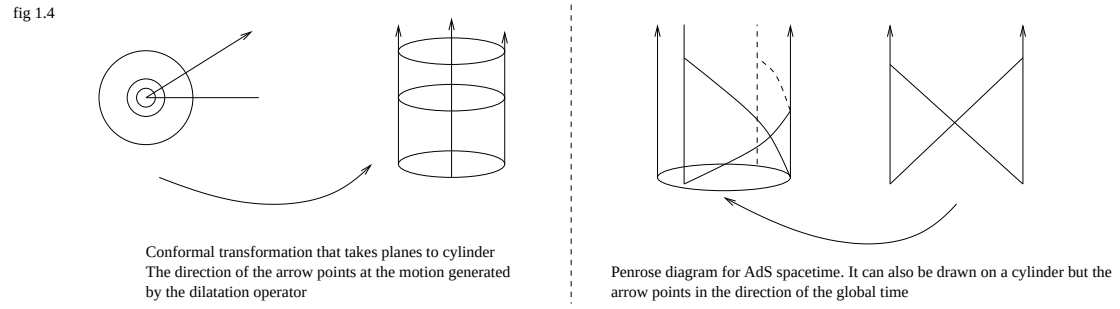

Figure 1.4: Conformal structures of anti de Sitter space

involved. Take the gravity calculations, for example. We need to dial down the string coupling constant to supress string interactions (the higher genus diagrams) and also take the limit $\alpha' \to 0$, which allows us to focus on the supergravity contributions. The corresponding limits on the field theory side is to take g_{YM} to zero and take the large N limit in such a way that the 't Hooft coupling $\lambda = g_{YM}^2 N$ is fixed but large. This will give us access to properties of the field theory at the planar level but at large 't Hooft coupling.

Next, we look at the symmetries of the two theories. We will focus on the bosonic part of the duality. The $\mathcal{N} = 4$, SU(N) super Yang-Mills on $R^{1,3}$ is a conformal theory. It has the conformal group SO(2,4) as its symmetry group. SO(2,4) also is the isomotry group of AdS_5. The generators of SO(2,4) includes the usual Poincare algebra plus dilatation $D = x^\mu \partial_\mu$ and the special conformal generator K_μ, which induces the transformation:

$$x'^\mu = \frac{x^\mu + a^\mu x^2}{1 + 2x^\nu a_\nu + a^2 x^2}$$

The scaling dimension $\triangle$ of an operator is defined by how it changes under dilataion.

$$x^\mu \to a x^\mu, O(x) \to O'(x) = a^{\triangle} O(ax)$$

From the commutation relations between the translation generator P_μ, D, and K_μ,[6] we see the translations are raising operators and the K_μ's are the lowering operators of the scaling dimension. In particular, the ones that are annhilated by K's are called primary operators. If we consider the Euclidean version of the theory, we can take the dilatation operator as the Hamiltonian. Since the theory is conformally invariant, the background spacetime can be replaced by $S^3 \times R^1$ fig(1.4). A state in the space corresponds to an insertion of an operator at the origin of $R^{1,3}$ and propagated with the dilatation generator. Propagation with the dilatation operator in this radial quantization actually does not map to translation along the global time coordinate of $AdS_5 \times S^5$. The correct combination in the Lorentzian sector is $H = \frac{1}{2}(P_0 + K_0) = \partial_t$, where t is the global time coordinate of AdS. However, the operator/ state correspondence has the advantage that the energy eigenvalues of a state is just the scaling dimension of the operator conjugate to it. In the $S^3 \times R^1$ picture

it is natural to denote the states by the scaling dimensions of the operators. This helps simplify the identification of the bulk and boundary Hilbert space. Since the background is the flat space we can use the isometries to show the Hilbert spaces according to the two quantization schemes are isomorphic to each other. The isometry group of the S^5 is SO(6). In the AdS/CFT picture it corespondes to the R-symmetry of the $\mathcal{N} = 4$ super Yang-Mills theory.

The mapping between states in the bulk and the operators on the boundary (remember their scaling dimensions label the states on the boundary) proceed as follows[7]:

$$< e^{\int_\partial \phi_0(x) O(x)} >_{CFT} = Z_{string}[\phi(x,z)|_{z=0} = \phi_0(x)] \tag{1.12}$$

where we have written the AdS metric in the form:

$$ds^2 = \frac{1}{z^2}(-dz^2 + dx_i^2) \tag{1.13}$$

These coordinates also only covers the Poincare patch, and the boundary is at $z = 0$ with the x_i's labeling it. In the following we will work in the Euclidean sector with $z \to iz$. Eqn(1.12) says the boundary conditions on the bulk fields are to be considered as sources for the boundary theory operators with the appropriate scaling dimension. We will consider here only scalar fields. The cases with higher spin particles can be generalized naturally by considering adding tensorial operators to the CFT generating functional. The string theory partition function is viewed as a functional of the boundary value of the bulk fields.

From the metric (1.13), it is easy to see the transformation $z \to az$, $x_i \to ax_i$ is an isometry. when restricted to the boundary, the above transformation is just the dilatation. If the operator has scaling dimension $\triangle$, in order for the exponent of the left hand side of (1.12) to be scaling invariant, the corresponding bulk field must have the behavior $\phi(z,x) \sim z^{\triangle'}\phi_0(x)$ with $\triangle' = 4 - \triangle$. If we solve the bulk scalar wave equation:

$$(z^2\partial_z^2 - 3zd_z + z^2\nabla_{transverse} - m^2)\phi_(z,x) = 0$$

with the ansatz $z^{\triangle'}\phi_0(x)$, we find there are two possible values for $\triangle' = 4$.

$$\triangle'_\pm = 2 \pm (4 + m^2)^{1/2} \tag{1.14}$$

The positive root gives regular solutions on the boundary, while the negative one makes the solution diverge. We will refer to the former as the normalizable mode and the latter as the nonnormalizable mode. In general the normalizability of a solution is defined with respect to the Klein Gordon inner product on the space-time. A general solution to the scalar field equation is a linear combination of the normalizable and non normalizable modes:

$$\phi(x,z) = \phi_0(x)z^{\triangle'_-} + \phi_1(x)z^{\triangle_+} \tag{1.15}$$

Also since $\triangle'_+ + \triangle'_- = 4$, it makes sense to associate a bulk field with $\triangle'_-$ to the boundary operator with scaling dimension $\triangle'_+$. This is also motivated by the requirement that the

bulk field is regular on the interior of the AdS space.

Having established the dictionary, the first thing to notice is (1.12) gives us a way of obtaining correlation functions of the field theory operators at large λ through perturbative supergravity calculations (the large N, large 't Hooft coupling limit is taken as outlined before). To do this, we need to obtain the general solutions of the bulk wave equation subject to certain boundary condition $\phi_0(x)$. In fact, we will relate the left hand side of (1.12) to the supergravity partition function evaluated at on shell bulk fields with their boundary behavior as free variables.

$$< e^{\int_\partial \phi_0(x) O(x)} >_{CFT} = e^{-I_{SUGRA}[\phi(x,z)|_{z=0}=\phi_0(x)]}_{saddle} \tag{1.16}$$

There is aIn other words we treat $\phi_0(x)$ as the source for its dual operator $O(x)$. The correlation functions are obtained by functional differentiation of both sides with respect to $\phi_0(x)$ evaluated at $\phi_0(x) = 0$. The bulk wave fuction can be derived perturbatively by propagating the boundary condintion in to the bulk with the help of the "boundry to bulk" propagators. These propagators satisfies the homogeneous wave equation every where in the bulk, but approaches a delta function source on the boundary[7].

$$\lim_{z_1 \to 0} G_{boundary/bulk}(z_1, x_1|0, x_2) = (\frac{z}{z_1^2 + (x_1 - x_2)^2})^{\triangle'_-} \to z_1^{\triangle'_-} \delta(x_1 - x_2) \tag{1.17}$$

For free scalar theories the bulk field is then

$$\phi(z_1, x_1) = \int_\partial dx_2 G_{boundary/bulk}(z_1, x_1|0, x_2)\phi_0(x_2) \tag{1.18}$$

In terms of these boundary to bulk propagators, the field theory correlation function can be represented geometrically as in fig(1.5).

Using (1.16)one can infer a particularly useful relation between a bulk field and its dual boundary field theory operator. Suppose we turn on in the bulk a scalar field of the form (1.15). If we differentiate both sides of (1.16) with respect to $\phi_0(x)$and evaluate at $\phi_0(x) = 0$, we obtain[8]

$$< O(x) >= \phi_1(x) \tag{1.19}$$

To illustrate the usefulness of this relation let us consider turning on a bulk vector field $A_\mu(x, z)$:

$$A_\mu(x, z) = A^0_\mu(x) g_0(z) + A^1_\mu(x) g_1(z) \tag{1.20}$$

where $g_0(z)$, $g_1(z)$ are the nonnormalizable and normalizable solutions to the equations of motion of the vector field, respectively. According to the discussion above this corresponds to adding a term $A^0_\mu(x) J^\mu(x)$ to the boundary field theory Lagrangian density and the boundary values of the vector field act as sources for an associated conserved current current $J_\mu(x)$. This enables us to analyze the boundary field in the presence of a background charge and current with expectations value given by

fig 1.5

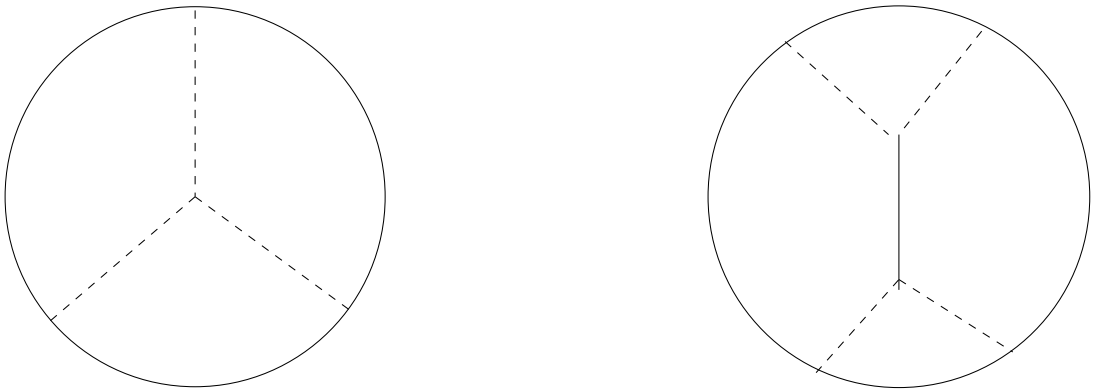

Bulk calculations of three and four point correlation functions. The circle is the boundary of AdS
The dotted lines are boundary to bulk propagators. The solid line is bulk to bulk propagator

Figure 1.5: Bulk calculations of boundary theory correlators

$$< J_\mu(x) >= A^1_\mu(x) \tag{1.21}$$

We will use this relation extensively in this thesis to study strongly coupled theory field theory phenomena at finite background charge and chemical potentials.

Despite the diffuculties in checking the AdS/CFT correspondence directly, many tests have been performed giving evidence for the validity of the duality. These tests usually involves calculating quantities in the boundary field theory with no dependence on the 't Hooft coupling (often the ones protected from quantum corrections by symmetries) and comparing with the corresponding supergravity/string theory objects according to the prescription (1.12): The spectrum of Chiral operators are invariant under change of the coupling. It is shown that the supergravity fields on AdS spacetime is in one-to-one correspondence with the chiral primary operators in the CFT. While single trace operators correspond to single particle states, multiple trace operators are dual to multiple particle states [6]. The decendents of a primary operator O (those obtained from acting derivatives or supercharges on the primaries), corresponds to excited states of the bulk field dual to O. Although the full spectrum of type IIB string theory on $AdS_5 \times S^5$ has not been mapped out entirely, it is conjectured the non-chiral primary operators will correspond to single string states with higher excitations. Gauging certain global symmetry on the field theory side results in quantum anomaly that comes only from the one loop diagrams, and thus can be trusted at the large λ regime. Such anomaly can be seen from the calculation of correlation functions of currents of the broken symmetry. Using the construction outlined above, the field theory and the supergravity calculation result in identical expressions for the anomaly in the large N limit [9]. Non-local operators such as Wilson loops in the boundary gauge theory of special shapes

are protected by super symmetry. Calculations from both the bulk and boundary points of view are also shown to match[13].

1.3 Adding Fundamentals

So far in our discussion, we have considered a brane setup where the degrees of freedom that survive the decoupling limit contain only those that transform in the adjoint representation of the gauge group, say $SU(N)$ for a stack of N D_3 branes in flat space. In order to use the gauge/gravity to analyze strongly coupled theories with matter content closer to QCD, we have to add additional fundamental sectors in the decoupled theory. This is accomplished in string theory by adding another set of D branes, which we will refer to as the flavor branes to the original stack of (color) branes that generates the adjoint sector of the theory. We will add N_f flavor branes, one for each species of fundamentals. The new degrees of freedom– the strings stretched between the flavor and the color branes, will transform from the point of view of the theory on the color branes in the fundamental represenation of gauge group [48]. The decoupling limit isolates the lowest energy string modes living at the intersections of the flavor and the color branes. The details of the resulting fundamental sector such as its mass, chrality, spin structure and the amount of (super)symmetry retained will depend on the specific branes used in the construction. For example in a well studied holographic model for supersymmetric QCD one uses $D7$ branes as flavor branes intersecting with a stack of color $D3$ branes. The model can be used to study quark and meson dynamics in a strongly coupled quark glueon plasma and its fundamental sector contains a $\mathcal{N}$ =2 hypermultiplet which consists of both bosonic and fermionic components[10]. In contrast, the fundamental sector of the model we will consider in chapter three has only massless chiral fermions and it breaks all supersymmetry [51]. This model can be used to study the chiral symmetry restoration transition in QCD[54].

On the gravity side, the geometries dual to general intersecting brane configurations have not been found. At $N_f \approx N$ the flavor branes backreact on the geometry and usually breaks symmetries rendering the Einstein's equations more difficult to solve. One can instead consider the case where $N_f << N$ ignoring the backreaction of the flavor branes by treating them as probes in the geometry dual to just having the color branes alone. Although there has been some recent progress towards finding the dual gravity solutions at general N_f/N [11, 12] these solutions are only generated numerically. They are only known at zero temperature and zero chemical potential and thus cannot be used to explore the phase diagram.

Many variants of the original AdS/CFT correspondence can be found by considering similar decoupling limits of dual descriptions of objects in string theory/M theory. In these variants the gravitational side need not be aysmptotically anti de Sitter while the dual gauge theories are generically not conformal[14] and it can sometimes be gauged matrix models[15, 16], Chern-Simons type theories[25] or even a nonlocal theory which has no explicit Lagrangian formulation–the little string theory[17]. The gauge/gravity dualities have also been checked beyond the supergravity limit. For example, a certain limit of $AdS_5 \times S^5$

along a null geodesic around the equator of the five sphere is shown to result in a spacetime on which the free string theory spectrum can be solved exactly in the light cone gauge. This background is a maximally supersymmetric plane wave solution of type IIB supergravity. The relevant string states live in a sector of the super Yang-Mills theory with large scaling dimensions and large R-charges. Coresponding limits on the field theory side are also shown to be dual to the string theory on the plane wave geometry[18]. We will now turn to finite temperature aspects of the AdS/CFT duality.

1.4 Hawking Page Phase Transition and Deconfinement Transition

Considering the $\mathcal{N} = 4$, SU(N) super Yang-Mills as living on the boundary of $AdS_5 \times S^5$, we have established a holographic picture for the AdS/CFT duality. If the duality is true to all orders of α' and N, we are to consider all backgrounds that are asymptotically AdS. This can be seen explicitly in (1.12) which asserts that the generating functional of the CFT can be computed by summing over all the bulk fields including variations of the background metric for the string theory as long as they are subjected to certain boundary conditions. The metrics that satisfies the bulk equations of motion may have different topological properties. These solutions are saddle points in the functional integral and integral maybe dominated by different saddles as we vary the parameters of the theory such as the temperature. When this happens the system goes through a phase transition. It is interesting to see how to describe topological changes in the bulk using the field theory language and how they are related to the phase diagram of the boundary theory.

There are two known solutions to Einstein's equations asymptotically AdS. The first one is the AdS spacetime (in this section, we will use the conventions of[3]:

$$ds_1^2 = (1 + r^2/b^2)dt^2 + \frac{dr^2}{1 + r^2/b^2} + r^2 d\Omega_{n-1}^2 \tag{1.22}$$

where b is related to the cosmological constant $\Lambda = \frac{n}{b^2}$. We will be calculating the Euclideanized partition function, the global time coordinate has been Wick rotated. The second solution is the Schwarzschild-AdS black hole:

$$ds_2^2 = (1 + r^2/b^2 - M/r^{n-2})dt^2 + \frac{dr^2}{(1 + r^2/b^2 - M/r^{n-2})} + r^2 d\Omega_{n-1}^2 \tag{1.23}$$

the temperature of the Euclidean black hole is determined by the requirement that the manifold is smooth and complete at the horizon $r_0 : 1 + r_0^2/b^2 - M/r_0^{n-2} = 0$. It is calculated to be:

$$T_H = \frac{r_0^2 + b^2}{2\pi b^2 r_0}$$

The topology of AdS spacetime is $R^n \times S^1$, and the Schwarzschild-AdS has $R^2 \times S^{n-1}$.

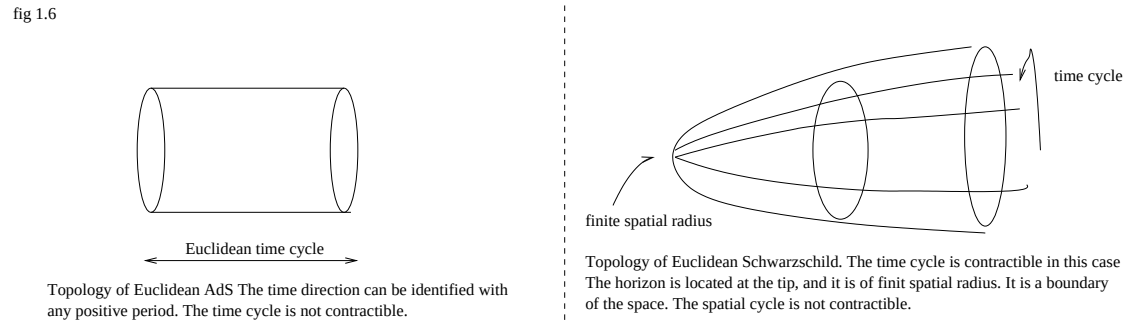

Figure 1.6: Topologies of anti de Sitter space and anti de Sitter black hole

They are dipicted in fig(1.6). There is a significant difference in the two cases. In ds_1^2, the temporal circle S^1 is not contractble and we can set the period of it to any positive number. In ds_2^2, the temporal circle is contractible provided it has the correct period $\beta = \frac{2\pi}{T_H}$, while it is the spatial sphere being not contractible. $r = r_0$ is a lower bound for the radial coordinate and the temporal circle pinches off at this point.

Hawking and Page[24] demonstrated that there is a gravitaional phase transition between AdS and AdS black hole. It is done by comparing the contributions to the partition function from the two geometries. Being solutions to the equations of motion, these are two saddle points for the Einstein-Hilbert Action with a cosmological constant:

$$I_{gravity} = I_{E-H} + I_{H-G}$$

$$= \frac{-1}{16\pi G_{n+1}} \int d^{n+1}x(g)^{1/2}(R + \frac{n(n-1)}{2b^2}) + \int_\partial K \tag{1.24}$$

where I_{H-G} is the Hawking-Gibbon's boundary term which cancells the contribution from varying the Ricci scalar to the equations of motion[23]. K is the extrinsic curvature on the boundary and G_{n+1} is the n+1 dimensional Newton's constant. On asymptotically AdS spacetimes the boundary term acctually evaluate to zero, and we will ignore it from now on. When plugging in solutions of Einstein's equation, the bulk term becomes:

$$I_{E-H} = \frac{n}{8\pi G_{n+1}} \int d^{n+1}x(g)^{1/2} \tag{1.25}$$

In both metrics $(g)^{1/2} = r^{n-1}$, however, the domains of integration in the t, and r coordinates are different. For AdS they are $t \in [0, \beta]$, $r \in [0, +\infty]$, where β could be any positive number and for Schwarzschild-AdS $t \in [0, \beta_H]$, $r \in [r_0, +\infty]$, where β_H is constraint to be the inverse Hawking temperature. This is a direct consequence of the topology difference between the two spacetimes. Note the radial coordinate is integrated all the way to infinity. Both contributions to the partition function have the same divergence due to the infinite volume.

In order to analyze the relative stability of the two saddle points, we need to regularize them. Following[24], we can subtract the AdS contribution from the black hole phase. To do so, however, we need to identify the two metrics on a large $r = R$ submanifold. Namely, we will need to match the circumference of the time circle on $r = R$

$$\beta_H(1 + \frac{R^2}{b^2} - \frac{M}{R^{n-2}})^{1/2} = \beta(1 + \frac{R^2}{b^2})^{1/2}$$

With the identification we found the differnce between the two solutions is:

$$\lim_{R\to\infty}(I_{E-H}^{S-AdS} - I_{E-H}^{AdS}) \propto \frac{b^2 r_0^{n-1} - r_0^{n+1}}{G_{n+1}(nr_0^2 + (n-2)b^2} \tag{1.26}$$

(1.21) turns zero at $r_0 = b$. From the usual thermodynamics relation $Z = e^{-I} = e^{-\beta F}$, we see that at small r_0 (low temperature), the AdS phase is energetically favorable, while at large r_0 (high temperature) S-AdS black hole is the dominant solution. There is a phase transition between AdS and S-AdS black hole. With the regularized S-AdS contribution to the partition function, we can also compute other thermodynamic quantities such as the energy and entropy of the black hole.

We now consider phase transitions in the boundary field theory. It is shown in [33, 34] at least in the small 't Hooft coupling limit the large N $\mathcal{N} = 4$ SU(N) super Yang-Mills theory on a compact manifold (here in particular we consider $S^1 \times S^3$), has a deconfinement phase transition. The transition is characterized by the behavior of the order parameter:

$$C_1 = \lim_{N\to\infty} \frac{F(\beta)}{N^2} \tag{1.27}$$

There exists a low temperature confined phase with $C_1 = 0$ (or $F(\beta > \beta_H) \sim O(1)$) and a high temperature deconfined phase $C_1 \sim O(1)$ (or $F(\beta < \beta_H) \sim O(N^2)$). $F(\beta)$ is the free energy of the theory and β is the period of the temperal circle. The large N limit is essential for the deconfinement transition to exist on a manifold with finite volume. On the other hand, it is also known that the $\mathcal{N} = 4$ SU(N) super Yang-Mills theory on the decompactified background $R^3 \times S^1$ is always in the deconfined phase. There is yet another order parameter for the deconfinement phase transition.

Consider the expectation value of a Wilson line operator in the gauge theory:

$$C_2 =< W(C) >=< Tr[Pe^{\int_C A}] > \tag{1.28}$$

In particular, we will consider the case when the Wilson line wraps around the temperal circle of the backgound. Introducing a Wilson line operator in the theory can be interpreted as adding an external static charge which transform in the fundamental representation of SU(N) (a quark) to the system. The expectation value of the Wilson line is related to the cost of free energy of introducing the quark.

$$< W(C) >\sim exp(-F(\beta)\beta) \tag{1.29}$$

In the confined phase, the field theory can be considered as a theory containing only glue balls at finite temperature. It takes an infinite amount of free energy to introduce an external charge, and therefore the expectation value of the Wilson line (C_2) is zero. In the deconfined phase the cost of free energy of such operation is finite and so is the order parameter C_2.

The authors of [32, 33] have utilized these order parameters and demonstrated deconfinement phase transition in weakly coupled large N gauge field theories on compact manifolds. Their result also shows in the confining phase the gauge theory spectrum has the Hagedorn behavior. The Hagedorn behavior is characterized by the exponential growth of the density of states with respect to increasing energy: $\rho(E) = e^{\beta_H E}$ Therefore, when computing the thermal partition function of the system, we get a critical temperature $\beta = \beta_H$, above which the thermal partition function diverges and the thermal ensemble is ill-defined.

$$Z_\beta = \int \rho(E) e^{-\beta E} \tag{1.30}$$

Studying the order parameters indincates the deconfinement transition could be either first order at a temperature below T_H, or second order happening right at T_H.

It is well known the spectrum of single string states also exhibits Hagedorn behavior [26]. The Hagedorn temperature can be considered as the temperature at which perturbative vacuum of string theory becomes unstable. This can be seen from the fact that some superstring states with nonzero winding around the thermal circle become tachyonic if the period of the thermal circle is smaller than certain critical value β_H [27]. It is argued that at any finite value of the string coupling there is corespondingly some kind of phase transition when the winding modes condense. The phase transition can again be first order below T_H or second order occuring at exactly the Hagedorn temperature. The former is not truely a Hagedorn transition in that the partition function is not dominated by contributions from states with arbitrily high energy, while the latter is. In the AdS/CFT correpondence, we are identifying the Hilbert space of the Yang-Mills theory with that of the string theory. It is natural to identify the Hagedorn behavior and the phase transitions on both sides of the picture as well. The winding modes can be heuristically identified with the temporal Wilson lines used as the order parameter of the deconfinement phase transition.

Going back to the strongly coupled field theory limit. According to AdS/CFT duality, this correspondes to the regime where supergravity results can be trusted. The supergravity description of the Wilson lines is proposed to be[28]:

$$< W(C) >_{CFT} \sim e^{-S_C} \tag{1.31}$$

where S_C is the minimal area of a surface in the bulk bordered by C on the boundary of the spacetime. S_C is calculated with respect to the appropriate bulk background geometry. The proposal is motivated by the picture that we can view (low energy) excitations of open strings stretched between a stack of N D-branes and one distantly seperated D-brane as states of

fig 1.7

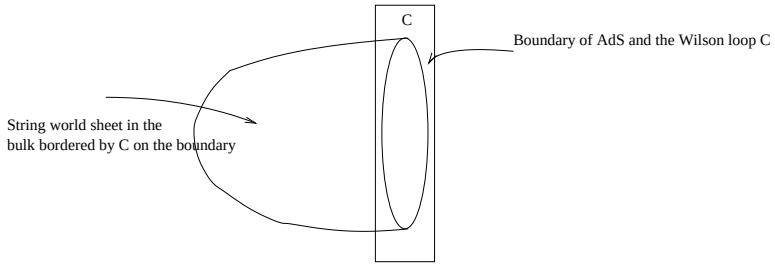

The expectation value of a Wilson loop operator C on the boundary can be approximated by the exponential of the area of string world sheets bordered by C

Figure 1.7: Bulk computation of the Wilson loop operator

very massive quarks, with the mass proportional to the seperation. (This is because open string ends carry Chan-Paton factors that transform in the fundamental of the SU(N)) If we take the quark to be static ($m \to \infty$), the string can be considered to be stretched between the bulk of AdS and its boundary. Since Wilson lines in gauge theory corresponde to insertion of such a massive quark, in view of the prescription (1.12), the expectation value of these operators on the boundary should be dual to (in the supergravity limit) the exponential of the area of the superstring world sheet with the boundary condition that it ends on C. fig(1.7). In the low temperature phase, according to (1.21), the bulk geometry is that of the pure AdS. However, it has the topology such that the temperal circle is not contractable.

Thus it is not the border of any string world sheet, and $< W(C) >= 0$. When the temperature is high, the dominating state in the bulk is the Schwarzscild-AdS black hole background. The black hole geometry admits contractable temporal circles, and thus C is the boundary of some string world sheet configuration. $< W(C) >$ is nonzero. The above result suggests that we can associate the confined phase in the boundary field theory to the bulk AdS geometry and the deconfined phase to the black hole background [3]. More importantly, the deconfinement phase transition is dual to the Hawking-Page phase transition. As we have seen in (1.21), the Hawking Page phase transition is a first order one. It is also understood that it happens at a temperature lower than the energy scale where stringy corrections become important, that is, it happens below the Hagedorn temperature.

From the above analysis, we can make the following congecture: in the large N, weak 't Hooft coupling limit, $\mathcal{N} = 4$ SU(N) super Yang-Mills has deconfinement phase transition, which could be identified with the Hagedorn behavior in the free superstring theory. It is not clear, however, what is the phase beyond the Hagedorn temperature on the string theory side. (For more interesting speculations on this point see [32]) When the 't Hooft coupling

is large, we can approximate bulk theory by classical supergravity. The deconfinement phase transtion in the gauge theory is mapped to the Hawking-Page phase transition. The phase transition is first order and is below the Hagedorn temperature. Notice that the information about the deconfinement phase transition in the strong coupling limit is only obtained through the help AdS/CFT, since we have no control over the perturbation theory when λ is large.

1.5 Plan of the Thesis

In this thesis we summarize three of our work using the gauge/gravity dualities to investigate strongly coupled phenomena in gravity, QCD like gauge theories and condensed matter physics.

First, we consider the thermodynamics of large N_c pure Yang Mills theory on a small compact space. The size of the compact space R provides us with an effective infrared cut off for spectrum of the theory . By taking $1/R$ to be much larger than the strong coupling scale Λ_{QCD} all the massive modes become weakly coupled due to asymptotic freedom. This enables us to integrate out these degrees of freedom and obtain an effective theory that is a unitary matrix model [32]. We analyze the phase diagram of the theory as a function of temperature by identifying the saddle point with the lowest free energy. In doing so we find that the system goes through a deconfinement transition as the temperature is raised. We extract the order of the phase transition and also find interesting intermediate phases. Our analysis sheds light on the structure of the theory near the transition. In the flat space limit ($R \to \infty$)the deconfinement transition occurs when the coupling is large and is only accessible through lattice simulations or toy models. By comparing with the numerical results, we propose possible phase diagrams that connect the weak and strong coupling regimes. As we will review below, in the dual picture, the deconfinement transition is connected to the formation of black holes. Our work provides information on possible modifications of black hole thermodynamics by stringy corrections and the Hagedorn transition in perturbative string theory.

Next we use the gauge/gravity duality to study the effects of finite baryon chemical potential on the phase structure of QCD like gauge theories. It is well known that the QCD phase diagram possesses many interesting features as a function of the baryon chemical potential even at zero temperature. Again, aside from the region of very high chemical potential where the coupling becomes small, we have very little analytic understanding of these interesting phase structures. Especially at intermediate values of the baryon chemical potential –the region of particular importance to nuclear physics, the numerical techniques also become very expensive as the action becomes complex valued. We consider the Sakai-Sugimoto model which consists of intersecting D branes whose low energy limit has exactly the field content of large N_c nonsupersymmetric QCD with chiral fermions. Specifically, the adjoint sector is generated by a stack of N_c D_4 branes while the fundamental sector of both chiralities are introduced through inclusion of N_f number of D_8 and anti D_8 branes [51]. The theory has a

well defined gravity dual at strong coupling in the quenched approximation where the flavor branes can be treated as probes in the background generated by the color branes. The gauge theory side exhibits deconfinement transition and chiral symmetry restoration [54]. These phase transitions are realized on the gravitational side through the topological changes of the background geometry and embeddings of the flavor branes, respectively. Along the baryon chemical potential axis we identify a first-order transition from vacuum to a phase with finite baryon density as the chemical potential is increased. Gravitational interpretations of the quark Fermi surface and the chiral density wave are also proposed.

Thirdly we study a setup in gravity theory whose field dual undergoes a transition to a superconducting state as the temperature is lowered. Recently, the gravitational duals to various interesting phenomena in condensed matter systems have been constructed including the Nerst effect [22], quantum Hall effect[20, 21] and superconductivity/superfluidity[92]. Specifically, it is shown by Gubser[114] that an Abelian-Higgs model placed in an anti-de Sitter black hole background develops a scalar hair at sufficiently low temperatures. The condensation of a scalar field in the bulk is mapped to an operator developing an expectation value which breaks the global $U(1)$ symmetry in the boundary theory and can be used as an order parameter for the phase transition. Using the duality, the boundary value of the electromagnetic vector potential gives the supercurrent velocity. In the presence of the condensate, the frequency dependent conductivity in the field theory shows a delta function divergence at zero frequency and has a gap. This suggests that the system is in a superconductor/superfluid state. We have studied carefully the superfluid solution at zero frequency. The phase diagram was analyzed as a function of temperature and the superfluid velocity v_s. We find that the critical temperature where the system transitions from superfluid to normal state decreases with increasing v_s. It was also observed that the transition is second order at low values of the superfluid velocity. A critical point exists in the phase diagram across which the transition switches to first-order. This agrees qualitatively with the analysis at weak couplings using the BCS theory.

Chapter 2

A Second Order Deconfinement Transition for Large N 2+1 Dimensional Yang-Mills Theory on a Small S^2

2.1 Introduction

The phase diagram of QCD has attracted much interest in modern particle physics research. It is well-known that the theory has qualitatively different behaviors at low and high temperatures. In particular at high temperatures the effective degrees of freedom of the theory are gluons and quarks, while they are confined into color singlet states such as glueballs and mesons as the temperature is lowered . The transition separating the two phases is conjectured to be a smooth crossover but becomes sharp as the ratio of the number of flavors to the number of colors reduced [29]. However in flat space, near the phase transition the theory is strongly coupled and there is no analytic approach to understanding the nature of the transition. Note that even in the deconfined phase near the transition the physics has also been shown to be strongly coupled[19]. In this chapter, we follow [33] to study the thermodynamics of large N pure 2+1 dimensional Yang-Mills theory on a spatial S^2 with radius much smaller than the scale set by the dimensionful coupling of the gauge theory. In this limit, the asymptotic free nature of the nonabelian gauge theory renders the dimensionless coupling $\lambda = g^2 NR$ is small, so the thermodynamics can be studied in perturbation theory. The thermal partition function is given by the path integral for the Euclidean theory on $S^2 \times S^1$, where the S^1 has radius given by the inverse temperature $\beta = T^{-1}$. From this path integral expression, we integrate out all modes apart from the trace of the Polyakov loop,[1]

$$u = \frac{1}{N}\mathrm{tr}(U) = \frac{1}{N}\mathrm{tr}Pe^{i\int_{S^1} A} \ ,$$

giving us an effective action for u, the standard order parameter for confinement. The free energy costs of adding a single external quark to the system space F_q and $u\ e^{-F_q/T}$. F_q is infinite in the confined phase as the flux lines emanating from the quark has no place to end but is finite in onthe deconfined phase. This effective action takes the form (valid for

[1]Here A is averaged over the S^2.

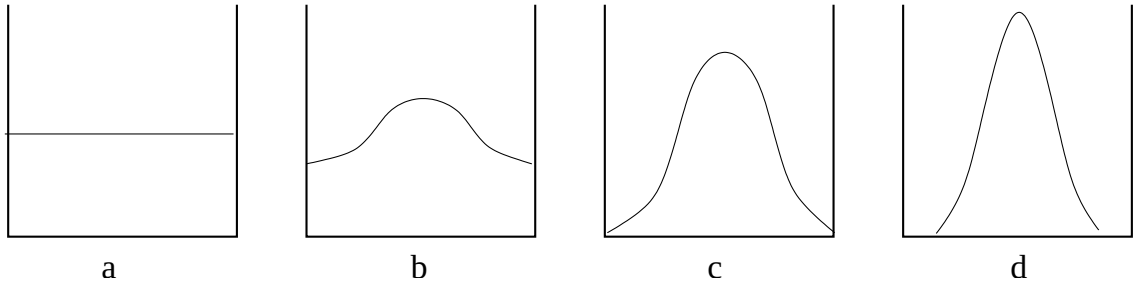

Figure 2.1: Distribution of Polyakov loop eigenvalues on unit circle (horizontal axis) in confined phase (a), in gapless phase above second order deconfinement transition (b), at third-order gapping transition (c), and in high-temperature gapped phase (d).

$|u| \leq 1/2$)

$$S_{eff}(u) = f(T,\lambda)|u|^2 + \lambda^2 b(T)|u|^4 + \mathcal{O}(\lambda^4) \; . \tag{2.1}$$

For low temperatures, f is positive, and so the saddle-point configuration has $u = 0$. At some temperature $T_H = T_H^0 + \mathcal{O}(\lambda)$, f becomes negative, so $u = 0$ is no longer the minimum action configuration. The three-loop calculation in this paper shows that the coefficient b is positive at the critical temperature, so as f becomes negative, $|u|$ develops an expectation value gradually, resulting in a second-order phase transition.

The situation here is in contrast to the 3+1 dimensional case, where the analogous calculation [33] revealed a negative value for $b(T_H)$. In that case, the deconfinement transition is first order, characterized by a discontinuous change in the eigenvalue distribution for the unitary matrix U from the uniform distribution (eigenvalues equally distributed around the unit circle) to a non-uniform distribution with a gap (i.e. a region of the circle where no eigenvalues are present). In terms of the eigenvalue distribution, the continuous transition we find here corresponds to a continuous change from the uniform distribution to an increasingly non-uniform distribution. As argued in [32], at a temperature

$$T_2 = T_H + \frac{1}{2}\lambda^2 b(T_H)/f'(T_H)$$

the minimum value of the eigenvalue density will reach zero, as depicted in figure 2.1, and the eigenvalue distribution will develop a gap for higher temperatures. This results in an additional third-order phase transition of Gross-Witten type, so the phase diagram for pure Yang-Mills theory on $S^2 \times S^1$ contains at least three distinct phases (uniform, non-uniform, gapped).

The basic setup for our calculation and the calculation itself are presented in sections 2 and 3 of this chapter. We then consider the implications of our results for the full phase diagram as a function of temperature and spatial radius. In section 4, we argue that in the high-temperature limit for fixed radius the theory effectively reduces to pure two-dimensional Yang-Mills theory on a spatial S^2. This theory has a third order phase transition as the radius

of the sphere is varied [38], suggesting that our phase diagram has an additional third order transition line coming from large temperature along the curve

$$TR \sim 1/(\lambda R) \ .$$

It is tempting to conjecture that this third-order transition line connects up with the one emerging from the critical temperature at small radius (as in figure 2.6b). Indeed, these are qualitatively very similar: while the latter transition is associated with the development of a gap in the eigenvalue distribution for the Polyakov loop, the two-dimensional Yang-Mills theory transition is associated with the development of a gap in the eigenvalue distribution for the Wilson loop around the equator of the sphere (or any other maximal-area non-intersecting loop) [40]. On the other hand, we have not been able to show any direct relation between the two order parameters (which we can choose to be the minimum value of the eigenvalue density for these two Wilson loops). Further, it is possible that the high temperature transition ceases to be sharp as we decrease the temperature.

In section 5, we consider the fate of the actual deconfinement transition line as the radius is increased and the possible forms for the full phase diagram. At large volume, we can appeal to lattice results, which for finite N suggest that there is a second order deconfinement transition for $N = 2, 3$ (and possibly $N = 4$), a weak first order transition for $N = 5$ and a stronger first-order transition for $N = 6$ [35]. It is believed that the transition should continue to strengthen as N is increased. If this is correct, the large N theory would be expected to exhibit a first order deconfinement transition, and there must be a point along the deconfinement transition line at some critical radius, where the deconfinement transition switches from second order to first order. We argue that there are two qualitatively different behaviors of the Polyakov loop effective potential that can lead to such a point. These correspond either to a tricritical point at which both quadratic and quartic terms in an effective action vanish, or to a triple point, separating three distinct phases. The simplest possible phase diagrams consistent with the available information are presented in figure 2.6.

We conclude in section 6 with a few comments on the implications for a possible gravitational dual theory of the existence of three distinct phases.

2.2 The Setup

In this section we will briefly review the results and techniques developed in [32–34] and apply them to analyze the thermodynamic properties of $2 + 1$ dimensional, large N pure Yang-Mills theory living on a two-sphere of radius R. As argued in [32], asymptotically free gauge theories become weakly coupled at small volume, in this case when $\lambda = g^2 NR$. This is because all modes with the exception of the constant mode of A_0 on $S^2 \times S^1$ (which we denote by α), are massive, with masses $\geq 1/R$. We thus have an effective IR cutoff on the renormalization group flow of the coupling $g^2_{YM}N$. The massive modes may be integrated out directly in perturbation theory, yielding an effective action for the zero-mode α, or more

precisely, for the constant $SU(N)$ matrix $U = e^{i\beta\alpha}$. The result of [32] shows that in the large N limit, the matrix model undergoes a Hagedorn-like transition at some critical temperature, which corresponds to a deconfinement transition in the gauge theory. We note that the large N limit is essential for the theory on a compact manifold to exhibit a sharp phase transition.

2.2.1 Basic Setup

The thermal partition function of pure $SU(N)$ Yang-Mills theory on S^2 at temperature T can be evaluated by the Euclidean path integral of the theory on the manifold $S^2 \times S^1$, with the radius of the circle S^1 equal to $\beta = \frac{1}{T}$. The action of the theory is:

$$\mathcal{L} = \frac{1}{4}\int_0^\beta dt \int d^2x \mathrm{tr}(F_{\mu\nu}F^{\mu\nu}). \tag{2.2}$$

To perform this computation we will work in the gauge:

$$\partial_i A^i = 0 \tag{2.3}$$

where $i = 1, 2$ runs over the sphere coordinates, and ∂_i are (space-time) covariant derivatives.

This does not completely fix the gauge, as we can still make spatially independent gauge transformations. To completely fix the gauge we also impose

$$\partial_t \int_{S^2} A_0 = 0. \tag{2.4}$$

so we choose the constant (on the sphere) mode of A_0 to be independent of time. We define:

$$\alpha = \frac{g_{YM}}{\omega_2}\int_{S^2} A_0, \tag{2.5}$$

where ω_2 is the volume of the 2-sphere.

The mode α is a zero mode of the theory which is always strongly coupled and cannot be integrated out perturbatively. Because of this, we will compute the path integral of the theory in two steps. First we will integrate out all other modes which are massive to generate an effective action for the zero mode α. Then we will analyze the effective action for α. In other words, we will do the path integral in the following order:

$$Z = \int DA\, d\alpha\, e^{-S[A,\alpha]} = \int d\alpha \int dA\, e^{-S[A,\alpha]} = \int d\alpha\, e^{-S_{eff}[\alpha]} \tag{2.6}$$

As explained in [32] the effective action for α can be written completely in terms of the unitary matrix $U \equiv e^{i\beta\alpha}$ in the form:

$$S_{eff} = \sum_m C_{m,-m} Tr(U^m)Tr(U^{-m}) + \lambda\beta \sum_{m,n} C_{m,n,-m-n} Tr(U^m)Tr(U^n)Tr(U^{-m-n})/N$$

$$+ \quad \lambda^2\beta \sum_{m,n,p} C_{m,n,p,-m-n-p} Tr(U^m)Tr(U^n)Tr(U^p)Tr(U^{-m-n-p})/N^2 + \dots \tag{2.7}$$

Then the free energy of the theory is given by the matrix integral:

$$Z(\beta) = e^{-\beta F} = \int [dU] e^{-S_{eff}(U)} \tag{2.8}$$

where, as discussed in [32], the Fadeev-Popov determinant of the gauge fixing transforms the integral over α to an integral over the gauge group with Haar measure $[dU]$. Note U is the holonomy of the gauge field around the temporal circle. We thus have an effective action for the temporal Wilson loop, whose expectation value is the standard order parameter for the deconfinement transition.

In the large N limit, we can evaluate the integral using saddle point techniques. Introducing the eigenvalue distribution $\rho(\theta) = \sum_i \delta(\theta - \theta_i)/N$ where θ_i are the eigenvalues of α, $i = 1..N$ and defining $u_n = \int d\theta \rho(\theta) e^{in\theta} = Tr(U^n)/N$ the effective action takes the form:

$$Z[\beta] = \int [du_n][d\bar{u}_n] e^{-N^2 S'_{eff}[u_n, \bar{u_n}; \beta, \lambda]} \tag{2.9}$$

with

$$\begin{aligned} S'_{eff} &= \sum_m (1/m - C_{m,-m}) u_m \bar{u_m} + \lambda\beta \sum_{m,n} C_{m,n,-m-n} u_m u_n \bar{u_{m+n}} \\ &+ \lambda^2\beta \sum_{m,n,p} C_{m,n,p,-m-n-p} u_m u_n u_p \bar{u_{m+n+p}} + ... \end{aligned} \tag{2.10}$$

where the extra $1/m$ comes from the Vandermonde determinant obtained in going to the variables u_n.

Note that $u_n = 0$ is a stationary point at all temperatures. It corresponds to the uniform distribution of the eigenvalues of U. The stability of this saddle point depends on the values of the coefficients $C_{n,m,...}$. As we will show in the next subsection, the coefficient of $|u_1|^2$ is positive at small T but becomes negative as we increase the temperature. This signals that the $u_n = 0$ phase becomes unstable and the system undergoes a phase transition. As explained in [32], near the transition temperature the u_1 mode becomes massless, while the $u_{n>1}$ modes remain massive. We will further integrate out these higher moments to obtain an effective action for u_1 near T_H to analyze the order of the phase transition. To achieve this we will need the coefficient of the quartic term in u_1. The relevant terms in (2.10) are:

$$\begin{aligned} S'_{eff} &= (1 - C_{1,-1})|u_1|^2 + (1/2 - C_{2,-2})|u_2|^2 + ... \\ &+ \lambda\beta[C_{1,1,-2}(u_1^2 \bar{u_2} + u_2 \bar{u_1}^2) + ...] \\ &+ \lambda^2\beta C_{1,1,-1,-1}|u_1|^4 + ... \end{aligned} \tag{2.11}$$

For the saddle point configuration, the higher modes u_n are determined by minimizing the effective action over u_n for fixed u_1, so we have

$$u_2 = -\lambda\beta \frac{C_{1,1,-2}}{(1/2 - C_{2,-2})} u_1^2 + O(\lambda^2) \tag{2.12}$$

This gives the effective action:

$$S'_{eff}(u_1) = (1 - C_{1,-1})|u_1|^2 + \lambda^2 \beta b_c |u_1|^4 + ... \tag{2.13}$$

where

$$b_c = -\beta^2 C_{1,1,-2}(\beta)^2/(1/2 - C_{2,-2}(\beta)) + \beta C_{1,1,-1,-1} + O(\lambda) \tag{2.14}$$

As discussed in[32], the sign of b evaluated at the critical temperature determines the order of the phase transition. If $b_c < 0$ the transition is first order and occurs at the Hagedorn temperature T_H at zero coupling, but slightly below T_H at small but finite coupling (they are the same up to order λ^2). If $b_c > 0$ there are two phase transitions. The first one occurs at exactly T_H and is second order, while the second one is a Gross-Witten type third order phase transition happening above T_H. The third order phase transition occurs at the point where the eigenvalue distribution of U develops a gap. Our goal will be to compute the coefficients $C_{n,m,...}$ to the appropriate order in perturbation theory to obtain b_c. The $C_{2,-2}$ requires a one loop calculation, while $C_{1,1,-2}$ and $C_{1,1,-1,-1}$ require two and three loop calculations respectively.

2.2.2 One Loop Free Energy

It is shown in [32] that the coefficient $C_{m,-m}$ can be extracted by computing the one loop partition function of the theory . It turns out that:

$$C_{m,-m} = -\frac{z_V(x^m)}{m} \tag{2.15}$$

where $x = e^{-\beta/R}$ and $z_V(x)$ is the single particle partition function

$$z_V(x) = \sum_{\triangle} n(\triangle) x^{-\beta\triangle} \tag{2.16}$$

In our case $\triangle^2$ are the eigenvalues of the Laplacian on the unit two sphere acting on the vector spherical harmonics surviving the gauge fixing, while $n(\triangle)$ is the multiplicity of each mode. More specifically $\triangle_h^2 = h(h+1)$, $n(\triangle_h) = 2h+1$, $h = 1, 2, ...$ The Hagedorn temperature is determined by the point where the u_1 mode become unstable:

$$z_V(x_c) = 1 \tag{2.17}$$

We are not able to get a closed form for $z_V(x)$, but numerically we find:

$$x_c \simeq 1.195097 \tag{2.18}$$

so the Hagedorn temperature of the free theory on a two-sphere of radius $R = 1$ is:

$$T_H \simeq 0.302675 \tag{2.19}$$

Similarly,

$$C_{2,-2} = -\frac{z_V(x_c^2)}{2} = 0.38155 \tag{2.20}$$

2.2.3 Gauge Fixed Action

Formally, the thermal partition function is of the form

$$Z[\beta] = \int [d\alpha][dA_0'][dA_i] \triangle_1 \triangle_2 e^{-S[\alpha, A_0', A_i; \beta]} \tag{2.21}$$

where $\triangle_1$, $\triangle_2$ are the Fadeev-Popov determinants associated with (2.3), (2.4) respectively and $\beta = 1/T$ is the size of the time circle. The prime on A_0' signals that the constant mode has been removed. As shown in [32], $\triangle_2$ can be combined with $[d\alpha]$ to give the integration measure of a unitary matrix $[dU]$ with $U = e^{i\beta\alpha}$. On the other hand, $\triangle_1$ is

$$\det \partial_i D^i = \int \mathcal{D}c\mathcal{D}\bar{c} e^{-\mathrm{tr}(\bar{c}\partial_i D^i c)} \tag{2.22}$$

where D^i denotes a gauge covariant derivative

$$D_i c = \partial_i - i g_{YM}[A_i, c] \tag{2.23}$$

and c and $\bar{c}$ are complex ghosts in the adjoint representation of the gauge group. With our gauge choice, the quadratic terms in the Yang-Mills action(2.2) take the form

$$-\int d^3x \mathrm{tr}\left(\frac{1}{2}A_i(\widetilde{D}_0^2 + \partial^2)A^i + \frac{1}{2}A_0'\partial^2 A_0' + \bar{c}\partial^2 c\right) \tag{2.24}$$

where

$$\widetilde{D}_0 X \equiv \partial_0 X - i[\alpha, X]. \tag{2.25}$$

The interaction terms in (2.2) are given by

$$\begin{aligned}\int d^3x \mathrm{tr}(\quad & i g_{YM}\widetilde{D}^0 A^i[A_i, A_0'] - i g_{YM}[A^i, A'^0]\partial_i A_0' - i g_{YM}\partial_i A_j [A^i, A^j] + \\ & \frac{g_{YM}^2}{4}[A_i, A_j][A^j, A^i] - \frac{g_{YM}^2}{2}[A_0', A_i][A'^0, A^i] - i g_{YM}\partial_i \bar{c}[A_i, c]).\end{aligned} \tag{2.26}$$

We wish to obtain the effective action by

$$e^{-S_{eff}[U;\beta,\lambda]} = \int [dc][dA_0'][dA_i] e^{-S_{1loop}} < e^{-S_{int}} > . \tag{2.27}$$

The result is an effective theory for a constant $SU(N)$ matrix $U = e^{i\beta\alpha}$

$$Z[\beta] = \int [dU] e^{-S_{eff}[U;\beta,\lambda]}. \tag{2.28}$$

2.3 The Perturbative Calculation

In this section, we summarize the computation of the two and three loop diagrams. As we are on S^2, it will be convenient to expand the fields in terms of the vector and scalar spherical harmonics on S^2. As a result, the spatial momentum integrals in the Feynman diagrams can be replaced by sums over the quantum numbers of the generators of $SU(2)$. We will first set up the conventions that facilitate the computation.

2.3.1 Spherical Harmonics Expansion on S^2

The basic set-up for the computation was described in section 2 of [32]. As in the $3+1$ case, it will be useful to write the action explicitly in terms of a set of spherical harmonic integrals. We will denote the scalar and vector spherical harmonics on S^2 by $S^\alpha(\theta)$ and $V_i^\beta(\theta)$, where $\alpha = (j_\alpha, m_\alpha)$ and $\beta = (j_\beta, m_\beta)$ are the $SU(2)$ quantum numbers for the various modes. Our conventions for the vector spherical harmonics can be found in appendix A. Note for $S^{j,m}$ and $V_i^{j,m}$ the j quantum number starts at $j = 0$, $j = 1$, respectively. In terms of these, we have:

$$\begin{aligned} A_0'(t,\theta) &= \sum_\alpha a^\alpha(t) S^\alpha(\theta); \\ A_i(t,\theta) &= \sum_\beta A^\beta(t) V_i^\beta(\theta); \\ c(t,\theta) &= \sum_\alpha c^\alpha(t) S^\alpha(\theta). \end{aligned} \tag{2.29}$$

We will denote the complex conjugate of S^α by $S^{\bar\alpha}$. On S^2, the complex conjugation for scalar spherical harmonics is the same as inverting the sign of m_α and multiplying by $(-1)^{m_\alpha}$. We also denote the complex conjugate of V_i^β by $V_i^{\bar\beta}$. The complex conjugation for vector spherical harmonics has the effect of changing the sign of m_β and multiplying by $(-1)^{m_\beta+1}$. The scalar spherical harmonics are an orthonormal basis of functions on S^2,

$$\int_{S^2} S^\alpha S^{\bar\beta} = \delta^{\alpha\beta}. \tag{2.30}$$

In terms of these spherical harmonics, we can define

$$\begin{aligned} C^{\alpha\beta\gamma} &= \int_{S^2} S^\alpha \vec{V}^\beta \cdot \vec{\nabla} S^\gamma, \\ D^{\alpha\beta\gamma} &= \int_{S^2} \vec{V}^\alpha \cdot \vec{V}^\beta S^\gamma, \\ E^{\alpha\beta\gamma} &= \int_{S^2} (\vec{\nabla} \times \vec{V}^\alpha) \cdot (\vec{V}^\beta \times \vec{V}^\gamma) \end{aligned} \tag{2.31}$$

They appear as effective couplings of various interaction terms in the pure Yang Mills Lagrangian. These integrals can be computed explicitly using properties of $SU(2)$. We will list

the expressions for C, D and E in the appendix. Note that C is antisymmetric in α and γ, D is symmetric in α and β, and E is antisymmetric in β and γ. Using these expressions, the quadratic part of the action for pure Yang Mills theory on the two sphere becomes

$$S_2 = \int dt \mathrm{tr} \left(\frac{1}{2} A^{\bar{\alpha}} (-D_\tau^2 + j_\alpha(j_\alpha+1)) A^\alpha + \frac{1}{2} a^{\bar{\alpha}} j_\alpha(j_\alpha+1) a^\alpha + \bar{c}^{\bar{\alpha}} j_\alpha(j_\alpha+1) c^\alpha \right). \quad (2.32)$$

The cubic interactions are

$$\begin{aligned} S_3 = g_{YM} \int dt \mathrm{tr}(\quad & i\bar{c}^{\bar{\alpha}} [A^\gamma, c^\beta] C^{\bar{\alpha}\gamma\beta} + 2i a^\alpha A^\gamma a^\beta C^{\alpha\gamma\beta} \\ & -i[A^\alpha, D_\tau A^\beta] a^\gamma D^{\alpha\beta\gamma} - i A^\alpha A^\beta A^\gamma E^{\alpha\beta\gamma}), \end{aligned} \quad (2.33)$$

and the quartic interactions are given by

$$\begin{aligned} S_4 = g_{YM}^2 \int dt \mathrm{tr}(\quad & - \frac{1}{2} [a^\alpha, A^\beta][a^\gamma, A^\delta] \left(D^{\beta\bar{\lambda}\alpha} D^{\delta\lambda\gamma} + \frac{1}{j_\lambda(j_\lambda+1)} C^{\alpha\beta\bar{\lambda}} C^{\gamma\delta\lambda} \right) \\ & - \frac{1}{2} A^\alpha A^\beta A^\gamma A^\delta \left(D^{\alpha\gamma\bar{\lambda}} D^{\beta\delta\lambda} - D^{\alpha\delta\bar{\lambda}} D^{\beta\gamma\lambda} \right)). \end{aligned} \quad (2.34)$$

2.3.2 Effective Vertices

Since the action is quadratic in a and c, these may be integrated out explicitly to give additional effective vertices. As discussed in detail in [33], we have two types of effective vertices. The A type vertices arise from loops of a and c. The B type vertices are from open strings of a's containing two vertices linear in a and some number of quadratic a vertices. Both involve divergences proportional to $\delta(0)$. As for the 3+1 dimensional theory on S^3, all divergent contributions proportional to $\delta(0)$ cancel. In particular the contributions from the a and c loops completely cancel out with the divergent parts in the B type effective vertices. We thus have only the non-divergent contributions from the latter. Computationally, we will keep only the vertices appearing in the Lagrangian above which contain no temporal component a and ghosts c. In addition, we will also have the second type of effective vertices, but can ignore any contributions proportional to $\delta(0)$ arising from contractions of $\nabla_\tau A$s in these. The B type vertices are:

$$\begin{aligned} B_4 &= \frac{g_{YM}^2}{2} \frac{D^{\alpha_1\beta_1\gamma} D^{\alpha_2\beta_2\bar{\gamma}}}{j_\gamma(j_\gamma+1)} \mathrm{tr}([A^{\alpha_1}, D_\tau A^{\beta_1}][A^{\alpha_2}, D_\tau A^{\beta_2}]), \\ B_5 &= -i g_{YM}^3 \frac{D^{\alpha_1\beta_1\lambda} C^{\bar{\lambda}\gamma\bar{\sigma}} D^{\alpha_2\beta_2\sigma}}{j_\lambda(j_\lambda+1) j_\sigma(j_\sigma+1)} \mathrm{tr}([A^{\alpha_1}, D_\tau A^{\beta_1}][A^\gamma, [A^{\alpha_2}, D_\tau A^{\beta_2}]]), \\ B_6 &= \frac{g_{YM}^4}{2} \left(3 \frac{D^{\alpha_1\beta_1\sigma} C^{\bar{\sigma}\gamma_1\tau} C^{\bar{\tau}\gamma_2\lambda} D^{\alpha_2\beta_2\bar{\lambda}}}{j_\lambda(j_\lambda+1) j_\sigma(j_\sigma+1) j_\tau(j_\tau+1)} + \frac{D^{\alpha_1\beta_1\sigma} D^{\gamma_1\lambda\bar{\sigma}} D^{\gamma_2\bar{\lambda}\bar{\tau}} D^{\alpha_2\beta_2\tau}}{j_\sigma(j_\sigma+1) j_\tau(j_\tau+1)} \right) \\ & \qquad \mathrm{tr}([[A^{\alpha_1}, D_\tau A^{\beta_1}], A^{\gamma_1}][[A^{\alpha_2}, D_\tau A^{\beta_2}], A^{\gamma_2}]). \end{aligned} \quad (2.35)$$

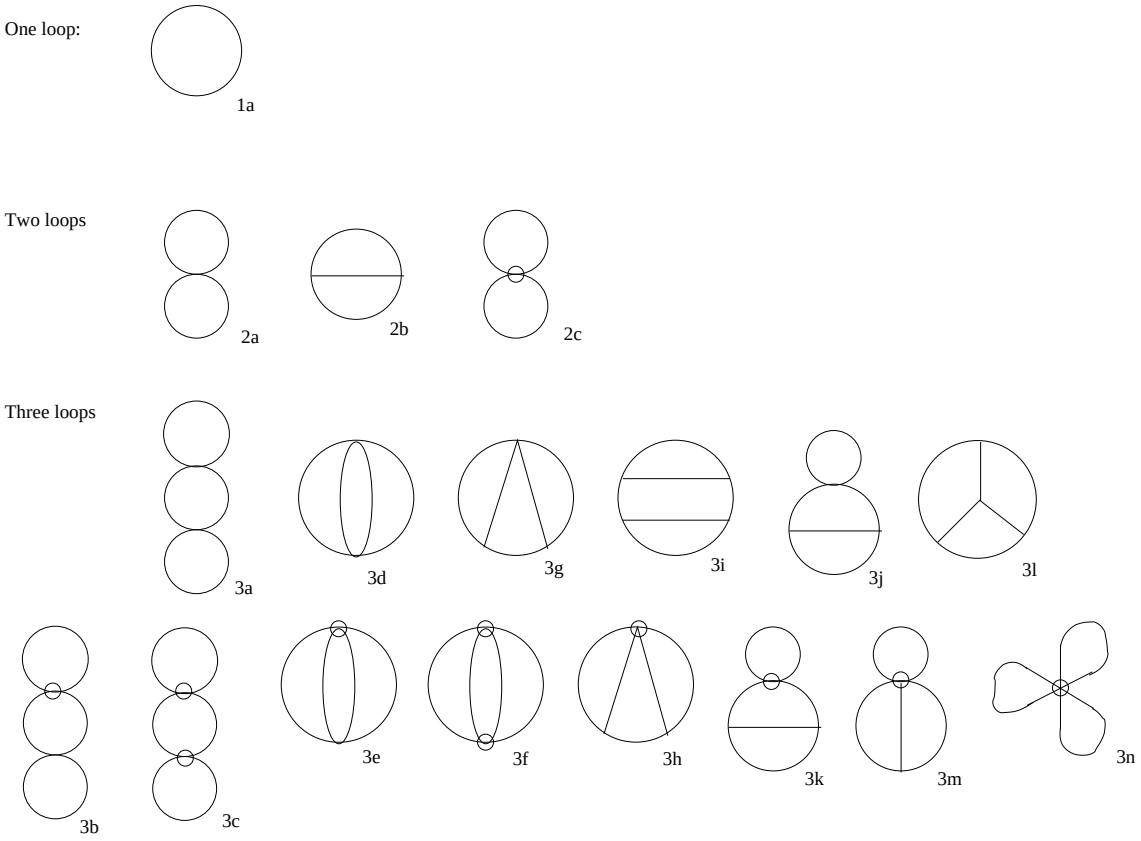

Figure 2.2: The diagrams contributing to the free energy up to 3-loop order. In this figure we present a particular planar form for each diagram, but in some cases the same diagram may also be drawn in the plane in different ways.

The relevant diagrams contributing to the vacuum energy at one, two and three loops are shown in figure 2.2. They are the same as those in 3+1 Yang-Mills theory on S^3. The B type vertices are denoted by circles.

2.3.3 Propagators

The propagators from the quadratic part of the action are

$$\langle \bar{c}^{\bar{\alpha}}_{ab}(t) c^{\beta}_{cd}(t') \rangle = \frac{1}{L_\alpha} \delta^{\alpha\beta} \delta(t-t') \delta_{ad} \delta_{cb}, \tag{2.36}$$

$$\langle a^{\alpha}_{ab}(t) a^{\beta}_{cd}(t') \rangle = \frac{1}{L_\alpha} \delta^{\alpha\bar{\beta}} \delta(t-t') \delta_{ad} \delta_{cb}, \tag{2.37}$$

$$\langle A^{\alpha}_{ab}(t) A^{\beta}_{cd}(t') \rangle = \delta^{\alpha\bar{\beta}} \Delta^{ad,cb}_{j_\alpha}(t-t'), \tag{2.38}$$

$$\langle D_\tau A^{\alpha}_{ab}(t) A^{\beta}_{cd}(t') \rangle = -\langle A^{\alpha}_{ab}(t) D_\tau A^{\beta}_{cd}(t') \rangle = \delta^{\alpha\bar{\beta}} D_\tau \Delta^{ad,cb}_{j_\alpha}(t-t'), \tag{2.39}$$

$$\langle D_\tau A^{\alpha}_{ab}(t) D_\tau A^{\beta}_{cd}(t') \rangle = \delta^{\alpha\bar{\beta}} \delta(t-t') \delta_{ad} \delta_{cb} - \delta^{\alpha\bar{\beta}} L^2_\alpha \Delta^{ad,cb}_{j_\alpha}(t-t'), \tag{2.40}$$

where the (adjoint $\otimes$ adjoint)-valued function $\Delta_{j_a}(t)$ solves

$$(-D_\tau^2 + j_\alpha(j_\alpha+1)) \Delta_{j_\alpha}(t) = \delta_{j_\alpha}(t) \tag{2.41}$$

explicitly on $[0, \beta)$,

$$\Delta^{ad,cb}_{j_a}(t) = \frac{e^{i\alpha t}}{2L_a} \left(\frac{e^{-L_a t}}{1 - e^{i\alpha\beta} e^{-L_a \beta}} - \frac{e^{L_a t}}{1 - e^{i\alpha\beta} e^{L_a \beta}} \right) \tag{2.42}$$

where $L_a = (j_a(j_a+1))^{1/2}$ and α is short for $\alpha^{ad} \otimes 1^{cb} - 1^{ad} \otimes \alpha^{cb}$. The quantity that will appear in computation is $\Delta_{j_a}(t_1 - t_2)$ where t_1 and t_2 range between 0 and β so that the argument of $\Delta_{j_a}(t)$ takes value between $-\beta$ and β. What we will use in computation are the full propagators:

$$\Delta_{j_a}(t) = \Theta(t) \frac{1}{2L_a} \left(\frac{e^{(i\alpha - L_a)t}}{1 - e^{i\alpha\beta} e^{-L_a\beta}} + \frac{e^{(i\alpha + L_a)(t-\beta)}}{1 - e^{-i\alpha\beta} e^{-L_a\beta}} \right) + \Theta(-t) \frac{1}{2L_a} \left(\frac{e^{(i\alpha - L_a)(t+\beta)}}{1 - e^{i\alpha\beta} e^{-L_a\beta}} + \frac{e^{(i\alpha + L_a)t}}{1 - e^{-i\alpha\beta} e^{-L_a\beta}} \right) \tag{2.43}$$

$$D_t \Delta_{j_a}(t) = \Theta(t) \frac{1}{2} \left(-\frac{e^{(i\alpha - L_a)t}}{1 - e^{i\alpha\beta} e^{-L_a\beta}} + \frac{e^{(i\alpha + L_a)(t-\beta)}}{1 - e^{-i\alpha\beta} e^{-L_a\beta}} \right) + \Theta(-t) \frac{1}{2} \left(-\frac{e^{(i\alpha - L_a)(t+\beta)}}{1 - e^{i\alpha\beta} e^{-L_a\beta}} + \frac{e^{(i\alpha + L_a)t}}{1 - e^{-i\alpha\beta} e^{-L_a\beta}} \right) \tag{2.44}$$

2.3.4 Two Loops

In this section, we will compute the coefficients $C_{1,1,-2}$ from the two loop diagrams. The two loop diagrams contributing to the effective potential are shown in figure 2.2. In particular, we will only need to extract the coefficients multiplying $trUtrUtrU^{\dagger 2}+trU^{\dagger}trU^{\dagger}trU^2$ in each diagram. Fortunately, these coefficients turn out to be non-divergent. No regularizations are required for them. The two loop diagrams can be computed to give
2a:

$$F_{2a} = \sum_{m's,j_\gamma} -\frac{\beta g_{YM}^2}{2}(D^{\alpha\beta\gamma}D^{\bar{\alpha}\bar{\beta}\bar{\gamma}} - D^{\alpha\bar{\alpha}\gamma}D^{\beta\bar{\beta}\bar{\gamma}})\triangle_{j_\alpha}(0,\alpha_{ab})\triangle_{j_\beta}(0,\alpha_{bc}) \tag{2.45}$$

2b:

$$F_{2b} = \sum_{m's}\frac{\beta g_{YM}^2}{2}\int dt \triangle_{j_\alpha}^{ab,bc}(t)\triangle_{j_\beta}^{cb,de}(t)\triangle_{j_\gamma}^{ed,ba}(t)(-E^{\alpha\beta\gamma}E^{\bar{\alpha}\bar{\beta}\bar{\gamma}} + 2E^{\alpha\beta\gamma}E^{\bar{\beta}\bar{\alpha}\bar{\gamma}}) \tag{2.46}$$

2c:

$$F_{2c} = \sum_{m's}\beta g_{YM}^2\frac{D^{\alpha\beta\gamma}D^{\bar{\alpha}\bar{\beta}\bar{\gamma}}}{j_\gamma(j_\gamma+1)}(D_t\triangle_{j_\alpha}(0,\alpha_{ab})D_t\triangle_{j_\beta}(0,\alpha_{ac}) + j_\beta(j_\beta+1)\triangle_{j_\alpha}(0,\alpha_{ab})\triangle_{j_\beta}(0,\alpha_{ac})) \tag{2.47}$$

We have used the notation $\triangle_{j_\alpha}(0,\alpha_{ab})$ to signal that the propagator participates in both the a and b index loop in the sense $\alpha^a\otimes 1^b - 1^a\otimes\alpha^b$. We isolate the coefficient of $trUtrUtrU^{\dagger 2}$ in each of the above and get:
2a:

$$\beta g_{YM^2}\sum_{j_\alpha,j_\beta}\frac{(2j_\alpha+1)(2j_\beta+1)}{16\pi^2}\frac{e^{-\beta(L_\alpha+L_\beta)}+e^{-\beta(L_\alpha+2L_\beta)}+e^{-\beta(2L_\alpha+L_\beta)}}{4(j_\alpha(j_\alpha+1)(j_\beta(j_\beta+1))^{1/2}} \tag{2.48}$$

2b:

$$\begin{aligned}
&\beta\frac{g_{YM}^2}{2}\sum_{j_\alpha,j_\beta,j_\gamma}(-\widetilde{A}^2(j_\beta,j_\gamma,j_\alpha) - 2\widetilde{A}(j_\beta,j_\gamma,j_\alpha)\widetilde{A}(j_\alpha,j_\gamma,j_\beta))\frac{1}{8L_\alpha L_\beta L_\gamma}[\frac{1}{L_\alpha+L_\beta+L_\gamma}\\
(\quad & e^{-(L_\beta+2L_\gamma)\beta}+e^{-(L_\alpha+2L_\beta)\beta}+e^{-(L_\gamma+2L_\alpha)\beta}+e^{-(2L_\alpha+L_\beta)\beta}+e^{-(2L_\beta+L_\gamma)\beta}+e^{-(2L_\gamma+L_\alpha)\beta})\\
+\quad & \frac{(e^{-(L_\beta+2L_\gamma)\beta}-e^{-(L_\alpha+L_\gamma)\beta})}{L_\alpha-L_\beta-L_\gamma}+\frac{(e^{-(2L_\alpha+L_\gamma)\beta}-e^{-(L_\alpha+L_\beta)\beta})}{-L_\alpha+L_\beta-L_\gamma}\\
+\quad & \frac{(e^{-(L_\alpha+2L_\beta)\beta}-e^{-(L_\beta+L_\gamma)\beta})}{-L_\alpha-L_\beta+L_\gamma}+\frac{(e^{-(L_\alpha+L_\gamma)\beta}-e^{-(2L_\alpha+L_\beta)\beta})}{L_\alpha+L_\beta-L_\gamma}\\
+\quad & \frac{(e^{-(L_\beta+L_\gamma)\beta}-e^{-(L_\alpha+2L_\gamma)\beta})}{L_\alpha-L_\beta+L_\gamma}+\frac{(e^{-(L_\alpha+L_\beta)\beta}-e^{-(2L_\beta+L_\gamma)\beta})}{-L_\alpha+L_\beta+L_\gamma}]
\end{aligned} \tag{2.49}$$

2c:

$$\beta g_{YM}^2\sum_{j_\alpha,j_\beta,j_\gamma}\quad\frac{R_1(j_\alpha,j_\beta,j_\gamma)}{j_\gamma(j_\gamma+1)}[\frac{1}{4}[(e^{-\beta(L_\alpha+L_\beta)}-e^{-\beta(L_\alpha+2L_\beta)}-e^{-\beta(2L_\alpha+L_\beta)})$$

$$+ \quad (\frac{j_\beta(j_\beta+1)}{j_\alpha(j_\alpha+1)})^{1/2}(e^{-\beta(L_\alpha+L_\beta)}+e^{-\beta(L_\alpha+2L_\beta)}+e^{-\beta(2L_\alpha+L_\beta)})]] \qquad (2.50)$$

To obtain the above expressions, we have used several properties of the scalar and vector spherical harmonics. These properties as well as the definitions of $\widetilde{A}(j_\beta, j_\gamma, j_\alpha)$, $R_1(j_\beta, j_\gamma, j_\alpha)$ are listed in the appendix. We will numerically evaluate the momentum sums. The results are:

Diagram	*Value*
$2a$	0.000609
$2b$	-0.013068
$2c$	0.00346

With these values we obtain:

$$\frac{-\beta_c C_{1,1,-2}(\beta_c)^2}{(\frac{1}{2}-C_{2,-2}(\beta_c))} = -0.000816. \qquad (2.51)$$

2.3.5 Three Loops

To determine the order of the phase transition we will also need the coefficient $C_{1,1,-1,-1}$ from the three loop diagrams. The three loop diagrams contributing to the effective potential are the same as those in 3+1 dimension. We will now list the expressions for the three loop diagrams. We will use the notation

$$\widehat{E}^{abc} \equiv E^{abc} + E^{bca} + E^{cab}, \qquad (2.52)$$

which is totally antisymmetric in its indicies.
We find the following expressions for the diagrams
3a:

$$F_{3a} = -\frac{\beta g_{YM}^4}{2}(D^{\alpha\gamma\lambda}D^{\bar\alpha\delta\bar\lambda}D^{\beta\bar\delta\tau}D^{\bar\beta\bar\gamma\bar\tau} - 2D^{\alpha\bar\alpha\lambda}D^{\gamma\delta\bar\lambda}D^{\beta\bar\gamma\tau}D^{\bar\beta\bar\delta\bar\tau} + D^{\alpha\bar\alpha\lambda}D^{\gamma\delta\bar\lambda}D^{\beta\bar\beta\tau}D^{\bar\gamma\bar\delta\bar\tau}) \int dt\ \Delta_{j_\alpha}(0,\alpha_{ab})\Delta_{j_\gamma}(t,\alpha_{ca})\Delta_{j_\partial}(t,\alpha_{ac})(\Delta_{j_\beta}(0,\alpha_{ad})+\Delta_{j_\beta}(0,\alpha_{dc})), \qquad (2.53)$$

3b:

$$F_{3b} = \beta g_{YM}^4(D^{\alpha\gamma\lambda}D^{\bar\alpha\delta\bar\lambda} - D^{\alpha\bar\alpha\lambda}D^{\gamma\delta\bar\lambda})\frac{D^{\bar\gamma\beta\rho}D^{\bar\delta\bar\beta\bar\rho}}{j_\rho(j_\rho+1)} \Big\{\Delta_{j_\alpha}(0,\alpha_{ab})(D_\tau\Delta_{j_\beta}(0,\alpha_{ad})+D_\tau\Delta_{j_\beta}(0,\alpha_{dc})) \int dt\ (D_\tau\Delta_{j_\gamma}(t,\alpha_{ac})\Delta_{j_\delta}(t,\alpha_{ca}) - \Delta_{j_\gamma}(t,\alpha_{ac})D_\tau\Delta_{j_\delta}(t,\alpha_{ca})) +\Delta_{j_\alpha}(0,\alpha_{ab})(\Delta_{j_\beta}(0,\alpha_{ad})+\Delta_{j_\beta}(0,\alpha_{dc}))$$

$$\int dt\ (j_\beta(j_\beta+1)\Delta_{j_\gamma}(t,\alpha_{ac})\Delta_{j_\delta}(t,\alpha_{ca}) - D_\tau\Delta_{j_\gamma}(t,\alpha_{ac})D_\tau\Delta_{j_\delta}(t,\alpha_{ca}))\Big\}, \tag{2.54}$$

3c:

$$\begin{aligned}
F_{3c} &= -\frac{\beta g_{YM}^4}{2}\frac{D^{\alpha\gamma\lambda}D^{\bar\alpha\delta\bar\lambda}D^{\bar\gamma\beta\rho}D^{\bar\delta\bar\beta\bar\rho}}{j_\lambda(j_\lambda+1)j_\rho(j_\rho+1)} \\
&\int dt(\Delta_{j_\beta}(0,\alpha_{ad})+\Delta_{j_\beta}(0,\alpha_{dc})) \\
&\quad \big\{(j_\alpha(j_\alpha+1)j_\beta(j_\beta+1)+j_\gamma(j_\gamma+1)j_\delta(j_\delta+1))\Delta_{j_\alpha}(0,\alpha_{ab})\Delta_{j_\delta}(t,\alpha_{ac})\Delta_{j_\gamma}(t,\alpha_{ca}) \\
&\quad -j_\beta(j_\beta+1)D_\tau\Delta_{j_\gamma}(t,\alpha_{ca})(4D_\tau\Delta_{j_\alpha}(0,\alpha_{ab})\Delta_{j_\delta}(t,\alpha_{ac})+2\Delta_{j_\alpha}(0,\alpha_{ab})D_\tau\Delta_{j_\delta}(t,\alpha_{ac})) \\
&\quad -2j_\delta(j_\delta+1)\Delta_{j_\alpha}(0,\alpha_{ab})\Delta_{j_\delta}(0,\alpha_{ac})\big\} \\
&+\int dt(D_\tau\Delta_{j_\beta}(0,\alpha_{ad})+D_\tau\Delta_{j_\beta}(0,\alpha_{dc})) \\
&\quad \big\{j_\gamma(j_\gamma+1)\Delta_{j_\gamma}(t,\alpha_{ca})(4D_\tau\Delta_{j_\delta}(t,\alpha_{ac})\Delta_{j_\alpha}(0,\alpha_{ab})+2\Delta_{j_\delta}(t,\alpha_{ac})D_\tau\Delta_{j_\alpha}(0,\alpha_{ab})) \\
&\quad -2D_\tau\Delta_{j_\alpha}(0,\alpha_{ab})D_\tau\Delta_{j_\delta}(t,\alpha_{ac})D_\tau\Delta_{j_\gamma}(t,\alpha_{ca}) \\
&\quad -2(D_\tau\Delta_{j_\alpha}(0,\alpha_{ab})\Delta_{j_\delta}(0,\alpha_{ac})+2\Delta_{j_\alpha}(0,\alpha_{ab})D_\tau\Delta_{j_\delta}(0,\alpha_{ac}))\big\}\,,
\end{aligned} \tag{2.55}$$

3d:

$$\begin{aligned}
F_{3d} &= -\frac{\beta g_{YM}^4}{4}D^{\alpha\gamma\lambda}D^{\beta\delta\bar\lambda}D^{\bar\alpha\bar\gamma\rho}D^{\bar\beta\bar\delta\bar\rho} \\
&\qquad \int dt\Delta_{j_\alpha}(t,\alpha_{ab})\Delta_{j_\beta}(t,\alpha_{bc})(2\Delta_{j_\gamma}(t,\alpha_{cd})\Delta_{j_\delta}(t,\alpha_{da})+\Delta_{j_\delta}(t,\alpha_{cd})\Delta_{j_\gamma}(t,\alpha_{da})) \\
&- \frac{\beta g_{YM}^4}{4}D^{\alpha\beta\lambda}D^{\gamma\delta\bar\lambda}D^{\bar\gamma\bar\beta\rho}D^{\bar\alpha\bar\delta\bar\rho} \\
&\qquad \int dt\Delta_{j_\alpha}(t,\alpha_{ab})\Delta_{j_\beta}(t,\alpha_{bc})(\Delta_{j_\gamma}(t,\alpha_{cd})\Delta_{j_\delta}(t,\alpha_{da})-4\Delta_{j_\delta}(t,\alpha_{cd})\Delta_{j_\gamma}(t,\alpha_{da}))\Big\},
\end{aligned} \tag{2.56}$$

3e:

$$\begin{aligned}
F_{3e} &= \beta g_{YM}^4(2D^{\alpha\delta\lambda}D^{\beta\gamma\bar\lambda}-D^{\alpha\beta\lambda}D^{\gamma\delta\bar\lambda}-D^{\alpha\gamma\lambda}D^{\beta\delta\bar\lambda})\frac{D^{\bar\gamma\bar\delta\rho}D^{\bar\alpha\bar\beta\bar\rho}}{j_\rho(j_\rho+1)} \\
&\qquad \int dt\,\big\{D_\tau\Delta_{j_\alpha}(t,\alpha_{ba})\Delta_{j_\beta}(t,\alpha_{ad})\Delta_{j_\gamma}(t,\alpha_{cb})D_\tau\Delta_{j_\delta}(t,\alpha_{dc})) \\
&\qquad\quad -\Delta_{j_\alpha}(t,\alpha_{ba})D_\tau\Delta_{j_\beta}(t,\alpha_{ad})\Delta_{j_\gamma}(t,\alpha_{cb})D_\tau\Delta_{j_\delta}(t,\alpha_{dc}))\big\}\,,
\end{aligned} \tag{2.57}$$

3f:

$$\begin{aligned}
F_{3f} &= -\frac{\beta g_{YM}^4}{2}\frac{D^{\alpha\gamma\lambda}D^{\beta\delta\bar\lambda}D^{\bar\alpha\bar\gamma\rho}D^{\bar\beta\bar\delta\bar\rho}}{j_\lambda(j_\lambda+1)j_\rho(j_\rho+1)} \\
&\quad \big[4\Delta_{j_\alpha}(0,\alpha_{ab})D_\tau\Delta_{j_\delta}(0,\alpha_{cd})D_\tau\Delta_{j_\beta}(0,\alpha_{da}) \\
&\qquad -2(j_\beta(j_\beta+1)+j_\delta(j_\delta+1))\Delta_{j_\alpha}(0,\alpha_{ab})\Delta_{j_\delta}(0,\alpha_{cd})\Delta_{j_\beta}(0,\alpha_{da}) \\
&\quad +\int dt\,\big\{\Delta_{j_\alpha}(t,\alpha_{ab})\Delta_{j_\gamma}(t,\alpha_{bc})\Delta_{j_\delta}(t,\alpha_{cd})\Delta_{j_\beta}(t,\alpha_{da})
\end{aligned}$$

$$
\begin{aligned}
& j_\gamma(j_\gamma+1)(j_\delta(j_\delta+1)+j_\beta(j_\beta+1)) \\
& +2D_\tau\Delta_{j_\alpha}(t,\alpha_{ab})D_\tau\Delta_{j_\gamma}(t,\alpha_{bc})D_\tau\Delta_{j_\delta}(t,\alpha_{cd})D_\tau\Delta_{j_\beta}(t,\alpha_{da}) \\
& -4j_\gamma(j_\gamma+1)\Delta_{j_\alpha}(t,\alpha_{ab})\Delta_{j_\gamma}(t,\alpha_{bc})D_\tau\Delta_{j_\delta}(t,\alpha_{cd})D_\tau\Delta_{j_\beta}(t,\alpha_{da})\big\}\big] \\
- & \frac{\beta g_{YM}^4}{2}\frac{D^{\alpha\beta\lambda}D^{\gamma\delta\bar{\lambda}}D^{\bar{\alpha}\bar{\gamma}\rho}D^{\bar{\beta}\bar{\delta}\bar{\rho}}}{j_\lambda(j_\lambda+1)j_\rho(j_\rho+1)} \\
& \big[4D_\tau\Delta_{j_\alpha}(0,\alpha_{ab})D_\tau\Delta_{j_\gamma}(0,\alpha_{bc})\Delta_{j_\beta}(0,\alpha_{da}) \\
& -2j_\alpha(j_\alpha+1)\Delta_{j_\alpha}(0,\alpha_{ab})\Delta_{j_\gamma}(0,\alpha_{bc})\Delta_{j_\beta}(0,\alpha_{da}) \\
& -2\Delta_{j_\alpha}(0,\alpha_{ab})D_\tau\Delta_{j_\gamma}(0,\alpha_{bc})D_\tau\Delta_{j_\beta}(0,\alpha_{da}) \\
& +\int dt\,\big\{D_\tau\Delta_{j_\alpha}(t,\alpha_{ab})D_\tau\Delta_{j_\gamma}(t,\alpha_{bc})D_\tau\Delta_{j_\delta}(t,\alpha_{cd})D_\tau\Delta_{j_\beta}(t,\alpha_{da}) \\
& +j_\alpha(j_\alpha+1)j_\delta(j_\delta+1)\Delta_{j_\alpha}(t,\alpha_{ab})\Delta_{j_\gamma}(t,\alpha_{bc})\Delta_{j_\delta}(t,\alpha_{cd})\Delta_{j_\beta}(t,\alpha_{da}) \\
& +2j_\delta(j_\delta+1)\Delta_{j_\alpha}(t,\alpha_{ab})D_\tau\Delta_{j_\gamma}(t,\alpha_{bc})\Delta_{j_\delta}(t,\alpha_{cd})D_\tau\Delta_{j_\beta}(t,\alpha_{da}) \\
& -4(j_\delta+1)^2D_\tau\Delta_{j_\alpha}(t,\alpha_{ab})D_\tau\Delta_{j_\gamma}(t,\alpha_{bc})\Delta_{j_\delta}(t,\alpha_{cd})\Delta_{j_\beta}(t,\alpha_{da})\big\}\big]\,,
\end{aligned}
\tag{2.58}
$$

3g:

$$
\begin{aligned}
F_{3g} &= \beta g_{YM}^4\widehat{E}^{\alpha\delta\rho}\widehat{E}^{\gamma\beta\bar{\rho}}(D^{\bar{\alpha}\bar{\gamma}\lambda}D^{\bar{\beta}\bar{\delta}\bar{\lambda}}-\frac{1}{2}D^{\bar{\alpha}\bar{\beta}\lambda}D^{\bar{\gamma}\bar{\delta}\bar{\lambda}}-\frac{1}{2}D^{\bar{\alpha}\bar{\delta}\lambda}D^{\bar{\beta}\bar{\gamma}\bar{\lambda}}) \\
&\quad \int dtdt'\Delta_{j_\beta}(t',\alpha_{da})\Delta_{j_\gamma}(t',\alpha_{cd})\Delta_{j_\delta}(t,\alpha_{bc})\Delta_{j_\alpha}(t,\alpha_{ab})\Delta_{j_\rho}(t'-t,\alpha_{ac}),
\end{aligned}
\tag{2.59}
$$

3h:

$$
\begin{aligned}
F_{3h} &= \beta g_{YM}^4\frac{1}{j_\lambda(j_\lambda+1)}D^{\alpha\gamma\lambda}D^{\beta\delta\bar{\lambda}}\widehat{E}^{\bar{\alpha}\bar{\gamma}\rho}\widehat{E}^{\bar{\delta}\bar{\beta}\bar{\rho}} \\
&\quad \int dt_1dt_2\; D_\tau\Delta_{j_\alpha}(t_1,\alpha_{ab})\Delta_{j_\gamma}(t_1,\alpha_{bc})\Delta_{j_\rho}(t_1-t_2,\alpha_{ca}) \\
&\quad\quad (\Delta_{j_\delta}(t_2,\alpha_{cd})D_\tau\Delta_{j_\beta}(t_2,\alpha_{da})-D_\tau\Delta_{j_\delta}(t_2,\alpha_{cd})\Delta_{j_\beta}(t_2,\alpha_{da})) \\
&+ \beta g_{YM}^4\frac{1}{j_\lambda(j_\lambda+1)}D^{\alpha\beta\lambda}D^{\gamma\delta\bar{\lambda}}\widehat{E}^{\bar{\alpha}\bar{\gamma}\rho}\widehat{E}^{\bar{\delta}\bar{\beta}\bar{\rho}} \\
&\quad \int dt_1dt_2\; D_\tau\Delta_{j_\alpha}(t_1,\alpha_{ab})\Delta_{j_\beta}(t_2,\alpha_{da})\Delta_{j_\rho}(t_1-t_2,\alpha_{ca}) \\
&\quad\quad (\Delta_{j_\delta}(t_2,\alpha_{cd})D_\tau\Delta_{j_\gamma}(t_1,\alpha_{bc})-D_\tau\Delta_{j_\delta}(t_2,\alpha_{cd})\Delta_{j_\gamma}(t_1,\alpha_{bc})),
\end{aligned}
\tag{2.60}
$$

3i:

$$
\begin{aligned}
F_{3i} &= -\frac{\beta g_{YM}^4}{4}\widehat{E}^{\alpha\beta\rho}\widehat{E}^{\bar{\alpha}\sigma\bar{\beta}}\widehat{E}^{\bar{\sigma}\delta\gamma}\widehat{E}^{\bar{\delta}\bar{\rho}\bar{\gamma}} \\
&\quad \int dt_1dt_2dt_3\Delta_{j_\alpha}(t_1-t_2,\alpha_{ab})\Delta_{j_\beta}(t_1-t_2,\alpha_{bc})\Delta_{j_\gamma}(t_3,\alpha_{cd}) \\
&\quad\quad \Delta_{j_\delta}(t_3,\alpha_{da})\Delta_{j_\rho}(t_1-t_3,\alpha_{ca})\Delta_{j_\sigma}(t_2,\alpha_{ac}),
\end{aligned}
\tag{2.61}
$$

3j:

$$
F_{3j} = \beta g_{YM}^4(D^{\alpha\rho\lambda}D^{\beta\bar{\rho}\bar{\lambda}}-D^{\rho\bar{\rho}\lambda}D^{\alpha\beta\bar{\lambda}})\widehat{E}^{\bar{\alpha}\tau\sigma}\widehat{E}^{\bar{\beta}\bar{\sigma}\bar{\tau}}
$$

$$\int dtdt' \Delta_{j_\rho}(0,\alpha_{ab})\Delta_{j_\beta}(t-t',\alpha_{ac})\Delta_{j_\sigma}(t',\alpha_{ad})\Delta_{j_\alpha}(t,\alpha_{ca})\Delta_{j_\tau}(t',\alpha_{dc}), \quad (2.62)$$

3k:

$$\begin{aligned} F_{3k} &= \beta g_{YM}^4 \frac{1}{j_\lambda(j_\lambda+1)} D^{\alpha\beta\lambda} D^{\bar\alpha\gamma\bar\lambda} \widehat{E}^{\bar\beta\rho\sigma} \widehat{E}^{\bar\gamma\bar\sigma\bar\rho} \\ &\int dt_1 dt_2 \ \Delta_{j_\rho}(t_1-t_2,\alpha_{cd})\Delta_{j_\sigma}(t_1-t_2,\alpha_{da}) \\ &\quad \big\{ 2D_\tau\Delta_{j_\alpha}(0,\alpha_{ab})\Delta_{j_\beta}(t_1,\alpha_{ac})D_\tau\Delta_{j_\gamma}(t_2,\alpha_{ca}) \\ &\quad +\Delta_{j_\alpha}(0,\alpha_{ab})D_\tau\Delta_{j_\beta}(t_1,\alpha_{ac})D_\tau\Delta_{j_\gamma}(t_2,\alpha_{ca}) \\ &\quad -j_\alpha(j_\alpha+1)\Delta_{j_\alpha}(0,\alpha_{ab})\Delta_{j_\beta}(t_1,\alpha_{ac})\Delta_{j_\gamma}(t_2,\alpha_{ca})\big\}, \end{aligned} \quad (2.63)$$

3l:

$$\begin{aligned} F_{3l} &= -\frac{\beta g_{YM}^4}{12} \widehat{E}^{\alpha\beta\tau} \widehat{E}^{\bar\beta\gamma\rho} \widehat{E}^{\bar\gamma\bar\alpha\sigma} \widehat{E}^{\bar\rho\bar\sigma\bar\tau} \\ &\int dt_1 dt_2 dt_3 \Delta_{j_\alpha}(t_2-t_3,\alpha_{ab})\Delta_{j_\beta}(t_3-t_1,\alpha_{ac})\Delta_{j_\gamma}(t_1-t_2,\alpha_{ad}) \\ &\quad \Delta_{j_\rho}(t_1,\alpha_{dc})\Delta_{j_\sigma}(t_2,\alpha_{bd})\Delta_{j_\tau}(t_3,\alpha_{cb}), \end{aligned} \quad (2.64)$$

3m:

$$\begin{aligned} F_{3m} &= 4\beta g_{YM}^4 \frac{D^{\alpha\beta\lambda} C^{\bar\lambda\bar\alpha\rho} D^{\gamma\delta\bar\rho} \widehat{E}^{\bar\beta\bar\gamma\bar\delta}}{j_\lambda(j_\lambda+1)j_\rho(j_\rho+1)} \\ &\int dt (D_\tau\Delta_{j_\alpha}(0,\alpha_{ab})\Delta_{j_\beta}(t,\alpha_{ca}) - \Delta_{j_\alpha}(0,\alpha_{ab})D_\tau\Delta_{j_\beta}(t,\alpha_{ca})) \\ &\quad (\Delta_{j_\gamma}(t,\alpha_{dc})D_\tau\Delta_{j_\delta}(t,\alpha_{ad}) - D_\tau\Delta_{j_\gamma}(t,\alpha_{dc})\Delta_{j_\delta}(t,\alpha_{ad})) \\ &+ 2\beta g_{YM}^4 \frac{D^{\alpha\delta\lambda} C^{\bar\lambda\beta\rho} D^{\gamma\bar\delta\bar\rho} \widehat{E}^{\bar\alpha\bar\gamma\bar\beta}}{j_\lambda(j_\lambda+1)j_\rho(j_\rho+1)} \\ &\int dt \big\{ D_\tau\Delta_{j_\alpha}(t,\alpha_{ab})\Delta_{j_\beta}(t,\alpha_{bd})D_\tau\Delta_{j_\gamma}(t,\alpha_{da})\Delta_{j_\delta}(0,\alpha_{ca}) \\ &\quad +2D_\tau\Delta_{j_\alpha}(t,\alpha_{ab})\Delta_{j_\beta}(t,\alpha_{bd})\Delta_{j_\gamma}(t,\alpha_{da})D_\tau\Delta_{j_\delta}(0,\alpha_{ca}) \\ &\quad -j_\delta(j_\delta+1)\Delta_{j_\alpha}(t,\alpha_{ab})\Delta_{j_\beta}(t,\alpha_{bd})\Delta_{j_\gamma}(t,\alpha_{da})\Delta_{j_\partial}(0,\alpha_{ca})\big\}, \end{aligned} \quad (2.65)$$

3n:

$$\begin{aligned} F_{3n} &= \beta g_{YM}^4 \frac{D^{\alpha\gamma\rho} D^{\beta\bar\gamma\sigma}}{j_\rho(j_\rho+1)j_\sigma(j_\sigma+1)} \left(3\frac{C^{\bar\rho\bar\alpha\lambda} C^{\bar\lambda\bar\beta\bar\sigma}}{j_\lambda(j_\lambda+1)} + 3\frac{C^{\bar\rho\bar\beta\lambda} C^{\bar\lambda\bar\alpha\bar\sigma}}{j_\lambda(j_\lambda+1)} + D^{\bar\alpha\bar\lambda\rho} D^{\bar\beta\lambda\bar\sigma} + D^{\bar\alpha\bar\lambda\bar\sigma} D^{\bar\beta\lambda\bar\rho} \right) \\ &\quad \big\{ D_\tau\Delta_{j_\alpha}(0,\alpha_{cb})\Delta_{j_\gamma}(0,\alpha_{ac})D_\tau\Delta_{j_\beta}(0,\alpha_{ad}) \\ &\quad +2D_\tau\Delta_{j_\alpha}(0,\alpha_{cb})D_\tau\Delta_{j_\gamma}(0,\alpha_{ac})\Delta_{j_\beta}(0,\alpha_{ad}) \\ &\quad -j_\gamma(j_\gamma+1)\Delta_{j_\alpha}(0,\alpha_{cb})\Delta_{j_\gamma}(0,\alpha_{ac})\Delta_{j_\beta}(0,\alpha_{ad})\big\} \\ &- \beta g_{YM}^4 \frac{D^{\alpha\gamma\rho} D^{\beta\bar\gamma\sigma}}{j_\rho(j_\rho+1)j_\sigma(j_\sigma+1)} \left(3\frac{C^{\bar\rho\bar\alpha\lambda} C^{\bar\lambda\bar\beta\bar\sigma}}{j_\lambda(j_\lambda+1)} + D^{\bar\alpha\bar\lambda\rho} D^{\bar\beta\lambda\bar\sigma} \right) \end{aligned}$$

$$\begin{aligned}
&\big\{D_\tau\Delta_{j_\alpha}(0,\alpha_{ab})\Delta_{j_\gamma}(0,\alpha_{ac})D_\tau\Delta_{j_\beta}(0,\alpha_{ad})\\
&\quad+2D_\tau\Delta_{j_\alpha}(0,\alpha_{ab})D_\tau\Delta_{j_\gamma}(0,\alpha_{ac})\Delta_{j_\beta}(0,\alpha_{ad})\\
&\quad+j_\gamma(j_\gamma+1)\Delta_{j_\alpha}(0,\alpha_{ab})\Delta_{j_\gamma}(0,\alpha_{ac})\Delta_{j_\beta}(0,\alpha_{ad})\big\}\\
-\quad&\beta g_{YM}^4\frac{D^{\alpha\gamma\rho}D^{\bar\alpha\bar\gamma\sigma}}{j_\rho(j_\rho+1)j_\sigma(j_\sigma+1)}\left(3\frac{C^{\bar\rho\beta\lambda}C^{\bar\lambda\bar\beta\bar\sigma}}{j_\lambda(j_\lambda+1)}+D^{\lambda\beta\bar\rho}D^{\bar\lambda\bar\beta\bar\sigma}\right)\\
&\big\{2D_\tau\Delta_{j_\alpha}(0,\alpha_{ab})D_\tau\Delta_{j_\gamma}(0,\alpha_{ad})\Delta_{j_\beta}(0,\alpha_{bc})\\
&\quad+(j_\alpha(j_\alpha+1)+j_\gamma(j_\gamma+1))\Delta_{j_\alpha}(0,\alpha_{ab})\Delta_{j_\gamma}(0,\alpha_{ad})\Delta_{j_\beta}(0,\alpha_{bc})\big\}\,. \qquad (2.66)
\end{aligned}$$

Again, we will only need to extract the coefficients multiplying $trUtrUtrU^\dagger trU^\dagger$ in each diagram. These coefficients turn out to be non-divergent as well. No regularizations are required for them. At the three loop level, the Feynman diagrams have very complicated expressions. However, they all have the following strucure:

$$\sum_{j's,m's} G_{j's,m's}I_{j's}(trU,trU^\dagger)). \qquad (2.67)$$

where $G_{j's,m's}$ are the group theory factors coming from the vertices in each diagram. $I_{j's}(trU,trU^\dagger)$ come from the propagators. We will expand $I_{j's}(trU,trU^\dagger)$ in powers of trU, $trU^\dagger$ to extract the coefficients of $trUtrUtrU^\dagger trU^\dagger$. Fortunately, the relevant terms in $I_{j's}(trU,trU^\dagger)$ are very similar to those in 3+1 dimensions, which have been computed [36]. To apply them, we only need to replace the masses of the propagators $(j_\alpha+1)^2_{3+1}\to(j_\alpha(j_\alpha+1))_{2+1}$. With these we can evaluate the angular momentum sums numerically. The results are

Diagram	*Value*	*Diagram*	*Value*
$3a$	-0.000182	$3b$	0.000008
$3c$	0.000432	$3d$	-0.000187
$3e$	-0.0001396	$3f$	0.0001399
$3g$	0.0021095	$3h$	0.00685
$3i$	-0.005715	$3j$	0.00197
$3k$	0.000779	$3l$	-0.00195
$3m$	0.000752	$3n$	0.001682

The total three loop contribution is

$$C_{1,1,-1,-1}=0.001237 \qquad (2.68)$$

We thus obtain the coefficient $b_c=0.00503>0$. Thus, we conclude that the deconfinement transition is second order, followed at a slightly higher temperature by a continuous transition in which the eigenvalue distribution develops a gap.

2.4 High Temperature Limit

In this section, we consider the behavior of the theory at general values of the spatial radius in the limit where the temperature is very large (compared with either the inverse spatial radius or the gauge coupling). In this limit, the Kaluza-Klein modes on the thermal circle become very massive, and the theory is well described by an effective two-dimensional theory on S^2. This theory contains a two-dimensional gauge field together with an adjoint scalar coming from the zero mode of A_0 on the thermal circle. As in the more familiar 3+1 dimensional case, this scalar receives a Debye mass at one loop, corresponding to screening of electric charge. In our case, the mass was calculated in [39] to be

$$m^2 \sim \lambda T \ln\left(\frac{T}{\lambda}\right),$$

where the logarithm arises from a resummation of infrared divergent diagrams[2]. For $T \gg \lambda$, this mass is much larger than the scale $M \sim \sqrt{\lambda_2} = \sqrt{\lambda T}$ associated with the two-dimensional Yang-Mills theory, so the model should be effectively described by pure two-dimensional Yang-Mills theory on S^2 (as long as the sphere radius is larger than m^{-1}). This theory has a third-order phase transition at $R \sim \lambda_2^{-\frac{1}{2}} \gg m^{-1}$ [38], so we conclude that our phase diagram has an additional phase transition line coming from large temperature along the curve

$$TR \sim 1/(\lambda R)\ .$$

An important question is whether this transition remains sharp for large but finite values of the temperature or whether it becomes smoothed out, either for any non-infinite value of the temperature (i.e. any finite A_0 mass) or below some particular temperature. For high temperatures, the question should correspond to asking about the fate of the phase transition in the two-dimensional theory when the mass of an adjoint scalar is reduced from infinity. Unfortunately, even this question seems difficult to approach since the theory is no longer solvable with the adjoint scalar.

The persistence of a sharp phase transition would be guaranteed if there were some order parameter associated with the transition. In the pure two-dimensional Yang-Mills theory on S^2, there is in some sense an order parameter for the phase transition, namely the eigenvalue distribution for a maximal area Wilson loop which divides the sphere into two equal areas.[3] This eigenvalue distribution is gapped for radii less than the critical radius, but ungapped above it [40]. Away from infinite temperature (where the full theory is on $S^2 \times S^1$), it will

[2]Strictly speaking, there are no infrared divergences since we are working on a spatial sphere. Nevertheless, this infinite volume result should be valid as long as the geometrical infrared cutoff scale $1/R$ is smaller than the dynamical infrared cutoff scale m. In this case, we are still required to resum a large number of (finite) diagrams to get the leading contribution to the mass. For smaller radii, the geometrical infrared cutoff dominates and the effective scalar mass will be given by the one-loop contribution.

[3]The precise shape of the loop is unimportant since the theory is invariant under area-preserving diffeomorphisms.

presumably no longer be true that the expectation value of a spatial Wilson loop will depend only on the enclosed area, so the extension of the order parameter to finite temperatures is ambiguous. We could for example choose to focus on the Wilson loop around the equator of the S^2, and it will certainly be true that the full phase diagram will divide into regions for which the eigenvalue distribution for this Wilson loop is gapped or ungapped, but it isn't clear that the boundary of this region should correspond to some non-smooth behavior of the free energy away from the infinite temperature limit.

If the high-temperature phase transition does remain sharp, an intriguing possibility is that it connects on to the third order phase transition line that originates at the critical temperature in the small volume limit (as in figure 2.6b). Indeed, in the limits where we have analytic control, both of these phase transitions are third-order transitions associated with gapping for the eigenvalue distribution of Wilson lines. To investigate whether the two transitions might be the same, one approach would be to study the behavior of the eigenvalue distribution for the Polyakov loop in the vicinity of the high-temperature transition. This distribution should be close to a delta function in this high-temperature regime, but could still be either gapped or ungapped depending on how the eigenvalue distribution falls off away from the peak. A transition between these two possibilities may show up as a change in behavior for the eigenvalue distribution of the massive adjoint scalar in the effective two-dimensional theory, for example from a strictly localized distribution to one with an exponential tail. Unfortunately, we have not been able to determine whether such a transition occurs, so we leave it as a question for future work to determine whether the two third-order transitions are connected.

2.5 Possible Phase Diagrams

We have seen that for small sphere volumes, our gauge theory undergoes a second order deconfinement transition followed by a third order gapping transition as the temperature is increased. We would now like to understand in general the simplest possibilities for what happens to this behavior as the spatial volume is increased.

First, we expect of course that the deconfinement transition extends all the way to large volume, where the transition temperature should be of order λ. The simplest logical possibility is that the qualitative behavior we found is unchanged as we go to large volume. This would mean a second order deconfinement transition at large volume. By the conjecture of Svetitsky and Yaffe [37], the critical behavior should then be the same as a two-dimensional spin model invariant under the same global symmetry, in this case $Z_{N\to\infty} \sim U(1)$. This corresponds to an XY model, for which the transition should be of Kosterlitz-Thouless type.

However, if the expected extrapolation to large N of the lattice results mentioned in the introduction holds, the infinite volume transition should be first order for large N, so the Svetitsky-Yaffe predictions would not apply. In this case, which we will assume for the remainder of the section, there must be a critical sphere radius at which the deconfinement transition changes from second order to first order.

We will now argue that there are two different types of behavior possible at the critical radius. To understand this, consider the effective potential for the eigenvalue distribution evaluated at the deconfinement transition temperature for various values of the radius. Where the transition is second order, the potential at the transition temperature has a global minimum for the uniform eigenvalue distribution, with a vanishing second derivative along some direction. The effective potential develops a negative second derivative along this direction as we go above the transition temperature, and the global minimum smoothly moves away from the uniform eigenvalue distribution. There are two qualitatively different effects that can give rise to a change to first order behavior:

First, the effective potential evaluated at the transition temperature might develop a second global minimum at a point away from the uniform distribution for some value of the radius. In this case, if we move further along the line where the uniform distribution is marginally stable (dotted line in figure 2.3), this new minimum will (generically) become the global minimum, so we must have a first order transition to this new minimum occurring at some lower temperature. Thus, below this critical radius, the deconfinement transition is second order and follows the boundary along which a local instability develops around the uniform distribution. Above the critical radius, the transition is first order and follows the boundary along which we have two global minima. Generically this line of two minima will not terminate at the critical radius but will continue to smaller radii above the deconfinement temperature. Even at these smaller radii, it represents a phase transition, since below the line the minimum near the uniform distribution should be the global minimum, while above the line, the other minimum will be the global minimum. Thus, we have a triple point at the critical temperature and critical radius separating three distinct phases. If the second minimum is at the boundary of configuration space, the higher temperature transition will correspond to a gapping transition, but in this case a first order one, since the eigenvalue distribution jumps discontinuously. The phase diagram in the vicinity of the triple point is sketched in figure 2.3. We now explain the other possible behavior near the critical radius (depicted in figure 2.4). If we follow the curve along which a single marginally stable direction exists (with all other directions stable), it may happen that this direction becomes marginally unstable at some point (e.g. if the fourth derivative of the potential in the marginal direction switches from positive to negative). Such a point is known as a tricritical point. In this case, if we continue along the line where we have a single marginal direction, the global minimum of the potential will shift gradually away from the uniform distribution. The deconfinement transition then no longer coincides with the curve along which the uniform distribution becomes locally unstable, but occurs at some lower temperature where the minimum at the origin (which exists everywhere below the marginal stability line) takes the same value as the new nearby minimum. The deconfinement transition corresponds to a jump from the minimum at the origin (i.e. the uniform distribution) to the nearby minimum. It is therefore first order but with a latent heat which vanishes as we approach the tricritical point, where the two minima in the effective potential merge. Unlike the other scenario, there is no other phase boundary emerging from the point at which the deconfinement transition switches

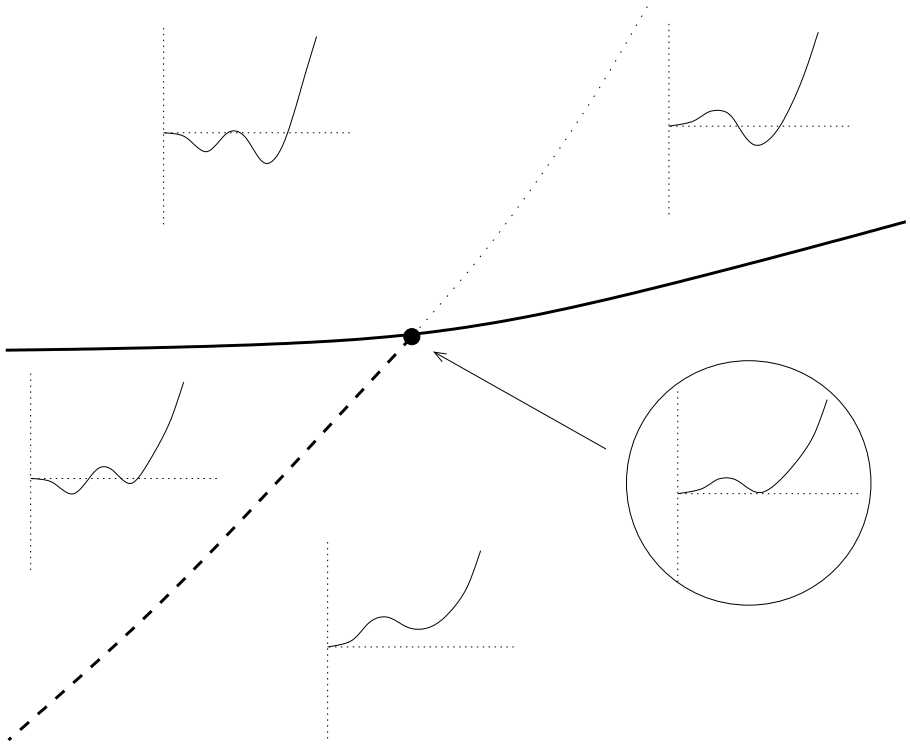

Figure 2.3: Phase diagram in the vicinity of the deconfinement transition when we have a triple point at the critical radius, with sketches of the effective potential in each region. Deconfinement transition switches from second order (dashed line) to first order (solid line). Dotted line is not a phase transition but represents boundary in deconfined phase of region for which local minimum exists at the origin.

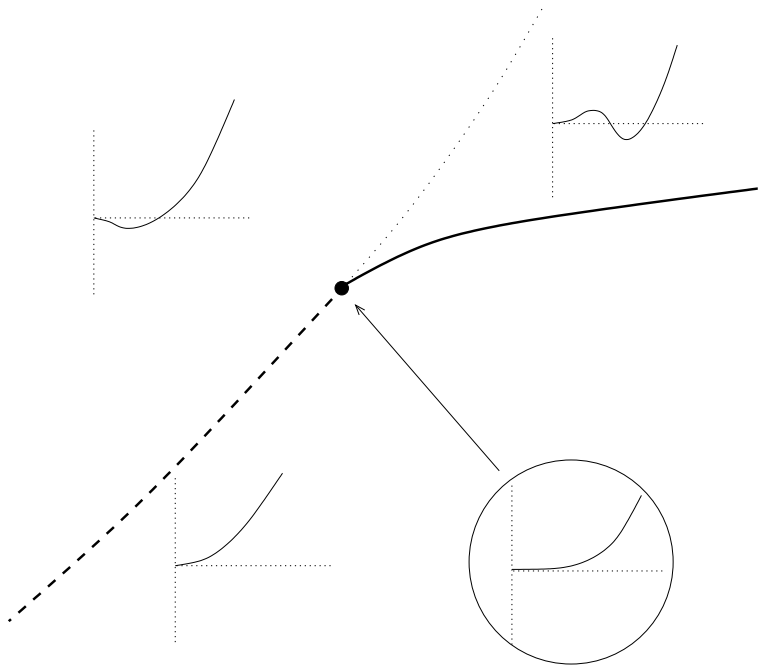

Figure 2.4: Phase diagram near the critical radius in the case when we have a tricritical point, with sketch of the effective potential in each region. Deconfinement transition switches from second order (dashed line) to first order (solid line). Dotted line is not a phase transition but represents boundary in deconfined phase of region for which local minimum exists at the origin.

behavior, since the line along which we have two equivalent minima simply ends at the tricritical point. In the present case, the first order deconfinement transition either to the left or right of the tricritical point is certainly to an ungapped phase. Both of these scenarios are realized in a simple toy model for a complex order parameter w with effective potential

$$S_{eff} = a|w|^2 + b|w|^4 + c|w|^6$$

and a boundary $|w| = 1$ for the configuration space. The phase diagram for this toy model as a function of the parameters a,b is shown in figure 2.5 for the two cases $c < 0$ and $c > 0$. In the first case, the switch from second order to first order behavior for the transition corresponds to a triple point, while in the second case, it corresponds to a tricritical point. Note that in the case $c > 0$, only the details of the potential near $w = 0$ are important, so any higher order terms can be ignored (so long as they do not give rise to a lower minimum). Thus, the behavior of the toy model in the vicinity of the tricritical point should precisely coincide with the behavior of the Yang-Mills theory if we have a tricritical point at the critical radius, since the effective action for u_1 will be of this form, with higher order terms that we can ignore.

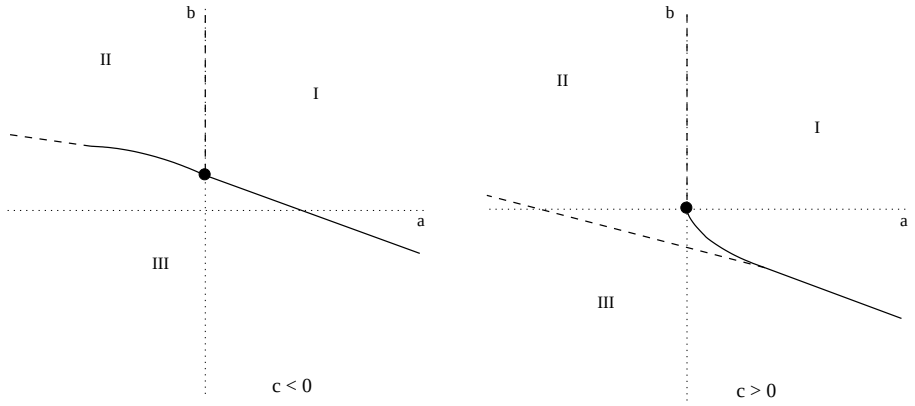

Figure 2.5: Phase diagram for toy model effective potential for $c < 0$ and $c > 0$ exhibiting the triple point and tricritical point behaviors. Phases I, II, and III correspond to having the global minimum at the origin, in the bulk of the configuration space away from the origin, and at the boundary of configuration space respectively. Solid and dashed lines represent first order and second order phase transitions respectively.

We can now comment on the possible forms for the full phase diagram, assuming that the large-volume transition is first order, so that there exists a change of behavior at some critical radius. If the effective potential is such that we have a triple point, the simplest possibility would be that the additional phase boundary coming from the tricritical point corresponds to a gapping transition, so that this phase boundary would connect with the third order gapping transition emerging from the zero-volume critical temperature. This requires there to be some radius at which the gapping transition switches from third order to first order. In this scenario, the full phase diagram would appear as in figure 2.6a. The fate of the high-temperature Douglas-Kazakov transition is unclear, though as we have discussed, it is possible that this phase boundary simply ends at some high temperature.

In the case where the effective potential gives rise to a tricritical point, the gapping phase boundary could either extend up to infinite temperature and be absent in the large volume limit (e.g. in the scenario where it connects with the Douglas-Kazakov transition at high temperatures), extend to large volume such that the first order deconfinement transition there would be followed by a gapping transition at some higher temperature, or end somewhere on the deconfinement phase boundary to the right of the tricritical point (as in the toy model for $c > 0$). These possibilities are shown in figure 2.6 b,c, and d respectively.

Further lattice studies should help distinguish between the possibilities in figure 2.6. In particular, while the distinction between gapped and ungapped eigenvalue distributions strictly exists only in the large N limit, recent studies at relatively large but finite values of N have provided clear suggestions of gapping transitions for eigenvalue distributions of spatial Wilson loops (see, for example [41]). Thus, it should be possible to determine whether the deconfinement transition at large volume is to a gapped or ungapped eigenvalue distribution,

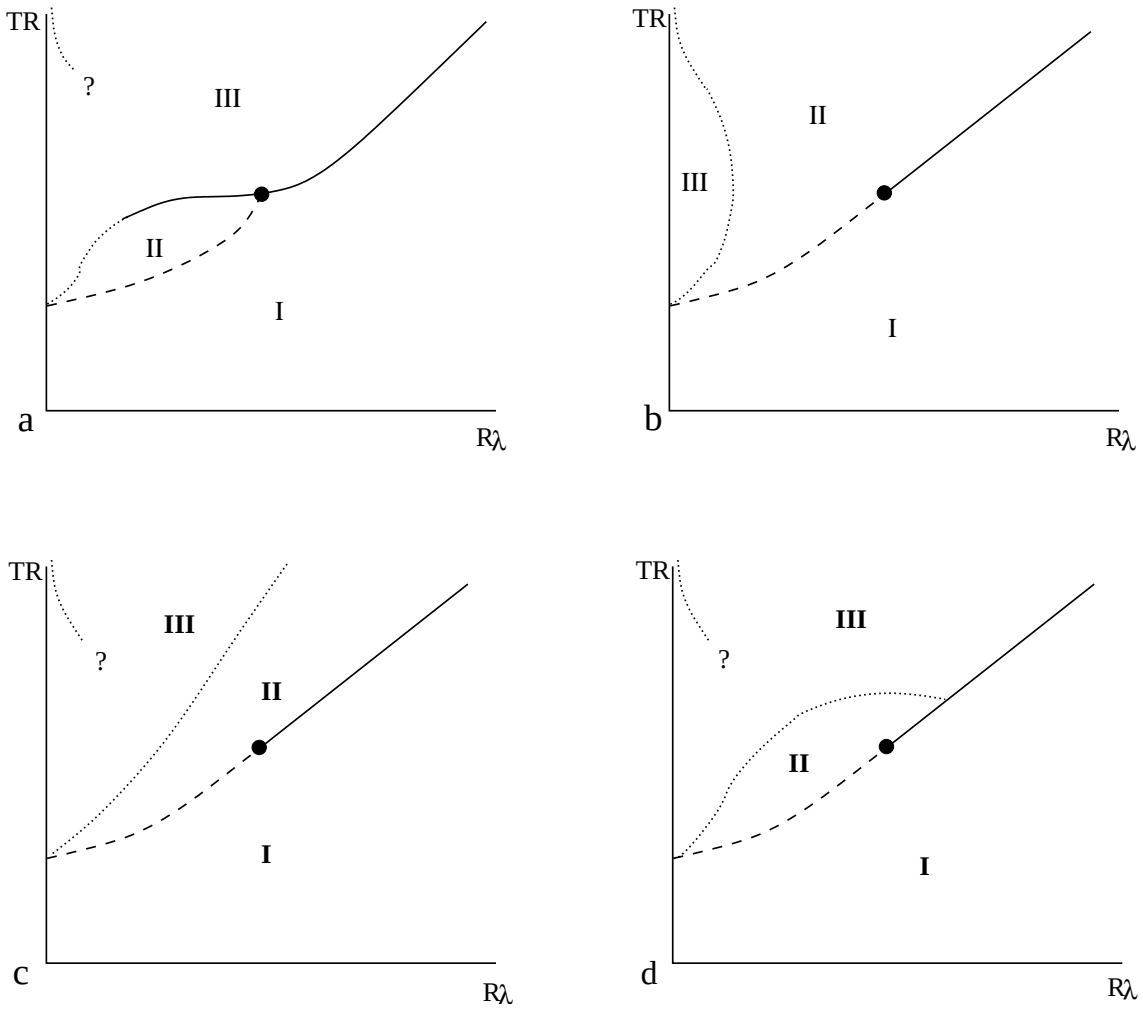

Figure 2.6: Simplest possible phase diagrams for large N pure Yang-Mills theory on S^2 as a function of sphere radius R and temperature T, assuming a first order deconfinement transition at large volume. Solid, dashed, and dotted lines correspond to first, second, and third order transitions respectively.

and in the latter case, whether there is an additional gapping transition at higher temperature (as in figure 2.6c). On the other hand, distinguishing between possibilities a) and d) may be difficult, since they differ only at intermediate values of the radius/coupling.

2.6 Conclusions

The main result of this paper is that pure large N two-dimensional Yang-Mills theory has a second order deconfinement transition at small spatial volume, with a third-order gapping transition at some higher temperature. This is is a qualitatively different behavior from pure Yang-Mills theory in 3+1 dimensions, and provides the first example of a gauge theory with a single-trace Lagrangian in more than two space-time dimensions for which the deconfinement transition is second order at small volume, and which therefore displays three distinct phases.

If the same behavior exists for some large N theory with a controllable gravity dual, it would be fascinating to understand what the new ungapped phase corresponds to on the gravity side. Generally, the deconfined phase of a large N gauge theory corresponds to a black hole geometry.[4] In $\mathcal{N} = 4$ SYM theory at strong coupling, the deconfinement transition corresponds on the gravity side to a first-order transition between the original $AdS^5 \times S^5$ spacetime with a thermal gas of supergravity particles to a large black hole spacetime [3]. On the other hand, in a theory with an intermediate ungapped phase on the field theory side, there should be a stable intermediate type of black-hole phase on the gravity side smoothly connected to both the no black hole phase and the big black hole phase.

[4]The argument [32] is that the non-zero expectation value for the Polyakov loop implies that a string worldsheet whose boundary wraps the thermal circle in the associated Euclidean spacetime can have finite area, and therefore the thermal circle must be contractible. In the Lorentzian picture, this is associated with the existence of a horizon.

Chapter 3

Cold Nuclear Matter In Holographic QCD

3.1 Introduction and Summary

QCD at finite temperature and chemical potential

The phase diagram of QCD as a function of temperature and baryon chemical potential (or alternatively baryon density) displays a rich variety of phases and transitions (for reviews, see [29, 44, 45]). However, apart from the regimes of asymptotically large temperature or chemical potential, where some analytic calculations are possible, and of zero chemical potential, where reliable lattice simulations are possible, our knowledge of the phase diagram is based exclusively on extrapolations and semi-empirical toy models. For intermediate values of the chemical potential, numerical simulation is plagued by a notorious 'sign problem' (see for example [45]), while analytic calculations are not possible due to strong coupling. Thus, while there has been significant progress recently in understanding the qualitative features of the phase diagram, reliable quantitative calculations that would definitively verify the proposed phase structure or determine the locations of various transitions or properties of the various phases seem a formidable challenge at present. A better understanding of the details of the phase diagram at intermediate chemical potential would have valuable applications, for example in understanding the physics of neutron-star interiors.

Holographic models of QCD

With the advent of the gauge theory / gravity duality [47], we have a new tool for studying the properties of certain strongly coupled gauge theories. While the original and most studied examples involve highly supersymmetric conformal gauge theories without fundamental matter, much progress has been made in constructing examples without supersymmetry [3], with confinement [3], with fundamental matter [48] and with chiral symmetry breaking [49]. We now have examples of gauge theories with a known gravity dual that share most of the qualitative features of QCD, and the duality permits analytic calculations that would be otherwise impossible.

It is obviously interesting to study these QCD-like theories in regimes for which neither analytic or numerical studies are currently possible in real QCD. One such regime is the near-equilibrium behavior of the theory at finite temperature . This has received a great

deal of attention recently (see [46] for a review) since calculations in holographic[5] models of QCD-like theories do a better job of explaining and predicting some properties of the quark-gluon plasmas produced in relativistic heavy-ion collisions than any other approach. In the present paper, our focus will be on another such regime as described above, the equilibrium properties at finite baryon chemical potential.

There is already a large literature on studies of gauge theories at finite chemical potential using gravity duals (see [50] and references therein). Many of these consider a chemical potential for R-charge in theories with only adjoint matter. There have been some some studies of the behavior of theories with fundamental matter at finite baryon chemical potential, but the early examples of holographic theories with fundamental matter had both bosonic and fermionic fields carrying baryon charge. In these cases, the physics at finite chemical potential involves Bose condensation rather than the formation of a Fermi surface. In order to get behavior similar to real QCD, it is essential to study a theory with baryon charge carried exclusively by fermionic fields. Such a model was constructed a few years ago by Sakai and Sugimoto [51], and it is this model that we will focus on the present work.

The Sakai-Sugimoto model

The details of the Sakai-Sugimoto model are reviewed in section 2. Briefly, the model gives a holographic construction of a non-supersymmetric $SU(N_c)$ gauge theory with N_f fundamental fermions. The gravity dual involves N_f D8-branes in the near-horizon geometry of N_c D4-branes wrapped on a spatial circle with anti-period boundary conditions for the fermions. In the geometry, the compact direction of the field theory together with the radial direction form a cigar-type geometry, in which the D8-branes are embedded as shown in figure 1. The other directions include an S^4 carrying N_c units of D4-brane flux and the $3+1$ directions of the field theory. In addition to N_f and N_c, the theory has a dimensionless parameter λ, the 't Hooft coupling at the field theory Kaluza-Klein scale.[6]

For small values of λ, the scale Λ_{QCD} where the running coupling becomes large is well below the field theory Kaluza-Klein scale, and the low-energy physics should be precisely that of pure $SU(N)$ Yang-Mills theory coupled to N_f massless (fermionic) quarks.[7] Unfortunately, in this limit, the dual gravity background is highly curved so we are not in a position to study it. For large λ on the other hand, the gravity background is weakly curved, and so via classical calculations on the gravity side of the correspondence, it should be possible to map out the phase diagram of the field theory as a function of temperature and chemical potential and quantitatively determine properties of the various phases.

We do not expect our results to agree quantitatively with real QCD (both because the

[5]Here 'holographic' is a now conventional term referring to the equivalence between a higher-dimensional gravitational theory and a lower-dimensional field theory.

[6]The model has another parameter, corresponding to the asymptotic separation between the D8-branes, but we focus exclusively on the case where the two stacks are on opposite sides of circle and extend down to the tip of the cigar.

[7]For recent work on adding quark masses, see [55, 56].

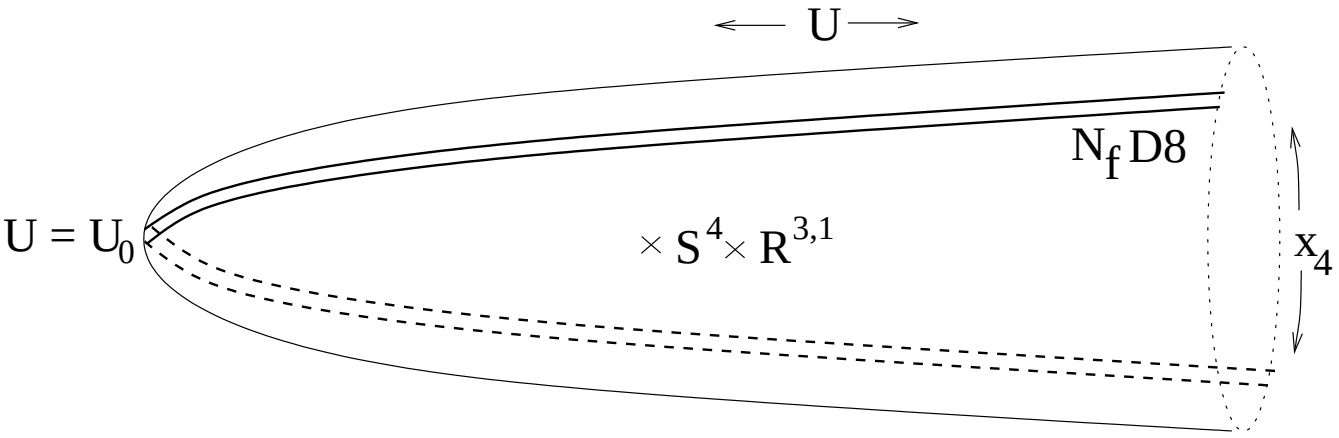

Figure 3.1: Type IIA string theory configuration for the Sakai-Sugimoto model.

Kaluza-Klein scale is not well separated from Λ_{QCD} for large λ and because the classical calculations give only the leading terms in the $1/N$ expansion), but it would certainly be interesting to have a precise understanding of the phase diagram for a theory that is so similar to QCD. Indeed, at least some features of the phase structure and the qualitative behavior of certain transitions are likely to be the same as in QCD, and we might even hope for rough quantitative agreement for quantities that are relatively insensitive to λ and N_c (we will discuss one such quantity below) .

The transition to nuclear matter

Our focus in this work will be on the part of the phase diagram for zero temperature and intermediate values of the baryon chemical potential. In real QCD, as we increase the chemical potential from zero, the equilibrium state (i.e. the ground state) continues to be the vacuum until some critical value of the chemical potential at which point it becomes advantageous for baryons to condense. A first approximation to this critical value is the baryon mass, since it is at this point where it becomes energetically favorable to add single baryons to the vacuum. In fact, the critical value is somewhat lower, since the baryons have a negative binding energy. At the critical value, we have a first order transition from the vacuum state to homogeneous nuclear matter with some minimal baryon density.[8] The best estimate for the critical chemical potential comes by studying the masses of atomic nuclei as a function of nucleon numbers [60]. These are fit very well by the Weizsacker-Bethe semiempirical mass formula, which includes a term proportional to the number of nucleons,

$$m_{vol} = -b_{vol} A$$

to take into account the energy $-b_{vol}$ due to strong interactions of each nucleon in the interior

[8]It is important to note that we are talking only about QCD and ignoring electromagnetism here. With electromagnetic interactions, the binding energy per nucleon is actually greater in iron nuclei than in homogeneous nuclear matter, so the transition to nuclear matter is preceded by a transition to solid iron.

of a nucleus with its neighbors plus the average kinetic energy per nucleon (non-zero due to Fermi-Dirac statistics). The best fit for this energy is

$$b_{vol} = 16 \text{ MeV} . \tag{3.1}$$

Ignoring electromagnetic interactions, this gives the binding energy per nucleon in the limit of large nuclei, and thus should be a good approximation to the value for homogeneous nuclear matter just beyond the transition. Thus, the critical chemical potential for the transition to nuclear matter in QCD should be approximately

$$\mu_c = M_B(1 - \frac{b_{vol}}{M_B}) \approx M_B(1 - 0.017) .$$

As we increase the chemical potential further, the baryon density and the energy per baryon will increase from their values just above the transition. Eventually we hit at least one more transition, to a phase characterized by quark-quark condensates [29].

In this paper, we will study the physics of the transition to nuclear matter in the Sakai-Sugimoto model at large λ. Via classical calculations in the dual gravitational theory, we will be able to determine the critical chemical potential and calculate the baryon density $n_B(\mu)$ and the energy per baryon $e_B(\mu)$ for μ above the transition.

Expectations at large N

Since our gravity calculations will give results corresponding to the large N_c limit of the field theory (with a fixed N_f), we should briefly recall the expectations for how baryons behave for large N_c [58]. In this limit, baryon masses and baryon-baryon interaction energies go as N_c, but the baryon size approaches a constant. Thus, we expect that both the baryon density above the transition and the binding energy per nucleon divided by the baryon mass to have a finite limit for large N_c. These properties indeed follow from our calculations.

One significant difference between the large N_c theory and ordinary QCD is the expected behavior at asymptotically large values of the chemical potential. In both cases, we have attractive interactions between excitations on the Fermi surface that result in an instability, but the nature of the resulting condensates is different. Whereas for $N_c = 3$ the instability is a BCS-type instability, believed to lead to a color superconductor phase, the dominant instability at large N_c is toward the formation of "chiral density waves" [64], inhomogeneous perturbations in the chiral condensate with wave number of order twice the chemical potential. This suggests that the ground state for large N_c QCD at large enough chemical potential is inhomogeneous, however the nature of the true ground state remains mysterious (see [66] for a recent discussion). We believe that our analysis sheds some light on this question, as we will discuss shortly.

Results for the Sakai-Sugimoto model

In the Sakai-Sugimoto model, a chemical potential for baryon number corresponds to a nonzero asymptotic value of the electrostatic potential on the D8-branes, equal on both

asymptotic regions of the D8-brane. Generally, this potential behaves asymptotically (for radial coordinate U to be described below) as

$$A_0 \sim \mu_B + E\frac{c}{U^{3/2}} + \dots \ .$$

The baryon density n_B is proportional to the asymptotic abelian electric flux E, so configurations with non-zero baryon density in the field theory correspond to D8-brane configurations with sources for the electric flux. These sources can be either string endpoints on the D8-branes which originate from D4-branes wrapped on the internal S^4 of the geometry [59] or (for $N_f > 1$) configurations of the Yang-Mills field carrying instanton charge [61, 62]. The latter can be thought of as the wrapped D4-branes dissolved into the D8-branes and expanding into smooth instanton configurations.

One flavor

For any value of chemical potential, we always have a trivial solution for which the electrostatic potential is constant on the D8-branes and the baryon density is zero. However we can also consider translation invariant configurations with a uniform baryon density. In the single flavor case, which we consider first, the bulk description of baryons is in terms of pointlike instantons, since there are no large instanton configurations in the abelian gauge theory of a single D8-brane. In this case, configurations with a uniform baryon density correspond to having some density of these pointlike instantons on the D8-brane. For a given value of the chemical potential greater than the critical value, we find some preferred distribution of charges on the D8-brane. The total baryon density for a given value of μ may be read off from the asymptotic value of the electric flux, and the result increases smoothly from 0 above the critical chemical potential, approaching an asymptotic behavior $n_B \propto \mu^{\frac{5}{2}}$. The charge distribution in the radial direction for a given value of μ represents the distribution of energies in the condensate of baryons in the field theory. In particular, the distribution has a sharp edge at some value of the radial coordinate which increases for increasing chemical potential, and this gives a bulk manifestation of the (quark) Fermi surface in the field theory.

For the single flavor case, the transition to nuclear matter is continuous, unlike QCD, but it may be expected that the single flavor case is different due to the absence of pions which usually play a crucial role in interactions between nucleons.

Two flavors

In the case with $N_f > 1$, we can have nonsingular instantons on the N_f coincident D8-branes, and the minimum energy configurations for large enough μ are should involve smooth configurations of the nonabelian gauge field carrying an instanton density. While we might expect this to be homogeneous in the field theory directions, we argue that there are no allowed configurations of the D8-brane gauge field that are spatially homogeneous in the three field theory directions such that the net energy density and baryon density in the field theory are both finite. Thus, any phase with finite baryon density is necessarily spatially inhomogeneous. This has a simple interpretation: it suggests that at large N_c, the nucleons retain their individual identities for any value of the chemical potential. Assuming that this holds true also for small λ where the theory becomes 2 flavor QCD, this suggests that the chiral density wave instability of the quark Fermi surface in large N_c QCD simply indicates that the quarks want to bind into nucleons even at asymptotically large densities. This is discussed further in section 5.

To avoid the complication of directly studying inhomogeneous configuration, we approximate these by certain singular homogeneous configurations, arguing that our approximation should become exact in the limit of large densities. Within the context of this approximation, we study the behavior of the system as a function of chemical potential.

Our model displays a first order transition to nuclear matter at some critical chemical potential that depends on the parameter λ, with the baryon density behaving as $n_B \propto \mu^3$

for large μ. In the limit of large λ, the critical value approaches the baryon mass, so the binding energy per nucleon is a vanishing fraction of the baryon mass at large λ.[9]

For large but finite λ, we find the behavior

$$\mu_c = M_B^0(1 + \frac{c}{\lambda} + \mathcal{O}\left(\frac{1}{\lambda^{\frac{3}{2}}}\right))$$

where M_B^0 is the large λ result for the baryon mass

$$M_B^0 = \frac{1}{27\pi} M_{KK} \lambda N_c \ .$$

On the other hand, the baryon mass for large but finite λ is [61, 62]

$$M_B = M_B^0(1 + \frac{c'}{\lambda} + \mathcal{O}\left(\frac{1}{\lambda^{\frac{3}{2}}}\right)) \ .$$

It is interesting that the result for the binding energy per nucleon at the threshold for nuclear matter formation,

$$E_{bind} = M_B - \mu_c \approx \frac{N_c}{27\pi} M_{KK}(c' - c) \ ,$$

is actually insensitive to the value of λ for large λ. Since we also know that this binding energy approaches some constant value in the limit of small λ (the large N_c QCD result with two massless flavors), then assuming a smooth behavior at intermediate values of λ, we can treat the large λ result as a prediction for the order of magnitude of the QCD result.[10] Noting that $M_{KK} \approx \Lambda_{QCD}$ for large λ, the value of the binding energy per nucleon extrapolated to $N_c = 3$ becomes

$$E_{bind} = \frac{1}{9\pi} \Lambda_{QCD}(c' - c) \approx 7 \text{ MeV}(c' - c)$$

In order to reliably compute the the numerical coefficients c and c', we require knowledge of the nonabelian analogue of the Born-Infeld action, and (in the case of c') probably corrections to this involving derivatives of field strengths. However, assuming $c' - c$ is of order one,[11] we do obtain the same order of magnitude as the QCD result (3.1). We are not aware of any other methods to reliably estimate this binding energy from first principles, so it is possible that a more complete calculation in the Sakai-Sugimoto model would represent the most reliable analytic prediction of this quantity.

[9] While this statement is derived in the context of our approximation, we argue that it should be true in the full model.

[10] Another example with similar insensitivity to λ for both large and small λ is the free energy of $\mathcal{N} = 4$ SUSY Yang-Mills theory. Here, it is indeed the case that the large λ result for the free energy gives a good prediction of the order of magnitude of the the small λ result (or vice versa).

[11] We must also assume that our approximation scheme at least gets the right power of λ in the correction to μ_c.

Outline

The remainder of the paper is organized as follows. In section 2, we review the Sakai-Sugimoto construction and collect various results necessary for our investigation. In section 3, we review the description of baryons in the Sakai-Sugimoto model and outline the basic approach for studying the theory at finite chemical potential. In section 4, we consider the single flavor case, calculating the baryon density as a function of chemical potential above the transition to nuclear matter. In section 5, we discuss the two flavor case, introduce our approximation, and set up a variational problem that determines the minimal energy configuration with a fixed baryon density (within our approximation). We then study the variational problem numerically for various values of chemical potential and baryon density to determine the critical chemical potential above which the minimum energy configuration has non-zero baryon density.

Related Work

Our work complements and extends various previous studies of the phase diagram for the Sakai-Sugimoto model. The behavior at finite temperature was analyzed in [54]. The behavior of the Sakai-Sugimoto model at finite chemical potential has also been discussed (with a different focus from the present paper) in [69, 70, 72]. Discussions of the finite density behavior in other holographic models of QCD include [50, 53, 73–75]

While this work was in progress, the paper [52] appeared, which has some overlap with the present work, in particular section 4.1.

3.2 The Sakai-Sugimoto Model

The basic setup for the Sakai-Sugimoto model [51] begins with the low-energy decoupling limit of N_c D4-branes wrapped on a circle of length $2\pi R$ with anti-periodic boundary conditions for the fermions [3]. Apart from N_c, this theory has a single dimensionless parameter

$$\lambda = \frac{\lambda_{D4}}{2\pi R} ,$$

the four-dimensional gauge coupling at the Kaluza-Klein scale. Because of the antiperiodic boundary conditions, the adjoint fermions receive masses of order $1/R$ while the scalars get masses of order λ/R due to one-loop effects. The coupling runs as we go to lower energies, becoming strong at a scale

$$\Lambda_{QCD} \sim \frac{1}{R} e^{\frac{-c}{\lambda}}$$

for some numerical constant c. As pointed out by Witten [3], for small λ, the dynamical scale Λ_{QCD} is far below the scale of the fermion and scalar masses and the Kaluza-Klein scale, so the dynamics should be exactly that of pure Yang-Mills theory.

The field theory here is dual to type IIA string theory on the near-horizon geometry of the branes. The Lorentzian metric, dilaton, and four-form field strength are given by

$$\begin{aligned} ds^2 &= \left(\frac{U}{R_4}\right)^{\frac{3}{2}} (\eta_{\mu\nu} dx^\mu dx^\nu + f(U) dx_4^2) + \left(\frac{R_4}{U}\right)^{\frac{3}{2}} (\frac{1}{f(U)} dU^2 + U^2 d\Omega_4^2) \\ e^\phi &= g_s \left(\frac{U}{R_4}\right)^{\frac{3}{4}} \\ F_4 &= \frac{2\pi N_c}{\omega_4} \epsilon_4 \end{aligned}$$

where ω_4 is the volume of a unit 4-sphere, ϵ_4 is the volume form on S^4, and

$$f(U) = 1 - \left(\frac{U_0}{U}\right)^3 .$$

The x_4 direction, corresponding to the Kaluza-Klein direction in the field theory, is taken to be periodic, with coordinate periodicity $2\pi R$, however, it is important to note that this x_4 circle is contractible in the bulk since the x_4 and U directions form a cigar-type geometry.

The parameters R_4 and U_0 appearing in the supergravity solution are related to the string theory parameters by

$$R_4^3 = \pi g_s N_c l_s^3 \qquad\qquad U_0 = \frac{4\pi}{9R^2} g_s N_c l_s^3$$

while the four-dimensional gauge coupling λ is related to the string theory parameters as

$$\lambda = 2\pi \frac{g_s N_c l_s}{R} .$$

In terms of the field theory parameters, the dilaton and string-frame curvature at the tip of the cigar (the IR part of the geometry) are of order $\lambda^{\frac{3}{2}}/N_c$ and $\sqrt{\lambda}$, so as usual, supergravity will be a reliable tool for studying the infrared physics when both λ and N_c are large (in this case, with $N_c >> \lambda^{\frac{3}{2}}$).

Note that this is opposite to the regime of λ where we expect pure Yang-Mills theory at low energies. However, we may still learn about pure Yang-Mills theory by studying this regime, since many qualitative features of the theory remain the same and we might expect further that certain quantitative features may be relatively insensitive to the value of λ (as for example with the free energy in $\mathcal{N} = 4$ SYM theory).

3.2.1 Adding Fundamental Matter

Now that we have defined the adjoint sector of the theory, we would like to add fundamental quarks. We keep the number of quark flavors fixed in the large N_c limit, but this means that the number of degrees of freedom in the fundamental fields (including the gauge field) is smaller than the number of degrees of freedom in the adjoint sector by a factor N_f/N_c.

Thus, for N_f fixed in the large N_c limit, the influence of the fundamental fields on the dynamics of the adjoint fields should be negligible.[12] In other words, what is known as the "quenched approximation" in QCD literature is exact in this limit. This implies that adding the additional matter does not modify the geometry, and indeed the construction of Sakai and Sugimoto (following earlier constructions) involves adding branes to the geometry which are treated in the probe approximation.

The Sakai-Sugimoto construction is motivated by the observation that the light open string modes living at a 3+1 dimensional intersection of D4-branes and D8-branes give rise to chiral fermion fields on the intersection without accompanying bosons. Thus, to the original D4-branes, which we can take to lie in the 01234 directions with the x_4 direction periodic, Sakai and Sugimoto consider adding a stack of N_f D8-branes and a stack of N_f anti-D8 branes separated at fixed locations in the x_4 directions and extended along the remaining directions. This configuration is unstable before taking a near horizon limit[13], nevertheless, one can obtain a stable configuration of the probe branes in the bulk geometry by fixing the asymptotic positions of the D8 and D8-bar stacks in the x_4 direction. The x_4 positions of the branes are free to vary as a function of the radial direction U in the bulk of the geometry, and charge conservation implies that the two stacks necessarily join up in the interior of the geometry. Thus, (in the zero-temperature situation that we are considering) we really have just a single set of D8-branes, bent so that the orientation in the two asymptotic regions is opposite (see figure 1).

The specific embedding of the D8-branes in the bulk depends on the asymptotic separation of the stacks (and also any distribution of matter on the branes), but we will focus exclusively on the case where the two asymptotic parts of the D8-brane stack sit at opposite sides of the D8 circle, in which case each side simply extends to the tip of the cigar along a line of constant x_4 as shown in figure 1. The corresponding field theory has all flavors massless.

3.2.2 D8-brane Action

To understand the physics of the probe D8-branes, we will need the action for the worldvolume D8-brane fields in the background above. We will begin by discussing the action for a single D8-brane before discussing the nonabelian generalization.

The Born-Infeld action for the worldvolume D8-brane fields (in the case of a single brane) is

$$S = -\mu_8 \int d^9\sigma e^{-\phi}\sqrt{-\det(g_{ab} + \widetilde{F}_{ab})}$$

[12]It would be quite reasonable to argue that we should keep N_f/N_c fixed for large N_c to obtain a theory that is most qualitatively similar to QCD, since then the number of degrees of freedom in the adjoint and fundamental sectors of the theory remain of the same order of magnitude for large N. However, this limit is much more difficult to study using supergravity, since then the back-reaction of the matter branes, to be described presently, must be taken into account.

[13]This instability is actually absent in the case we consider the stacks sit at opposite sides of the circle

where

$$\widetilde{F} \equiv 2\pi\alpha' F$$

We also have a Wess-Zumino term

$$S = \mu_8 \int e^{\widetilde{F}} \wedge \sum C \ .$$

Here, only the C_3 term contributes. Noting that F^3 is the derivative of the five-dimensional Chern-Simons form, ω_5 and integrating by parts, we get

$$S = -\mu_8 \int F_4 \wedge \omega_5 \ .$$

After integrating over the sphere, this gives

$$S = \frac{N_c}{24\pi^2} \int \omega_5(A) \tag{3.2}$$

where $d\omega_5 = F \wedge F \wedge F$. For a single D8-brane, $\omega_5 = A \wedge F \wedge F$.

To simplify the Born-Infeld action, we can choose to identify the worldvolume and spacetime coordinates in the sphere and the field theory directions, and parameterize the profile of the brane in the U and x_4 directions by $U(\sigma)$ and $X(\sigma)$ respectively (we will soon focus on the solution where $X(\sigma)$ is constant).

We will be interested only in time-independent configurations homogeneous and isotropic in the spatial directions of the field theory (which we label by indices i, j, k). The most general configurations we will consider will have non-zero $F_{\sigma i}$, F_{ij}, and $F_{0\sigma}$, all functions only of σ.

Integrating the determinant from the sphere directions over the sphere, we get a factor

$$\frac{8}{3}\pi^2 R_4^3 U$$

while the remaining five-dimensional determinant is

$$-\det(g_{\mu\nu} + \widetilde{F}_{\mu\nu}) = -(G_{00} g_{\sigma\sigma} + \widetilde{F}_{0\sigma}^2 + g_{00}\widetilde{F}_{\sigma i}(g+\widetilde{F})^{ij}\widetilde{F}_{\sigma j}) \det(G_{ij} + \widetilde{F}_{ij})$$

with

$$g_{\sigma\sigma} = G_{44}\partial_\sigma X \partial_\sigma X + G_{uu}\partial_\sigma U \partial_\sigma U \ .$$

Note that we are using G_{IJ} here to refer to the spacetime metric and g_{ab} for the worldvolume metric. The final result (in the Abelian case) is

$$\begin{aligned} S_{DBI} \ = \ -\frac{\mu_8}{g_s}\frac{8}{3}\pi^2 R_4^3 \int d^4x d\sigma U \Bigg\{ \left(\left(\frac{U}{R_4}\right)^{\frac{3}{2}} g_{\sigma\sigma} - \widetilde{F}_{0\sigma}^2\right)\left(\left(\frac{U}{R_4}\right)^3 + \frac{1}{2}\widetilde{F}_{ij}^2\right) \\ + \left(\frac{U}{R_4}\right)^3 \widetilde{F}_{\sigma i}^2 + (\frac{1}{2}\epsilon_{ijk}\widetilde{F}_{i\sigma}\widetilde{F}_{jk})^2 \Bigg\}^{\frac{1}{2}} \end{aligned} \tag{3.3}$$

This action is manifestly invariant under reparametrizations of σ. The nonabelian generalization of this action is known only up to F^6 terms. Up to order F^4, we symmetrize all of the nonabelian field strengths in expanding the square root and take an overall trace. However, this symmetrized trace prescription is known to fail beyond order F^4.

3.2.3 Chemical Potential for Baryon Charge

We would like to study the theory at finite chemical potential for baryon charge or alternatively, the theory with a modified Hamiltonian density

$$H = H + \mu B$$

where B is the baryon charge density operator

$$B = B_L + B_R = \psi_L^\dagger \psi_L + \psi_R^\dagger \psi_R \, .$$

This is equivalent to adding a term $-\mu B$ to the action since there are no time derivatives in B. Turning on the operator B in the boundary gauge theory with real coefficient μ should correspond to turning on some (real) non-normalizible mode in the gravity picture. From the original brane setup, we know that the operators B_L and B_R couple to the time-components of the $D8$ and $\bar{\text{D}}8$ brane gauge fields respectively. We will see below that the equations of motion for these fields require them to approach some constant values in the UV part of the geometry. If we describe the probe branes as above with a single gauge field for the whole configuration, then we have two such constant values,

$$A_\infty = A_0(\sigma = \infty)$$

and

$$A_{-\infty} = A_0(\sigma = -\infty)$$

These two values give the chemical potentials for the operators B_L and B_R.[14] Thus, to work at finite chemical potential for baryon number, we require that the value of A_0 in both asymptotic regions of the D8-brane approaches the constant μ_B.

3.2.4 Asymptotic Solutions

In the simple case where the D8-brane is at constant x_4 and we assume that only the electrostatic potential is turned on, the Born-Infeld action above reduces to

$$S_{DBI} = -\frac{\mu_8}{g_s}\frac{8}{3}\pi^2 R_4^{\frac{3}{2}} \int d\sigma d^4x U^{\frac{5}{2}} \left[\frac{1}{f(U)}\partial_\sigma U \partial_\sigma U - \partial_\sigma \widetilde{A} \partial_\sigma \widetilde{A}\right]^{\frac{1}{2}} \tag{3.4}$$

The reparametrization invariance allows us to chose $U(\sigma)$ to be whatever we like. For a given choice of U, the equation of motion for A away from any sources (which we assume are localized in the infrared part of the geometry) is

$$\partial_\sigma \left(\frac{\mu_8}{g_s}\frac{8}{3}\pi^2 R_4^{\frac{3}{2}} U^{\frac{5}{2}} \left[\frac{1}{f(U)}\partial_\sigma U \partial_\sigma U - \partial_\sigma \widetilde{A} \partial_\sigma \widetilde{A}\right]^{-\frac{1}{2}} \partial_\sigma \widetilde{A} \right) = 0 \tag{3.5}$$

[14] We give an argument in appendix A to establish that B_L and B_R are turned on with the same sign if A_∞ and $A_{-\infty}$ have the same sign.

The quantity in round brackets is analogous to the conserved electric flux. Integrating and rearranging, and choosing $\sigma = U$ (valid for either half of the brane), we get

$$\partial_u \widetilde{A} = \frac{E}{\sqrt{f(U)(U^5 + E^2)}} \ , \tag{3.6}$$

where E is an integration constant proportional to the conserved flux. Solving this, we find

$$\begin{aligned} \widetilde{A} &= \widetilde{A}_\infty - \int_U^\infty du \frac{E}{\sqrt{F(u)(u^5 + E^2)}} \\ &= \widetilde{A}_\infty + \frac{2}{3}\frac{E}{U^{\frac{3}{2}}} + \dots \end{aligned}$$

valid in the region outside the sources. The constant E is the normalizible mode of A_0 in the asymptotic solution, so the values of E for the two sides of the brane correspond to the expectation values for B_L and B_R in the field theory.

In general, the sum of the Es for the two halves of the brane (times $\frac{\mu_8}{g_s}\frac{8}{3}\pi^2 R_4^{\frac{3}{2}}(2\pi\alpha')$) is equal to the total charge density on the brane,

$$\frac{\mu_8}{g_s}\frac{8}{3}\pi^2 R_4^{\frac{3}{2}}(2\pi\alpha')(E_2 + E_1) = q$$

If we fix $A_\infty = A_{-\infty}$ as we have argued corresponds to a chemical potential for baryon number, and we assume that the sources are symmetric under a reflection in the σ direction, then for continuous A_0 we must have $E_1 = E_2$, and

$$\frac{\mu_8}{g_s}\frac{8}{3}\pi^2 R_4^{\frac{3}{2}}(2\pi\alpha')E = q/2 \tag{3.7}$$

Since the charge density in the bulk (divided by N_c) corresponds to the baryon density in the field theory, we obtain

$$n_B = \frac{\mu_8}{g_s N_c}\frac{16}{3}\pi^2 R_4^{\frac{3}{2}}(2\pi\alpha')E \tag{3.8}$$

3.3 Baryons

We have seen that configurations with non-zero baryon charge density (as measured by the asymptotic electric flux E) require sources for A_0 on the D8-branes. The basic source for A_0 is the endpoint of a fundamental string. In order to have some net charge, we need the number of string endpoints of one orientation to be unequal to the number of string endpoints of the other orientation. So we need a source for fundamental strings in the bulk. In our background, such a source is provided by D4-branes wrapped on S^4 [59]. These necessarily have N_c string endpoints, since the background D4-brane flux gives rise to N_c units of charge on the spherical D4-branes, so we need N_c units of the opposite charge (coming from the

string endpoints) to satisfy the Gauss law constraint. Thus, we can get a density of charge on the D8-brane by having a density of D4-branes wrapped on S^4 in the bulk, with N_c strings stretching between each D4-brane and the D8-brane.

In the case where we have $N_f > 1$ D8-branes, there is another possible picture of the configurations with baryons [61, 62]. To see this, note that a D4-brane / D8-brane system with four common worldvolume directions is T-dual to a D0-D4 system. In that case, it is well known that the D0-branes can "dissolve" in the D4-branes, where they show up as instanton configurations of the spatial non-abelian gauge field. Similarly, our baryon branes can dissolve in the D8-branes (if we have $N_f > 1$) and show up as instantons. Indeed, the Chern-Simons term (3.2) gives rise to a coupling

$$S = \frac{N_c}{8\pi^2} \int A_0 \mathrm{tr}(F \wedge F) \tag{3.9}$$

between the instanton charge density and the abelian part of the gauge field, showing that instantons act as a source for the electrostatic potential on the branes.

The question of which of these two pictures is more appropriate is a dynamical one, but it turns out that the dissolved instantons give rise to a lower energy configuration since the electrostatic forces prefer the instanton density to be delocalized [61, 62].

3.3.1 Baryon Mass

The baryon mass was estimated originally by Sakai and Sugimoto [51] as the energy of a D4-brane wrapped on S^4 and located at the tip of the cigar. Since we will also need to know the potential energy for such branes, we briefly recall the calculation. Starting with the Born-Infeld action for a D4-brane wrapping S^4,

$$S = -\mu_4 \int d^5\xi e^{-\phi} \sqrt{-\det(g_{ab})}$$

and integrating over the sphere, we get

$$S_{D4} = -\frac{\mu_4}{g_s} \frac{8}{3} \pi^2 R_4^3 \int dt U(t) \tag{3.10}$$

as the velocity independent term in the action (the negative of the potential energy). The minimum energy occurs for $U = U_0$, and this gives the baryon mass

$$M_B^0 = \frac{\mu_4}{g_s} \frac{8}{3} \pi^2 R_4^3 U_0 = \frac{1}{27\pi} \frac{1}{R} \lambda N_c$$

This agrees with the Yang-Mills action for a pointlike instanton configuration on the D8-brane [61]. Both of these calculations ignore the energy from the electric flux sourced either by the string endpoints coming from the wrapped D4-brane or by the instanton density. To

take this into account, the authors of [61] and [62] considered more general smooth instanton configurations with varying scale factor, inserting these into the Yang-Mills approximation to the D8-brane action. They found that the optimal size for the instanton behaves as $\lambda^{-\frac{1}{2}}$, and that the baryon mass is

$$M_B = M_B^0(1 + \frac{c'}{\lambda})$$

This method ignores the effects of the non-trivial geometry on the Yang-Mills configuration and also does not include effects from the α' corrections to the D8-brane effective action, which should be important, since for large λ, the instanton is small so that derivatives of the Yang-Mills field strength are large. Thus, as the authors point out, the numerical coefficient c' should probably not be trusted. On the other hand, an analysis of the effects of Born-Infeld corrections [61] indicates that at least the power of λ in the correction to the mass and in the instanton size should be reliable.

3.3.2 Critical Chemical Potential

We have seen that turning on a chemical potential in the gauge theory corresponds to including boundary conditions $A_0 = \mu$ for the two asymptotic regions of the D8-brane. For any μ, one solution consistent with these boundary conditions is to have constant A_0 everywhere on the brane. This represents the vacuum configuration in the field theory. However, beyond a certain critical chemical potential, this solution is unstable to the condensation of baryons.

The critical value of the chemical potential should not be larger than the baryon mass. At this value, a zero-momentum baryon has effectively negative energy in the modified hamiltonian, so it is advantageous to add baryons to the vacuum. If there were no interactions between the baryons, the critical chemical potential would be exactly the baryon mass. Note that even in the absence of interactions, the baryon density above the transition is limited by the Fermi statistics for the baryons for odd N or in any case by the Fermi statistics of the quarks. The condensate will have occupied all states whose Fermi energy is less than the chemical potential. In this case, the baryon density will rise smoothly from zero above the critical chemical potential and the transition will be second order.

With short range repulsive interactions, the story would be qualitatively similar, with a slower growth in the baryon density as the chemical potential is increased. In QCD, however, we have attractive interactions, and this lowers the critical chemical potential below the baryon mass. With the repulsive interactions, there is a specific nonzero value of the baryon density for which the energy per baryon is lowest, and when the chemical potential is increased to this value the baryon density jumps from zero to this density.

In the next sections, we will study this transition to nuclear matter in the Sakai-Sugimoto model for one flavor (section 4) and two flavors (section 5). In the first case, it appears that the transition is second order, unlike QCD, while in the multi-flavor case, we find some evidence for a more realistic first-order transition.

3.4 One Flavor Physics

In this section, we study the physics of the Sakai-Sugimoto model at finite chemical potential in the simpler case of a single quark flavor. Here, we have only a single D8-brane in the bulk, and we can use the abelian Born-Infeld action for our analysis. Since the abelian gauge theory does not support large instantons, the wrapped D4-branes cannot dissolve into the D8-branes, so the baryons are pointlike charges on the D8-brane that source the electrostatic potential. For chemical potential larger than the baryon mass, it is favorable for some of these baryons to condense, and we would now like to determine the baryon density as a function of chemical potential for μ above the critical value.

3.4.1 Localized Source Approximation

As a first approximation, we make the simplifying assumption that all the pointlike instantons sit at $U = U_0$. More realistically, the charge should spread out dynamically, via electrostatic repulsion; we will include this effect in section 4.2.

In our simple approximation, the relevant action is the Abelian Born-Infeld action (3.4), together with the action taking into account the baryon masses and their interaction with the electromagnetic field on the brane.

$$\begin{aligned} S &= -\frac{\mu_8}{g_s}\frac{8}{3}\pi^2 R_4^{\frac{3}{2}} \int dU d^4x U^{\frac{5}{2}} \left[\frac{1}{f(U)} - \partial_\sigma \widetilde{A}\partial_\sigma \widetilde{A}\right]^{\frac{1}{2}} \\ &\quad + \frac{n_B N_c}{2\pi\alpha'}\widetilde{A}(U_0) - n_B M_B^0 \end{aligned}$$

where the terms in the last line are the potential terms taking into account the energy from the charges in the electrostatic potential and the masses of the pointlike instantons.

To obtain the energy, we perform a Legendre transform, but it is convenient first to rewrite the first term in the second line as

$$\frac{n_B N_c}{2\pi\alpha'}\widetilde{A}(U_0) = \frac{n_B N_c}{2\pi\alpha'}\widetilde{A}_\infty - \int dU \frac{n_B N_c}{2\pi\alpha'}\widetilde{A}'(U)$$

since we will be holding $A(\infty) = \mu$ fixed. Performing the Legendre transform (which amounts to taking the negative of the action, since we are only looking at static configurations), and rewriting everything in terms of the electric flux (3.6), we find

$$\begin{aligned} \mathcal{E}_{flux} &= 2 \cdot \frac{\mu_8}{g_s}\frac{8}{3}\pi^2 R_4^{\frac{3}{2}} \int_{U_0}^{\infty} dU \frac{U^{\frac{5}{2}}}{\sqrt{f}}\left(\sqrt{1 + \frac{E^2}{U^5}} - 1\right) - (\mu - \mu_c)n_B \\ &= \frac{\mu_8}{g_s}\frac{16}{3}\pi^2 R_4^{\frac{3}{2}} U_0^{\frac{7}{2}} h(e) - (\mu - \mu_c)n_B \end{aligned}$$

where we have defined $e = E/U_0^{\frac{5}{2}}$ and

$$h(e) = \int_1^{\infty} dx (\sqrt{x^5 + e^2} - x^{\frac{5}{2}}) \frac{1}{\sqrt{1 - 1/x^3}} \, .$$

In the first term, we have included a factor of 2 to take into account the energy f rom both halves of the D8-brane.

For $\mu > \mu_c$, the combined energy from the string endpoints (or Chern-Simons action) and the D4-brane mass (or Born-Infeld energy of the instantons) is negative and should be proportional to n_B, while the energy from the flux is a positive function of n_B which behaves as n_B^2 for small n_B and $n_B^{\frac{7}{5}}$ for large n_B. Thus, there will be some positive value of n_B where the total energy is minimized.

Defining

$$\widetilde{\mu} = \frac{6\pi\alpha'\mu}{U_0} ,$$

so that $\widetilde{\mu} = 1$ corresponds to $\mu = M_B$, and using the relation (3.7) between n_B and E, the total energy may be written as

$$\mathcal{E} = \frac{\mu_8}{g_s}\frac{16}{3}\pi^2 R_4^{\frac{3}{2}} U_0^{\frac{7}{2}} \left(h(e) - \frac{1}{3}(\widetilde{\mu} - 1)e \right) ; .$$

From this, we find that the energy is minimized when

$$\frac{1}{3}(\widetilde{\mu} - 1) = h'(e) .$$

This can be inverted to determine the relationship between n_B (proportional to e) and μ above the transition. For small $\mu - \mu_c$, we find

$$e \sim \frac{1}{\pi}(\widetilde{\mu} - 1)$$

so

$$n_B \propto \mu - \mu_c \qquad \text{small } \mu - \mu_c .$$

For large μ we have

$$e \sim 0.021\widetilde{\mu}^{\frac{5}{2}}$$

so

$$n_B \propto \mu^{\frac{5}{2}} \qquad \text{large } \mu - \mu_c$$

3.4.2 Dynamical Charge Distribution

The analysis of the previous section assumed that all charges were localized at $U = U_0$. Presumably, the charges would prefer to spread out dynamically. To take this into account, we can define a charge distribution $\rho_B(U)$ which we would like to determine. For a given ρ, the action is given in terms of a Lagrangian density

$$\mathcal{L} = -CU^{\frac{5}{2}} \left(\frac{1}{f(U)} - \partial_\sigma \widetilde{A} \partial_\sigma \widetilde{A} \right)^{\frac{1}{2}} + \frac{N_c}{2\pi\alpha'} \widetilde{A} \rho_B - \frac{N_c}{6\pi\alpha'} U \rho_B .$$

where

$$C = \frac{\mu_8}{g_s}\frac{8}{3}\pi^2 R_4^{\frac{3}{2}} .$$

Here, the second term is the action arising from the string endpoints, while the third term takes into account the potential energy from the baryon masses (recalling that the action for a wrapped D4-brane at location U is proportional to U).

For a given ρ_B, the electric flux is determined by solving the equation of motion for $\widetilde{A}$,

$$(2\pi\alpha')\partial_U\left(\frac{\mu_8}{g_s}\frac{8}{3}\pi^2 R_4^{\frac{3}{2}}U^{\frac{5}{2}}\left[\frac{1}{f(U)}-\partial_U\widetilde{A}\partial_U\widetilde{A}\right]^{-\frac{1}{2}}\partial_U\widetilde{A}\right) = \rho_B(U)N_c \tag{3.11}$$

This gives

$$\rho_B(U) = \frac{C(2\pi\alpha')}{N_c}\partial_U E$$

where we have defined an electric flux

$$E(U) = U^{\frac{5}{2}}(\frac{1}{f(U)} - (\partial_U\widetilde{A})^2)^{-\frac{1}{2}}\partial_U\widetilde{A} .$$

We can now reexpress all terms in the action in terms of E and Legendre transform (which again amounts to switching the sign) to find the energy. We obtain

$$\frac{\mathcal{E}}{2C} = \int_{U_0}^{\infty} dU\left[\frac{1}{\sqrt{f}}(\sqrt{U^5+E^2}-U^{\frac{5}{2}})+\frac{1}{3}U\partial_U E\right] - \widetilde{A}_\infty E_\infty$$

where we have included an extra factor of 2 in the denominator on the left side since we are integrating over only half the brane on the right side. To maximize this, we can first minimize over all $E(U)$ such that $E(U_0)=0$, $E(U\to\infty)=E_\infty$, and $\partial_U E>0$ to determine $\mathcal{E}(E_\infty,\mu)$. Then we can minimize over E_∞.

Varying the energy functional with respect to E, we find that the energy functional is locally stationary if and only if

$$\frac{E}{(U^5+E^2)^{\frac{1}{2}}} = \frac{\sqrt{f(U)}}{3} \tag{3.12}$$

This satisfies $E=0$ for $U=U_0$ as desired but approaches arbitrarily large values for large U. On the other hand, our constraints $\partial_U E>0$ and $E(U\to\infty)\to E_\infty$ imply that E can never exceed E_∞. It is straightforward to check that the local contribution to the energy from a point U is a function of E that decreases from $E=0$ to the optimal value (3.12) and then increases again, so when the value (3.12) exceeds E_∞, the best we can do to minimize the energy is to set $E=E_\infty$. We conclude that the minimum energy configuration for fixed μ and fixed E_∞ is

$$\begin{array}{ll} E = \frac{U^{\frac{5}{2}}}{\sqrt{\frac{9}{f}-1}} & U < U_{max} \\ E = E_\infty & U \geq U_{max} \end{array} \tag{3.13}$$

Here U_{max} represents the extent of the charge distribution in the radial direction, and is related to E_∞ as

$$\frac{E_\infty}{(U_{max}^5 + E_\infty^2)^{\frac{1}{2}}} = \frac{\sqrt{f(U_{max})}}{3} \tag{3.14}$$

We can now write the energy as a function of E_∞, or more conveniently, U_∞ as follows. We define a function $g(x)$ by

$$g(x) = \frac{x^{\frac{5}{2}}}{\sqrt{\frac{9}{\widetilde{f}(x)} - 1}}$$

where

$$\widetilde{f}(x) = 1 - \frac{1}{x^3} \ ,$$

and define

$$H(x,g) = \frac{1}{\sqrt{f(x)}}(\sqrt{x^5 + g^2} - x^{\frac{5}{2}}) \ .$$

Then in terms of $u = U_{max}/U_0$ and , the energy is given by

$$\mathcal{E} = 2CU_0^{\frac{7}{2}} \left\{ \int_1^u dx H(x, g(x)) + \int_u^\infty H(x, g(u)) - \frac{1}{3}\int_1^u g(x)dx + \frac{1}{3}ug(u) - \frac{1}{3}\widetilde{\mu}g(u) \right\}$$

where as in the previous section, we define

$$\widetilde{\mu} = \frac{(6\pi\alpha')\mu}{U_0} \ .$$

We can now minimize this as a function of u. The result is

$$\widetilde{\mu} = u + 3\int_u^\infty dx \partial_g H(x, g(u))$$

To compare with the results of the previous section, we note that (using (3.14)) the dimensionless variable e proportional to the baryon mass is related to u by

$$\frac{e}{(u^5 + e^2)^{\frac{1}{2}}} = \frac{\sqrt{\widetilde{f}(u)}}{3} \ .$$

From these, we find that for small $u - 1$,

$$\widetilde{\mu} - 1 = c_1(u-1)^{\frac{1}{2}} \qquad c_1 \approx 1.814 \qquad \text{small } u - 1$$

or

$$e \sim \frac{1}{\pi}(\widetilde{\mu} - 1)$$

where we have used (3.14). Thus, for small e we obtain the same result as in the previous approximation, with

$$n_B \propto (\mu - \mu_c)$$

for small $\mu - \mu_c$, where the critical value of μ is as before. For large μ, we find

$$\widetilde{\mu} \to c_2 u \qquad c_2 \approx 1.697 \qquad \text{large } u$$

or

$$e \sim 0.0942 \widetilde{\mu}^{\frac{5}{2}} \ .$$

Again, we find that

$$n_B \propto \mu^{\frac{5}{2}} \ .$$

Thus, the qualitative behavior of $n_B(\mu)$ is the same as in the simplified model of the previous section, though the numerical coefficients come out different. We also found the behavior of the energy density:

$$\mathcal{E} \propto (\mu - \mu_c)^4$$

for $(\mu - \mu_c)$ small, and

$$\mathcal{E} \propto \mu^{7/2}$$

when μ is large.

It is interesting that (in this approximation) the charge distribution has a sharp edge at $U = U_{max}$ which progresses further and further towards the UV in the radial directions as the chemical potential is increased. In the field theory picture, the radial direction represents an energy scale, so the charge distribution we find in the bulk should be related to the spectrum of energies for the condensed baryons. The edge of the distribution is then a bulk manifestation of the Fermi surface.

Since our large N_c calculation does not distinguish between even and odd values of N_c, it is insensitive to whether or not the baryons are fermions or bosons. Thus, the Fermi surface that we see should probably be thought of as the quark Fermi surface. It is interesting that the fermionic nature of the quarks in the field theory arises in the bulk from the classical electrostatic repulsion between the instantons.

3.5 Two Massless Flavors

For $N_f = 2$, the authors of [61, 62] argued that single instantons on the D-brane prefer to grow to some finite size on the baryon in order to balance the electrostatic forces which tend to make the instanton spread out with the gravitational forces which prefer the instanton to be localized as much as possible near the IR tip of the D8-branes. From these considerations, we also expect that the minimum energy configurations with nonzero baryon density will involve some smooth configuration of the nonabelian gauge field on the D8-brane locally carrying an instanton density $\mathrm{tr}(F \wedge F)$. In this section, we consider such configurations.

The absence of homogeneous configurations

We first consider static, spatially homogeneous configurations, such that A_μ is translation invariant in the 3+1 directions of the field theory and rotationally invariant (up to a gauge transformation) in the three spatial directions (which we denote by an index i). The general configuration of the spatial gauge field with these symmetries is

$$A_\sigma = 0 \qquad\qquad A_i = \frac{1}{4\pi\alpha'}\sigma_i h(\sigma) \tag{3.15}$$

for an arbitrary function $h(\sigma)$. These give[15]

$$\widetilde{F}_{ij} = -\frac{1}{4\pi\alpha'}\epsilon_{ijk}\sigma_k h^2(\sigma) \qquad\qquad \widetilde{F}_{i\sigma} = -\frac{1}{2}\sigma_i h'(\sigma)\ . \tag{3.16}$$

From these, we find that

$$\widetilde{F}_{i\sigma}\widetilde{F}_{i\sigma} = \frac{3}{4}(h'(\sigma))^2\mathbb{1}_{2\times 2} \qquad\qquad \frac{1}{2}\widetilde{F}_{ij}\widetilde{F}_{ij} = \frac{3}{(4\pi\alpha')^2}h^4(\sigma)\mathbb{1}_{2\times 2}\ .$$

We see that unless both h and h' vanish for $\sigma \to \pm\infty$, the Yang-Mills action density integrated over σ will diverge, corresponding to an infinite energy density in the field theory. On the other hand, we find

$$(\widetilde{F}\wedge\widetilde{F})_{123\sigma} = \frac{1}{8\pi\alpha'}h^2(\sigma)h'(\sigma) = \frac{1}{24\pi\alpha'}\partial_\sigma(h^3(\sigma))\mathbb{1}_{2\times 2}\ .$$

In order that we have a configuration with finite baryon density in the field theory, we require that this instanton density, integrated over the sigma direction be non-zero[16]. But this requires that $h(\infty) \neq h(-\infty)$, and we have already seen that such a configuration will result in an infinite energy density in the field theory.

The apparent conclusion for the dual field theory is that *there are no spatially homogeneous configurations with finite non-zero baryon density and finite energy density.* Now, there certainly are non-homogeneous configurations with finite average energy density and finite average baryon density: we can simply take a periodic array of individual instantons. For large enough chemical potential (greater than the energy density divided by the baryon density), such configurations are favored over the vacuum, so we will certainly have a phase transition to a phase with nonzero baryon density as the chemical potential is increased. However, our observation suggest that this phase cannot be spatially homogeneous.

Interpretation of the inhomogeneity and origin of the chiral density wave

[15]We use conventions where $\{\sigma_i,\sigma_j\} = 2\delta_{ij}\mathbb{1}$ and recall that $\widetilde{F} \equiv (2\pi\alpha')F$.

[16]To see this, note that the abelian electrostatic potential A_0 couples to $\mathrm{tr}(F\wedge F)$, so that the change in the action upon a constant shift in A_0 (corresponding to a change in the baryon chemical potential) is $\int d\sigma \mathrm{tr}(F\wedge F)$.

The inhomogeneity of nuclear matter is not unexpected, and indeed is what we have for real nuclear matter at low densities (e.g. in the interior of large nuclei). It simply reflects the fact that the individual nucleons retain their identities (and therefore that the baryon density is clumped[17]). What is perhaps surprising is that the inhomogeneity seems to have a topological rather than a dynamical origin from the bulk point of view, following from basic properties of instantons. It follows that even at arbitrarily high densities, the nuclear matter will be inhomogeneous, though the scale of the inhomogeneities should become shorter and shorter as the instantons pack closer and closer together. This suggests an interpretation of the DGR "chiral density wave" instability of the quark Fermi surface [64] at asymptotically large chemical potential: that even at arbitrarily high densities, quarks in large N_c QCD bind into distinct nucleons, in contrast to the quark matter phase with homogeneous condensates that we expect at large μ for finite N_c. This may be related to the property that the density of a baryon diverges for large N_c and thus the baryon is more and more sharply defined in this limit.

Our approximation

The absence of homogeneous configurations with finite baryon density complicates the analysis of the phase transition and the properties of the nuclear matter phase. We will not attempt to study the inhomogeneous configurations directly here. Rather, we will describe an approach that approximates the inhomogeneous configurations with singular homogeneous configurations.

Our approach is motivated by the observation that in the limit of infinite baryon density, the bulk configuration should become homogeneous. Such homogeneous configurations are singular at the core, corresponding to a divergence of the instanton charge density. For example, we can have a self-dual configuration of the form (3.15) if we choose

$$h(\sigma) = \frac{1}{\sigma} \ . \tag{3.17}$$

This should arise from the limit of a periodic array of instantons for which the separation is taken to zero while adjusting the scale factors to yield a non-trivial configuration in the limit. We expect that some similar configuration[18] should arise in our case as the minimum energy configuration in the limit of infinite chemical potential.

As we move away from infinite density, the minimum energy configuration will only be approximately homogeneous. We expect, however, that the averaged field strengths and instanton density should be qualitatively similar to those for the configuration (3.17) but with finite values at $\sigma = 0$. This behavior can be achieved in a configuration of the form (3.15) for which h is an odd function like (3.17) but with some finite limit at $\sigma = 0$. Such configurations are singular at $\sigma = 0$, but we will ignore any effects associated with the singularity at $\sigma = 0$ since we are using our configurations to approximate non-singular

[17] Quantum mechanically this would be reflected in the behavior of density-density correlation functions.

[18] not necessarily self-dual since we are working with the D-brane effective action in a nontrivial geometry

inhomogeneous configurations that do not have any pathologies at $\sigma = 0$.[19] In particular, we might expect that our approximation becomes exact in the limit of infinite baryon density where we can have homogeneous configurations. We will find evidence below that supports the validity of this claim. More generally, we find results that are in accord with various physical expectations, providing further evidence for usefulness of our approximation.

3.5.1 Energy Density for Approximate Configurations

We would now like to analyze the behavior of the model as a function of chemical potential in the approximation where we consider only configurations of the form (3.15), taking h to be a monotonically increasing function for $\sigma > 0$ that takes some finite (negative) value at $\sigma = 0$ and vanishes for $\sigma \to \infty$. In practice, we work with the action for half the brane, assuming that h is an odd function so that all the field strengths are symmetric about $\sigma = 0$. As we mentioned above, such configurations are singular at $y = 0$ but we ignore any effects of the singularity, motivated by the expectation that the nonsingular contributions may provide a good approximation to the averaged quantities for the non-singular inhomogeneous configuration that we should really be studying.

The configuration of the spatial $SU(2)$ Yang-Mills field carries instanton density, and therefore acts as a source for the abelian electrostatic potential on the D8-branes. In order to determine the potential $A(U)$ for a given $h(U)$, we need the equation of motion for A, which should come from the non-abelian generalization of the Born-Infeld action (3.3) and the Chern-Simons action (3.9).

As we have noted, the nonabelian generalization of the Born-Infeld action (3.3) is known only up to F^6 terms. In the absence of the full result, we will work with a naive ordering prescription in which we simply insert our ansatz into the abelian expression (3.3) and (noting that each product of Fs above gives an identity matrix) evaluate the trace. This will give us results that are precisely correct in the limit where the field strengths are small and only the Yang-Mills terms in the action are important, but we should not trust numerical coefficients whose calculation depends on the higher order terms in the Born-Infeld action.

Inserting the ansatz (3.16) into (3.3), we find (in the $\sigma = U$ coordinates):

$$S_{DBI} = -\frac{\mu_8}{g_s}\frac{16}{3}\pi^2 R_4^3 \int d^4x dU U \sqrt{(\frac{1}{f(U)} - (\partial_U \widetilde{A})^2 + \frac{3}{4}(h'(U))^2)((U/R_4)^3 + \frac{3}{4}\frac{h^4(U)}{(2\pi\alpha')^2})} \tag{3.18}$$

while the Chern-Simons term (3.2) gives:

$$\begin{aligned} S &= \frac{N_c}{24\pi^2}\int \mathrm{tr}(A \wedge F \wedge F) \\ &= \frac{N_c}{128\pi^6(\alpha')^4}\int dU \widetilde{A}\partial_U(h^3(U)) \ . \end{aligned} \tag{3.19}$$

[19] This is similar in spirit to replacing a nonsingular charge distribution with a localized singular distribution with the same multipole moments.

If we define

$$G = \frac{1}{f(U)} + \frac{3}{4}(h'(U))^2$$

and

$$F = U\sqrt{(U/R_4)^3 + \frac{h^4(U)}{(4\pi\alpha')^2}}$$

then the action takes the form

$$S = -C\int dU F\sqrt{G - (\partial_U \widetilde{A})^2} + \widehat{k}\int \widetilde{A}\partial_U(h^3)$$

where

$$\widehat{k} = \frac{N_c}{128\pi^6(\alpha')^4}$$

and

$$C = \frac{16}{3}\pi^2\frac{\mu_8}{g_s}R_4^3$$

The equations of motion for the electrostatic potential A are

$$C\partial_U E = \widehat{k}\partial_U(h^3)$$

where

$$E = \frac{F\partial_U \widetilde{A}}{\sqrt{G - (\partial_U \widetilde{A})^2}}\ . \tag{3.20}$$

From this, we conclude that

$$\widehat{k}h^3 = C(E - E_\infty) \tag{3.21}$$

where we have determined the integration constant by demanding that h vanish as $U \to \infty$, as is required for finite energy configurations. Since E vanishes by symmetry at $U = U_0$ (assuming that there is no delta function charge distribution at $U = U_0$) we see that the asymptotic value of E is related directly to the value of h at $U = U_0$ by

$$\widehat{k}h_0^3 = -CE_\infty\ . \tag{3.22}$$

We may therefore rewrite (3.21) as

$$E = \frac{\widehat{k}}{C}(h^3 - h_0^3)$$

Using this result, the electrostatic potential may be determined in terms of h by inverting (3.20).

We may now write an expression for the energy density of a configuration for a given value of $h(U)$.

Starting with the actions (3.18) and (3.19), we can derive the 3+1 dimensional energy density via a Legendre transformation as we did earlier. We find

$$\mathcal{E} = C\int dU\left[F\sqrt{G-(\partial_U\widetilde{A})^2}-F_{h=0}\sqrt{G_{h=0}}\right]+\widehat{k}\int\partial_U\widetilde{A}(h^3-h_0^3)-\widehat{k}\widetilde{A}_\infty h_0^3$$

where we have subtracted off the energy density of the unexcited brane such that the vacuum state is normalized to zero energy. We can now rewrite the energy in terms of h, assuming that the equation of motion for A is obeyed. We have first

$$\mathcal{E} = C\left\{\int dU(\sqrt{G(F^2+E^2)}-F_0\sqrt{G_0}\right\}-C\widetilde{A}_\infty E_\infty$$

Now writing E in terms of h as above, changing variables to $x = U/U_0$, defining

$$y = -\frac{\sqrt{3}}{2}\frac{h}{U_0}\,, \tag{3.23}$$

$$\lambda_0 = \frac{2g_sN_cl_s}{3\sqrt{3}R}\,,$$

and

$$\widetilde{\mu} = \sqrt{3}R\mu = \frac{\lambda_0}{3}\frac{\mu}{M_B^{\lambda=\infty}}\,, \tag{3.24}$$

we finally have

$$\mathcal{E} = \frac{CU_0^{\frac{7}{2}}}{R_4^{\frac{3}{2}}}\left[\int_1^\infty dx\left\{\sqrt{\frac{1}{\widetilde{f}(x)}+(y'(x))^2}\sqrt{x^5+\lambda_0^2(x^2y^4+(y^3-y_0^3)^2)}-\frac{x^{\frac{5}{2}}}{\sqrt{\widetilde{f}(x)}}\right\}-\widetilde{\mu}y_0^3\right] \tag{3.25}$$

Using the definition (3.23), and the relations (3.22) and (3.7), we find that y_0 is related to the baryon density by

$$\begin{aligned} n_B &= \frac{\pi}{12\sqrt{3}}\left(\frac{4}{9\pi}\frac{g_sN_cl_s}{R}y_0\right)^3\frac{1}{R^3} \\ &= \frac{2}{27\pi^2}\lambda_0^3y_0^3\frac{1}{R^3} \end{aligned}$$

Thus, minimizing this expression for $\widetilde{\mu}=0$ and fixed y_0 will give the minimum energy density for a fixed baryon density, which we denote by

$$\mathcal{E}_{min}(y_0)$$

The energy density per baryon is then proportional to $\mathcal{E}_{min}/y_0^3$, and as we have argued above, the minimum of this gives the critical chemical potential. In the next section, we will analyze the functional (3.25), to obtain results for the behavior of $\mathcal{E}_{min}(y_0)$ and for the critical chemical potential.

3.5.2 Results

In this section, we discuss the evaluation of the baryon density for a given chemical potential based on minimizing the energy functional (3.25). Demanding that the functional is stationary under local variations of y gives a second order differential equation for y. For a given initial value y_0 we find that there is a particular value of the initial slope y_0' for which the solution approaches 0 as $x \to \infty$. For larger or smaller y_0' the solution approaches positive or negative infinity respectively for $x \to \infty$, giving a diverging energy functional, so the minimum energy configuration must correspond to the solution with boundary condition $y \to 0$ at $x \to \infty$.

Small Baryon Density

We first study $\mathcal{E}(y_0)$ in the regime where the baryon density is small. Since the full energy at finite μ takes the form

$$\mathcal{E}(y_0, \mu) = \mathcal{E}_{min}(y_0) - \widetilde{\mu} y_0^3 \ ,$$

it is important to determine the behavior of $\mathcal{E}_{min}(y_0)$ for small y_0. As long as the potential for $\mu = 0$ is quadratic (or linear) for small y_0, we must have a first order transition to some finite baryon density at a critical chemical potential rather than a continuous transition where the baryon density increases gradually from zero. The results we obtain at small y_0 are also very robust (within our approximation), since here all field strengths and derivatives are small, and the incompletely known α' corrections in the D8-brane effective action are not important.

The terms in (3.25) coming from the Yang-Mills action are simply the leading order kinetic and potential terms,

$$\mathcal{E} = \frac{C U_0^{\frac{7}{2}}}{R_4^{\frac{3}{2}}} \left\{ \int_1^\infty dx \left(\frac{1}{2} x^{\frac{5}{2}} \sqrt{\widetilde{f}(x)} (y'(x))^2 + \frac{1}{2} \lambda_0^2 \frac{1}{x^{\frac{1}{2}} \sqrt{f(x)}} y^4 \right) - \widetilde{\mu} y_0^3 \right\}$$

It is convenient to change variables to obtain a canonical kinetic term. Thus, we define u such that

$$\frac{du}{dx} = \frac{1}{x^{\frac{5}{2}} \sqrt{\widetilde{f(x)}}} = \frac{1}{\sqrt{x^5 - x^2}}$$

Choosing $u = 0$ to correspond to $x = 1$, we have

$$x(u) = \sec^{\frac{2}{3}}\left(\frac{3}{2} u\right) \ .$$

Note that $x = \infty$ corresponds to $u = \pi/3$, so we now have a finite domain, which is convenient for our later numerical methods. Dropping the overall constant and working at $\mu = 0$ for now, we have

$$\widetilde{\mathcal{E}} = \int_0^{\frac{\pi}{3}} du \left(\frac{1}{2} (y')^2 + \frac{1}{2} \lambda_0^2 x^2(u) y^4 \right) \tag{3.26}$$

Extremizing, this gives rise to the differential equation

$$y''(u) = 2\lambda_0^2 x^2(u) y^3(u) \tag{3.27}$$

As we discussed above, for a given $y(0) > 0$, solutions to this equation with slope larger or smaller than some critical value will approach positive or negative infinity as $u \to \pi/3$ and give rise to an infinite energy. The minimal energy configuration corresponds to the critical value of the initial slope for which the solution approaches zero at $u = \pi/3$. For $y_0 << 1/\lambda$, the solution is linear to a good approximation, since taking

$$y(u) = y_0(1 - \frac{3}{\pi}u) \tag{3.28}$$

we find that the right hand side of (3.27) is small enough that even the maximum value of y'' integrated over the interval would only change y' slightly.

Thus, for $y_0 << 1/\lambda$, the energy is given by inserting (3.28) into (3.26), and we find

$$\widetilde{\mathcal{E}}_{eff}(y_0) \sim \frac{3}{2\pi} y_0^2 + \mathcal{O}(\lambda^2 y_0^4) \qquad \text{small } y_0$$

Thus, the full energy $\mathcal{E}(y_0, \mu)$ is always positive for small enough y_0, and the transition to nuclear matter must be first order in our model.

While we can no longer trust the Yang-Mills approximation for large y_0 (of order $1/\sqrt{\lambda}$ or larger), it still interesting to look at behavior of the Yang-Mills terms in the energy functional in this regime. Continuing to use only the terms (3.26), a numerical study suggests the asymptotic behavior

$$\widetilde{\mathcal{E}}_{eff} \approx \frac{1}{3}\lambda_0 y_0^3$$

Note that this asymptotic growth in the energy density as a function of y_0 is not enough to stabilize the baryon density to finite values for $\widetilde{\mu}$ larger than value

$$\widetilde{\mu} = \frac{1}{3}\lambda_0 \ .$$

Comparing with (3.24), we see that this value corresponds precisely to $\mu = M_B^0$. Thus, we conclude that the α' corrections in the Born-Infeld action are essential for stabilizing the baryon density to finite values for large μ, and that without these, the baryon density would diverge beyond a critical chemical potential that exactly coincides with the large λ result for the baryon mass. In fact, we will see that at large λ the Born-Infeld corrections only modify this critical chemical potential by terms of order $\frac{1}{\lambda}$.

The Critical Chemical Potential

Now that we have demonstrated that there must be a first order phase transition to nuclear matter in our model, we would like to determine the critical value of μ above which a non-zero baryon density is favored, and the baryon density as a function of μ above this. Thus,

we repeat our numerical study from the previous section, but this time with the full energy functional. In this case, the differential equation for y (using the same coordinates) is

$$y'' = -\frac{5}{2x^6}(y')^3\frac{dx}{du} + ((y')^2 + x^5)\partial_y \ln H - y'\frac{dx}{du}(1 + \frac{(y')^2}{x^5})\partial_x \ln(H)$$

where

$$H(x,y) = \sqrt{1 + \lambda^2(\frac{y^4}{x^3} + \frac{1}{x^5}(y^3 - y_0^3)^2)}\ .$$

As before, the energy is minimized for a critical solution to this equation that approaches 0 at $u = \pi/3$.

Our results indicate that the energy $\mathcal{E}_{min}(y_0)$ behaves as a quartic function of y_0 for large y_0, so the Born-Infeld terms stabilize the baryon density to finite values for any value of μ. As we have discussed, the critical value of the chemical potential beyond which a nuclear matter phase is favored is given by the minimum value of the energy per baryon. Specifically, we have

$$\widetilde{\mu}_c = \min_{y_0}\frac{\widehat{\mathcal{E}}}{y_0^3};$$

We have numerically evaluated this critical chemical potential for large values of λ ranging from $\lambda = 10$ to $\lambda = 3000$. Our data for μ_{crit} at large λ are fit very well with a function

$$\mu_{crit} = M_B^0(A + c\lambda_0^{-1} + \mathcal{O}(\lambda_0^{-\frac{3}{2}})) \tag{3.29}$$

where the best fit values are

$$A \approx 1.000 \pm 0.001 \qquad c \approx 8 \pm 2$$

Thus, to very good accuracy, the critical value of the chemical potential approaches the baryon mass for large λ. Though our analysis using singular homogeneous configurations is an approximation, it is implausible that the almost exact agreement between the critical chemical potential and the baryon mass that we find here for large λ is a numerical coincidence. A more plausible explanation is that the ratio of the critical chemical potential to the baryon mass does approach 1 in the limit of large lambda, and that our approximation gets this leading result correct. This is in accord with the expectation that our approximation should become exact in the limit of large baryon density, since as we will see below, the baryon density just above the transition does approach infinity as λ becomes large.

Thus, we believe that a robust conclusion of our analysis is that the binding energy per nucleon for large λ is a vanishing fraction of the baryon mass.

The Binding Energy per Nucleon

To determine the actual value of the binding energy, we need to compare the subleading term in (3.29) with the subleading term in the baryon mass.

Even if our approximation is also correct for this subleading term, evaluating the coefficient c here depends crucially on the higher order terms in the Born-Infeld action. Since we have used the abelian D8-brane action together with an ad-hoc ordering prescription in lieu of the unknown full result for the effective action, we expect that the numerical value here is not reliable, However, the result that the correction is of order λ^{-1} (rather than e.g. $\lambda^{-\frac{1}{2}}$) should be robust.

Similarly, a correct calculation of c' in the result

$$M_B = M_B^0(1 + \frac{c'}{\lambda_0} + \dots)$$

for the baryon mass discussed in section 3.1 probably requires more complete knowledge of the non-abelian effective action. However, recalling that the leading order result for the baryon mass is proportional to λ, we see that the result for the binding energy per nucleon $(M_B - \mu_c)$ is actually relatively insensitive to λ for large λ. Since we also know that this binding energy approaches some constant value in the limit of small λ (the large N_c QCD result with two massless flavors), then assuming a smooth behavior at intermediate values of λ, we can treat the large λ result as a prediction for the order of magnitude of the QCD result.[20]

Noting that $M_{KK} \approx \Lambda_{QCD}$ for large λ, the value of the binding energy per nucleon extrapolated to $N_c = 3$ becomes

$$E_{bind} = \frac{1}{9\pi}\Lambda_{QCD}(c' - c) \approx 7 \text{ MeV}(c' - c)$$

As we have noted in the introduction, this is indeed of the same order of magnitude as the physical QCD result of $16MeV$ assuming that $c' - c$ is of order one.

3.5.3 Baryon Density above the Transition

We can also calculate the baryon density just above the transition. Our results suggest that just above the transition, the preferred value of y_0 for large λ behaves like

$$y_0 \to K\lambda^{-\frac{1}{2}}$$

for $K \approx 0.31$. This suggests that

$$n_B R^3 \propto \lambda^{\frac{3}{2}}$$

as λ is increased. This is consistent with the finding of Sakai and Sugimoto that the baryon size goes like $\lambda^{-\frac{1}{2}}$.

[20] Another example with similar insensitivity to λ for both large and small λ is the free energy of $\mathcal{N} = 4$ SUSY Yang-Mills theory. Here, it is indeed the case that the large λ result for the free energy gives a good prediction of the order of magnitude of the the small *lambda* result (or vice versa).

For large chemical potential, the result that the $\mu = 0$ energy density approaches y_0^4 for large y_0 implies that the baryon density minimizing $\mathcal{E}(y_0 \propto n_B^{\frac{1}{3}}) - \mu n_B$ for large μ is

$$n_B \propto \mu^3$$

Also, the energy density as a function of μ for large μ behaves as

$$\mathcal{E} \propto \mu^4$$

Note that the powers here are those appropriate for free fermions. We would like to understand this point better.

Chapter 4

Supercurrent: Vector Hair for an AdS Black Hole

4.1 Introduction

In the previous chapter we used explicit construction in string theory to achieve a brane configuration whose low energy limit can be used as a model for large N_c QCD.Using the gauge /gravity duality we were able to study strongly coupled physics in the model through relatively simple perturbative calculations in its supergravity dual. Here we attempt to use the gauge /gravity duality to analyze a broader class of phenomena in the strong coupling limit. In particular, we are interested in studying the gravity duals to superconductors/superfluids. The gravitational theory we study in this chapter cannot be embedded directly into string theory. However the string theory construction of the gravity duals to superconducting systems have recently been found [94] and they also possess the features we found in the present setup.In recent times, there have been various works which aim at constructing string theory (gravitational) duals to condensed matter systems [21, 22, 106–112].

A superconductor (or BEC in general) is one of the most studied systems in condensed matter physics [113] and is also equally important in the study of the phase diagram of QCD [29]. However there are certain aspects of superconductivity, e.g. high temperature superconductivity etc, that are still not completely understood. As superconductivity is a field theoretical phenomenon, it is interesting to ask if gauge gravity duality can be used to provide some insights into superconductivity. It turns out that there exists a gravitational system which closely mimics the behaviour of a superconductor. We will briefly describe the basic set up. Recently it has been shown by Gubser that in the AdS_4 background one can have condenstation of a charged scalar field [114][21]. It is shown that there exist solutions that allow for a condensing scalar to be coupled to the black hole if the charge on the black hole is large enough. The scalar couples to a $U(1)$ gauge field under which the black hole is charged, and its condensation breaks the gauge symmetry spontaneously, giving a mass to the gauge field. The exact backreacted gravity solution with the condensation of scalar field is difficult to find. In [92] the gauge fields and coupled scalar part of the Lagrangian has been solved and studied numerically, neglecting the gravity backreaction. It has also been shown that system undergoes a second order normal conductor/DC superconductor transition after the

[21]Possible ways to have scalar hair in asymptotically at EYMH systems (also related mechanism in non-abelian gauge gravity systems) has been discussed by authors (see [115–118] and references therein).

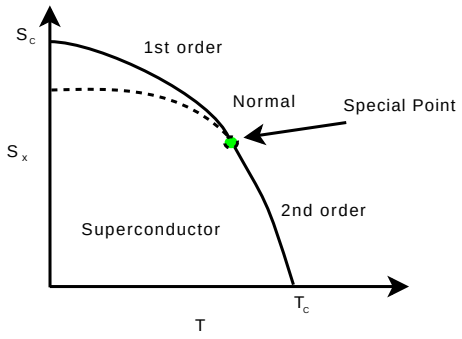

Figure 4.1: Phase diagram in S_x, T plane showing critical point, first order and second order transition. For $T < T_{sp}$ the phase transition is first order. The dotted line is the extension of second order transition line.

scalar condenses. Various related works discuss other aspects of superconductivity including partial discussions of Meissner effect and the non-abelian case [119–125].

Here we carry these investigations further by presenting a DC supercurrent type solution. Infinite DC conductivity in the dual field theory means that there are states in the field theory with time independent non-zero DC current (but without any external voltage). Such a phenomenon is well known in condensed matter systems. It is known from various experiments that the supercurrent can sustain itself for several years in a superconducting coil. In terms of AdS/CFT the above mentioned supercurrent states will correspond to a deformation of superconducting black holes by the spatial component of the gauge fields with a non-trivial radial dependence. We have numerically constructed such a solution. The solution may be thought as a vector hair to a superconducting AdS black hole and may be interpreted as a bound state of soliton and a black hole. As one would expect, a type of no-hair theorem [126] prevents any such non-trivial solution from occurring in the case of a normal (non-superconducting) AdS black hole.

We also have studied the interesting and novel phase diagram of such a system. It is shown that the critical temperature of the superconducting transition decreases with the introduction of a chemical potential for supercurrent and most interestingly at some point the order of phase transition changes from second order to first order. Thereby we have shown the existence of a "special point"[22] in the phase diagram, where the line of second order transitions ends and the first order transition begins (Fig 4.1). It has also been shown that the superconducting phase transits back to the normal phase at a certain value of the supercurrent (critical current). The associated transition may be second order or first order depending on temperature.

In this paper we start by discussing the equations and general setup (section 4.2), then

[22]This is actually a critical point. However we refrain from using the word "critical" to avoid any possible confusion with T_c, S_c etc.

we discuss the superconducting black hole solution studied in [92] and also introduce our supercurrent solution (section 4.3). In section 4.4 we discuss the various phase diagrams associated with our model. We also comment on some possible connection with superfluid phase diagram (section 4.5) and the issue of gravity backreaction (section 4.6). In the concluding section we discuss some future directions and open questions.

4.2 Equations and Accounting of the Boundary Conditions

In this section we will describe the setup on the gravity side which gives a superconducting system in the boundary theory. Following [92], we consider the planar limit of the four dimensional AdS black hole:

$$ds^2 = -f(r)dt^2 + \frac{dr^2}{f(r)} + r^2(dx^2 + dy^2) \tag{4.1}$$

where

$$f(r) = \frac{r^2}{L^2} - \frac{M}{r} \tag{4.2}$$

and L is the radius of the anti-de Sitter space and the temperature of the black hole (and also the boundary field theory) is given by

$$T = \frac{3M^{1/3}}{4\pi L^{4/3}} \tag{4.3}$$

In this note we will adopt the convention that $M = L = 1$. At the phenomenological level, superconductivity is usually modeled by a Landau-Ginzburg Lagrangian where a complex scalar field develops a condensate in a superconducting phase. In order to have a scalar condensate in the boundary theory, the authors of [92] introduce a $U(1)$ gauge field and a conformally coupled charged complex scalar field ψ in the black hole background. The Lagrangian of the system is:

$$L = \int dx^4\sqrt{-g}(-\frac{1}{4}F^{ab}F_{ab} - V(|\psi|) - |\partial\psi - iA\psi|^2), \tag{4.4}$$

where the potential is given by

$$V(|\psi|) = -2\frac{|\psi|^2}{L^2} \tag{4.5}$$

which corresponds to the conformal mass $m^2_{conf} = -2/L^2$. As argued in [92], the mass term is negative but above the Breitenlohner-Freedman (BF) bound [127] and thus does not cause any instability in the theory. As we will see below the presence of the vector potential effectively modifies the mass term of the scalar field as we move along the radial direction r

and allows for the possibility of developing hairs for the black hole in parts of the parameter space. Noticed that in our model there's no explicit specification of the Landau-Ginzburg potential for the complex scalar field. The development of a condensate relies on more subtle mechanisms for violations of the no hair theorem.

Here we consider the possibility of a DC supercurrent in this setup. For this purpose, we will have to turn on both a time component A_t and a spatial component A_x for the vector potential. We are interested in static solutions and will also assume all the fields are homogeneous in the field theory directions with only radial dependence. It is more convenient to analyze the system by making a coordinate transformation $z = 1/r$. The metric becomes:

$$ds^2 = -f(z)dt^2 + \frac{dz^2}{z^4 f(z)} + \frac{1}{z^2}(dx^2 + dy^2) \tag{4.6}$$

with

$$f(z) = \frac{1}{z^2} - z. \tag{4.7}$$

The horizon is now at $z = 1$, while the conformal boundary lives at $z = 0$. Like [92] we will also neglect the gravity back reaction of gauge and scalar fields. How this limit can be taken consistently is discussed in [92, 119]. The equations of motion for the fields in this coordinate system are:

$$\begin{aligned} \psi'' &+ \frac{f'}{f}\psi' + \frac{1}{z^4}\left(\frac{A_t^2}{f^2} - \frac{z^2 A_x^2}{f} + \frac{2}{L^2 f}\right)\psi = 0 \\ A_t'' &- 2\frac{\psi^2}{f z^4} A_t = 0 \\ A_x'' &+ \left(\frac{2}{z} + \frac{f'}{f}\right) A_x' - 2\psi^2 \frac{A_x}{z^4 f} = 0 \end{aligned} \tag{4.8}$$

To require regularity at the horizon we will have to set $A_t = 0$ at $z = 1$. Since we have a set of coupled equations, this will in turn give the constraints at the horizon

$$\begin{aligned} z\psi' &= \frac{2}{3}\psi - \frac{1}{3}z^2 A_x^2 \psi^2 \\ A_x' &= -\frac{2}{3}(\frac{\psi}{z})^2 A_x \\ A_t &= 0 \end{aligned} \tag{4.9}$$

where $z = 1$. Examining the behaviour of the fields near the boundary, we find

$$\begin{aligned} \psi &\sim \Psi_1 z + \Psi_2 z^2 + ... \\ A_t &\sim \mu - \rho z + ... \\ A_x &\sim S_x + J_x z + ... \end{aligned} \tag{4.10}$$

The constant coefficients above can be related to physical quantities in the boundary field theory using the usual dictionary in gauge/gravity correspondence. μ, ρ are the chemical potential and the density of the charge carrier in the dual field theory, respectively. J_x corresponds to the current, while S_x gives the dual current source. $\Psi_{1,2}$ are both coefficients multiplying normalizable modes of the scalar field equation. They are the expectation values of operators in the field theory.

$$\Psi_i \sim < \mathcal{O}_i > \tag{4.11}$$

In this paper, we will mainly study the $\Psi_1 = 0$ case and also briefly discuss $\Psi_2 = 0$ case. It turns out both exhibit similar behavior when it comes to DC superconductivity.

We want to parametrize our solutions in terms of dimensionless quantities. From the analysis in the appendix we see that T, μ, Ψ_1, S_x have dimension one, while ρ, Ψ_2, J_x have dimension two. The dimensionless combinations are $(\frac{T}{\mu}, \frac{S_x}{\mu}, \frac{J_x}{\mu^2}, \frac{\sqrt{<\mathcal{O}_2>}}{\mu}, \frac{<\mathcal{O}_1>}{\mu})$. With the regularity conditions (Eq. (4.9)) and $\Psi_1 = 0$ (or $\Psi_2 = 0$) , we are left with a two parameter family of solutions; which we characterize by two dimensionless quantities $\frac{T}{\mu}, \frac{S_x}{\mu}$. Since the effect of temperature is governed by $\frac{T}{\mu}$, we can in practice keep the temperature fixed and achive the same effect by changing $1/\mu$.

4.3 Nature of the Solution

4.3.1 Superconducting Black Hole

Here we discuss the space-time profile of the superconducting black hole solution found in [92] and put $A_x = 0$ in the Eq. (4.8). At a small value of μ the only solution to the set of equations 4.8 is given by,

$$\begin{aligned} A_t &= \mu(1-z) \\ \psi &= 0 \end{aligned} \tag{4.12}$$

The effective mass of the field ψ in this background is given by

$$m_{eff}^2 = -2 - \frac{A_t^2}{f(z)} \tag{4.13}$$

Hence, as we increase μ the effective mass becomes less than BF bound in a sufficiently large region of space and consequently a zero mode develops for the field ψ (Fig 4.2) at $1/\mu = 1/\mu_c \approx 0.146$. As μ is increased further the field ψ condenses and a new branch of solution shows up which has non-zero value of ψ. (As discussed in Eq. (4.11), there are two possible boundary condition for ψ. Here we concentrate on $\Psi_1 = 0$ case, $\Psi_2 = 0$ case is similar.) It has been argued in [92] that this new solution has a lower free energy than the regular black hole solution with $\psi = 0$ and there is a second order phase transition associated with this phenomenon. We present the phase diagram in the next chapter which may be

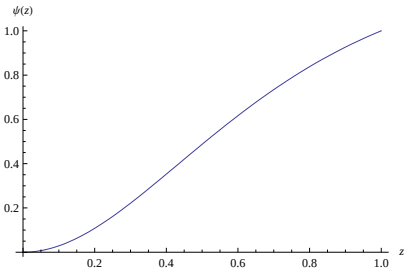

Figure 4.2: Zero mode of ψ at $\mu = \mu_c$ with a normalization $\psi = 1$ at the horizon.

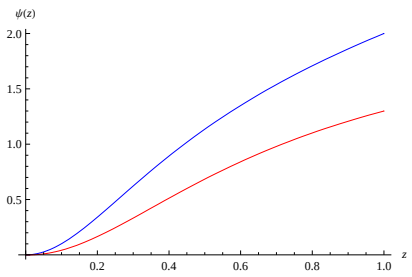

(a) Plot of $\psi(z)$.

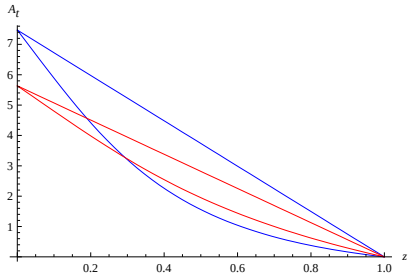

(b) Plot of $A_t(z)$, the curved ones. The straight lines are the plots of $A_t(z)$ for $\psi = 0$ case with the same value of $1/\mu$.

Figure 4.3: Plots of ψ and A_t at $1/mu \approx 0.105, 0.079$. μ is increasing from below.

thought as the $A_x = 0$ case in our context[23]. Here we will present the general nature of the solution.

We plot the solution for some generic values of $1/\mu \approx 0.105, 0.079$ (Fig 4.3(a), Fig 4.3(b)). As one can see, Ψ_2 increases as we increase the value of μ[24].

The conductivity of this system can be calculated by looking at the frequency (ω) dependent fluctuation equation of A_x in this back ground. It has been shown in [92] that imaginary part of conductivity has a pole at $\omega = 0$. Consequently the real part of the conductivity will have a delta function at $\omega = 0$. This example of an infinite DC conductivity is an example of superconductivity. In contrast to that an ordinary black hole (with $\psi = 0$) has a finite

[23] As we increase μ further there is a possibility of multi-nodal (in radial direction) solution, but as in [92] we will not consider such solutions. These solutions probably are thermodynamically unfavourable.

[24] Another interesting property is that as we increase μ, $\rho = A_t'(z)$ at the boundary $z = 0$ increases, however the charge of the black hole $\rho = A_t'(z_0)$ decreases. Although the the total charge of the configuration is increased by increasing μ, the condensation becomes more dense and carries most of the charge.

DC conductivity.

4.3.2 Supercurrent Solution

The conductivity is given by (from Eq. (4.11))

$$\sigma = \frac{J_x}{\dot{S}_x} \tag{4.14}$$

An infinite value of conductivity (as discussed at the end of the previous chapter) implies J_x may be non-zero even if the $\dot{S}_x = 0$. This is natural to expect in a superconductor, that current may flow without any applied voltage. Hence one may expect that one can deform the superconducting black hole solutions by turning on non-zero J_x (consequently a non-zero A_x). Here we have constructed such a solution numerically by solving the coupled Eq. (4.8). As we are solving the coupled equation our solution is valid for any value of A_x within the approximation scheme of neglecting gravity backreaction. The solution is characterized by two chemical potentials S_x, μ which are the boundary values of the fields A_x and A_t Eq. (4.11). To find this solution we start with fields satisfying appropriate boundary conditions near the black hole horizon Eq. (4.9) and integrate up to the boundary $z = 0$. Just like the case of superconducting black hole solution we can put either Ψ_1 or Ψ_2 to zero. Here we present the solution with $\Psi_1 = 0$, the case $\Psi_2 = 0$ is similar.

It should be noted that such a solution does not exist in an ordinary black hole background. From Eq. (4.8) we have for $\psi = 0$ case

$$\begin{aligned}
& A_x'' + (\frac{2}{z} + \frac{f'}{f})A_x = 0 && (4.15)\\
\Rightarrow\ & z^2 f A_x'' + (z^2 f)' A_x = 0 && (4.16)\\
\Rightarrow\ & z^2 f (z^2 f A_x')' = 0 && (4.17)\\
\Rightarrow\ & \frac{d^2}{dy^2} A_x = 0, \quad dy = \frac{dz}{z^2 f} && (4.18)\\
\Rightarrow\ & A_x = c_1 + c_2 y && (4.19)
\end{aligned}$$

Near the horizon $z^2 f(z) = -3(1-z) + \ldots$ Hence,

$$\begin{aligned}
y &\sim \log(1-z)\\
\Rightarrow F_{zx} &\sim \partial_z A_x \sim c_2 \frac{1}{1-z} && (4.20)
\end{aligned}$$

Energy density near the black hole horizon has a contribution from $g^{zz} g^{xx} F_{zx}^2$ term and consequently diverges as $1/(1-z)$ near the black hole horizon. Hence the only possible finite energy solutions are a constant ($c_2 = 0$,z independent) A_x solution with other fields given by

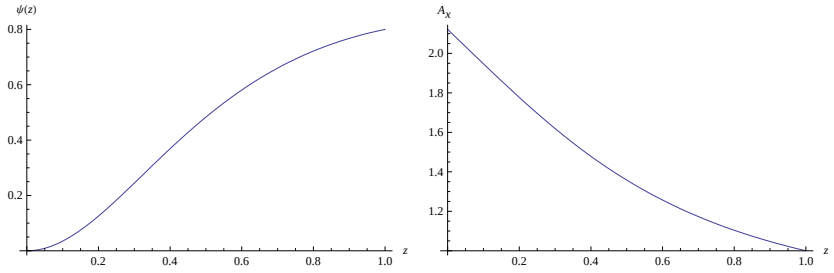

(a) Plot of ψ (b) Plot of A_x

Figure 4.4: Nature of solution for $\frac{1}{\mu} \approx 0.174$ and $\frac{S_x}{\mu} \approx 0.369$

Eq. (4.12). As discussed $J_x = 0$ for such solutions. Free energy competition between such a normal solution and supercurrent solution gives rise to an intricate phase diagram. Actually the order of superconducting phase transition changes from second order to first order as we tune the boundary value of A_x. It should also be noted that the introduction of field A_x changes the effective mass of the field ψ,

$$m_{eff}^2 = -2 - \frac{A_t^2}{f(z)} + z^2 A_x^2 \tag{4.21}$$

This implies that the introduction of too much A_x may destroy superconductivity and suggests the possibility of a cortical value of S_x, beyond which there is no superconductivity. These issues related to phase transition has been discussed in section 4.4. Here we will show how the solution looks like.

From Eq. (4.9), one may argue that the slope of the field ψ at the horizon changes sign as one turns on A_x. This may be seen from the solutions with generic conditions $1/\mu \approx 0.174, S_x/\mu \approx 0.369$ (Fig 4.4(a),4.4(b)) and $1/\mu \approx 0.087, S_x/\mu \approx 0.609$ (Fig 4.5(a),4.5(b)). As we turn on more S_x the value of ψ at the horizon decreases. Fig 4.4(a) shows one configuration which is near the phase boundary. Turning on S_x further will eventually destroy the condensate.

4.4 Results

4.4.1 $\Psi_1 = 0$

In this section we discuss the phase diagram associated with our solution. Let us for the moment set $\Psi_1 = 0$. This corresponds to choosing a boundary condition such that $\psi(z) \sim z^2$ at the boundary ($z \to 0$).

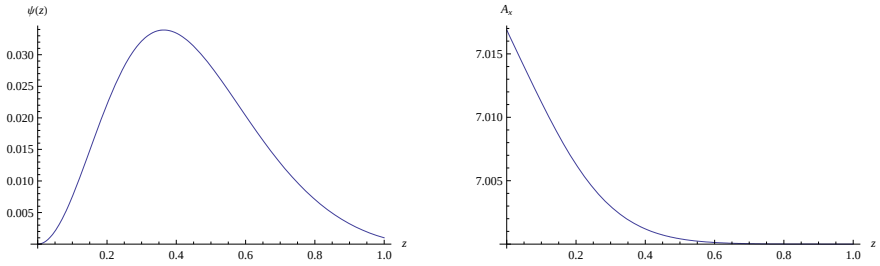

(a) Plot of ψ (b) Plot of A_x

Figure 4.5: Nature of solution for $\frac{1}{\mu} \approx 0.087$ and $\frac{S_x}{\mu} \approx 0.609$

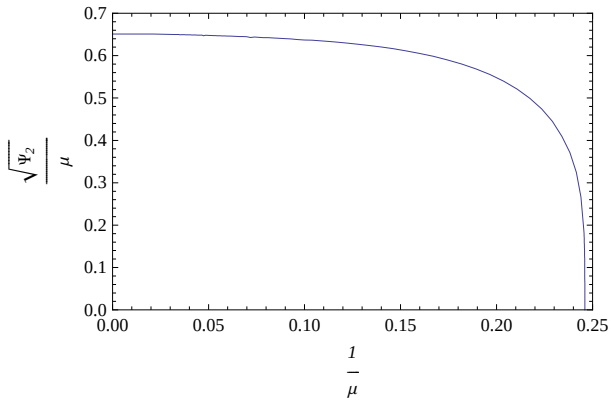

Figure 4.6: Plot of Ψ_2 as a function of $1/\mu$, for $A_x = 0$.

We first look at the case when $A_x = 0$. Solving for the condensate strength as a function of temperature or, equivalently, $1/\mu$ we get the curve shown in Fig 4.6. For small values of $1/\mu$ the condensate strength reaches a saturation value. Near the point $\Psi_2 = 0$ the curve has the dependence $\sqrt{\Psi_2}/\mu \sim (1/\mu - 1/\mu_c)^{1/2}$, as expected. This corresponds to a second order phase transition. If the parameter $1/\mu$ is increased further the condensate ceases to exist, i.e., $\psi(z) = 0$ beyond this point. The critical value $1/\mu_c = 0.246$. For a fixed boundary value of $\frac{1}{\mu}$ Solutions with $\Psi_2 \neq 0$ always has less free energy than the normal black hole solution given in Eq. (4.12).

μ Fixed, S_x Varying

Let us now consider the effect of turning on A_x. As explained in the section 4.2, turning on A_x has the effect of introducing a global $U(1)$ current J_x in the dual field theory. The

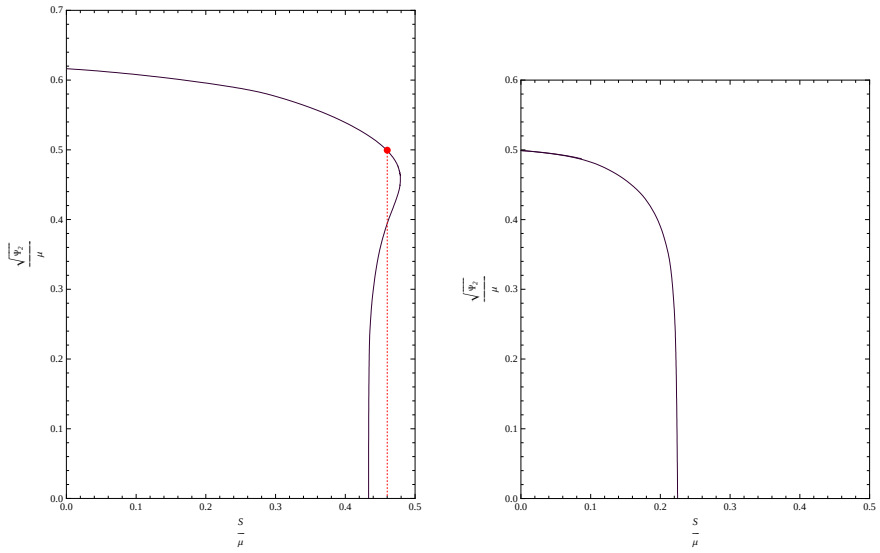

(a) $1/\mu = 0.146$ (b) $1/\mu = 0.217$

Figure 4.7: Phase structure in presence of a non-trivial A_x field. Vertical line in the left hand figure marks the first order transition.

boundary value of A_x, S_x acts as chemical potential for this current. In Fig 4.7 we plot the scaled condensate strength $\sqrt{\Psi_2}/\mu$ as a function of the scaled A_x chemical potential S_x/μ for different values of $1/\mu$. The plot on the left is for $1/\mu \approx 0.146$, while for the plot on the right $1/\mu \approx 0.217$. We see an interesting behaviour here: for all values of $1/\mu$ there is a critical value of the current above which there is no condensate. However, the nature of this transition seems to change with the value of $1/\mu$. For small values of this parameter, we seem to find a first order transition from the superconducting to the normal state when S_x reaches a critical value $S_{x,c}$(see Fig 4.7(a)). For values above a special value $1/\mu_{sp}$, the nature of the transition seems to change to second order (see Fig 4.7(b)). Note that the values of $1/\mu$ or temperature that we consider are below the usual critical temperature that exists for $A_x = 0$, which is at $\frac{1}{\mu_c} \approx 0.246$ in this case.

The critical value $S_{x,c}$ can determined by comparing the free energies of the solution with supercurrent solution and the $\psi = 0$ solution for the same value of $\frac{S_x}{\mu}$. In Fig 4.8 we plot the difference in free energies of the two branches as a function of S_x/μ. The figure on the left (Fig 4.8(a)) is for $1/\mu = 0.146$. We see the "swallow tail" curve typical of first order transitions. At $S_{x,c}/\mu = 0.46$ the branches cross, and the system jumps to the normal phase where the condensate ceases to exist. In the right hand side figure (Fig 4.8(b)), we again plot the free energy difference for $1/\mu = 0.217$. We see a smooth transition to the normal phase, which is second order. The critical value of S_x/μ is 0.22 in this case. Details of the

"swallow tail" diagram is discussed in a similar situation in the next subsection.

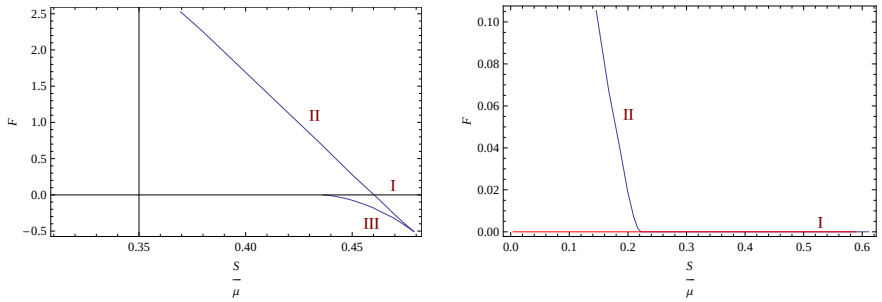

(a) $1/\mu \approx 0.146$ (b) $1/\mu \approx 0.217$

Figure 4.8: Free energy for the different phases.

We can also calculate the critical (or maximal) value of the "current" J_x. This can be done by reading off the current from a plot of S_x/μ vs J_x, shown in Fig 4.9. For the two cases considered above the critical currents are $J_{x,c} = 4.2$ and $J_{x,c} = 0.36$ respectively.

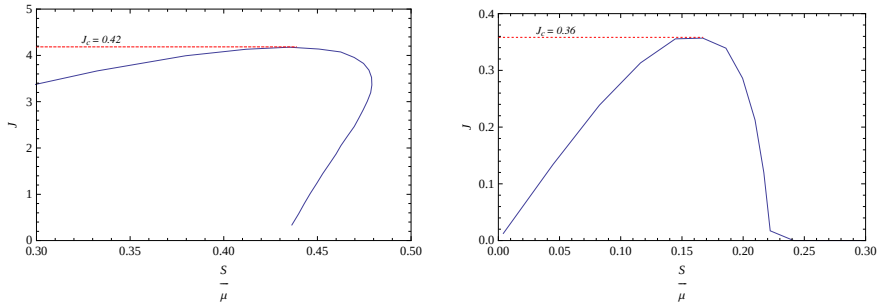

(a) $1/\mu \approx 0.146$ (b) $1/\mu \approx 0.217$

Figure 4.9: Plot of J_x as a function of S_x/μ.

S_x Fixed, μ Varying

In the above discussion, we explored the phase structure by taking constant $1/\mu$ sections. Equivalently, we can consider constant S_x/μ sections. Fig 4.10 shows the variation of the condensate $\sqrt{\Psi_2}/\mu$ with $1/\mu$, with $S_x/\mu = 0.1, 0.5$ respectively for the left and right hand side plots. The plot of the free energy difference between the normal and the supercurrent

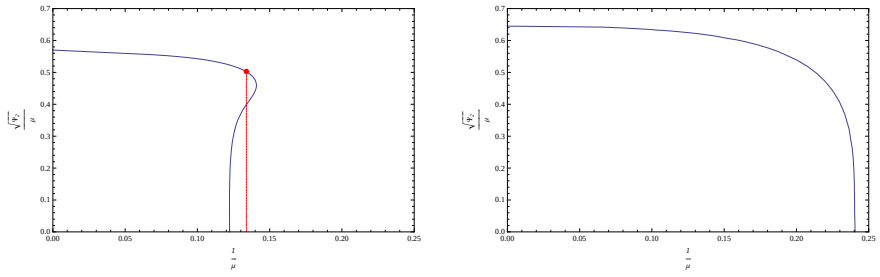

(a) $S_x/\mu = 0.1$ (b) $S_x/\mu = 0.5$

Figure 4.10: Phase structure in presence of a non-trivial A_x field. Vertical line in the left hand graph marks first order transition.

branches reveals the nature of the phase transition (see Fig 4.11). We see again that for small values of S_x/μ the phase transition is first order ($1/\mu_c = 0.134$), and it changes to second order for higher values of S_x/μ ($1/\mu_c = 0.24$). When the transition is first order there is three branches of solution. Similar to the phase diagram of AdS_5 black holes in global coordinate, there is one nucleation temperature ($1/\mu_N$) where there is generation of two new solutions. In Fig 4.10(a) $1/\mu_N \approx 0.14$. For a value of $1/\mu$ just below $1/\mu_N$, there are two possible solutions: the one with the higher value of condensate is stable (branch II), while the other one is unstable (branch III) (we have not done a local stability analysis, but this is the most likely case from the global stability.). The stable solution becomes dominant over the non-super conducting solution (branch I) at $\mu = \mu_c$. The unstable solution merges with the non-superconducting branch at an even lower value of $1/\mu$. The "swallow tail" diagram in Fig 4.11(a) shows this clearly. When the transition is of second order, there is no branch crossing and the non-superconducting solution becomes unstable for $\mu > \mu_c$ and the free energy of the condensate branch (II) is always less than the non-superconducting branch (I).

The critical value of the current J_x can be determined similarly as above.

In order to better understand the phase structure we can look at a three dimensional plot showing the variation of the three relevant dimensionless parameters in this case namely $1/\mu, S_x/\mu$ and $\sqrt{\Psi_2}/\mu$. This is shown in Fig 4.12. The curves in Fig 4.7 are constant $1/\mu$ sections of this plot, while Fig 4.10 shows constant S_x/μ sections. We can clearly see the change in the behaviour of $\sqrt{\Psi_2}/\mu$ as a function of S_x/μ with changing $1/\mu$. Below $1/\mu_{c'} = 0.22$ the dependence is non-monotonic, indicative of a first order transition. Above this value the dependence becomes monotonic and we have a second order phase transition.

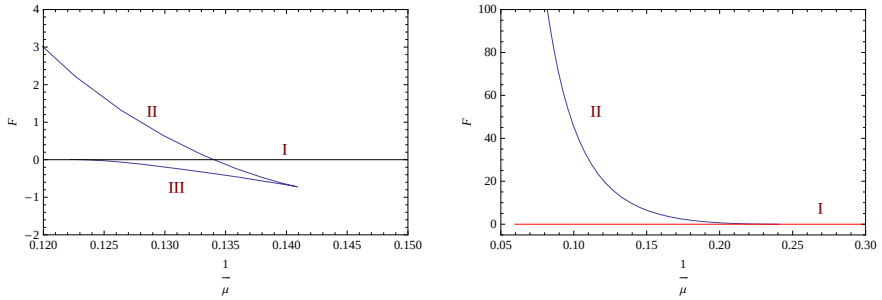

(a) $S_x/\mu = 0.5$ (b) $S_x/\mu = 0.1$

Figure 4.11: Free energy for the different phases.

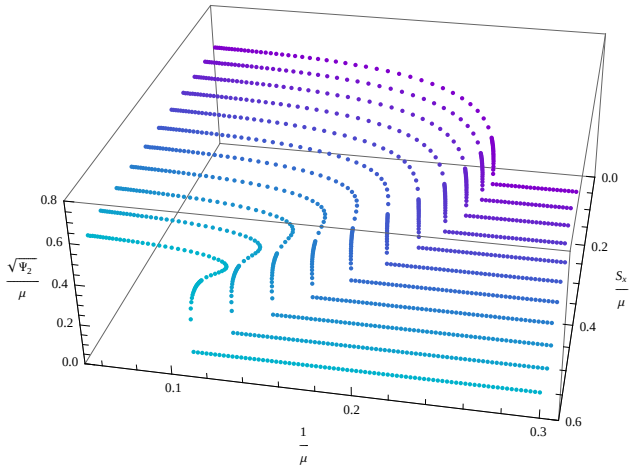

Figure 4.12: Plot of $\sqrt{\Psi_2}/\mu$ as a function of $1/\mu$ and S_x/μ.

Phase Boundary

We can also look at the phase structure on the S/μ, $1/\mu$ plane. The following figure (Fig 4.13) shows the result. The blue line indicates the region of second order phase transitions (the line in the right hand sign of the dot), which changes into first order at the red line (the line at the left hand side of the dot). The area enclosed by the transition line and the axes represent the condensate phase, while above the line the system is in the normal phase. The intercepts of this curve with the axes define two critical points: at $S_x = 0$, there is a second order phase transition as $1/\mu$ is increased at $1/\mu_c = 0.246$, while near $1/\mu = 0$ there is a first

order phase transition with increase in S_x/μ at $S_{x,c}/\mu = 0.874$.

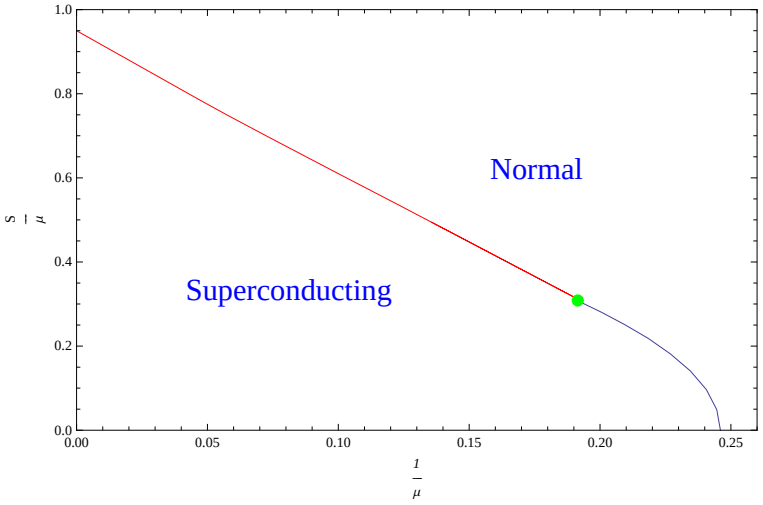

Figure 4.13: Phases of the Abelian Higgs model. The nature of the phase transition changes from second order (blue line) to first order (red line) at the "special point" (green dot).

4.4.2 $\Psi_2 = 0$

We now consider the case where $\Psi_2 = 0$. This corresponds to the boundary condition when $\psi(z) \sim z$ as $z \to 0$. Then for $A_x = 0$ we get the dependence of the scaled condensate strength Ψ_1/μ on $1/\mu$ shown in Fig 4.14. Near $1/\mu = 0$ the condensate strength diverges[25], while near the critical value of $1/\mu = 1/\mu_c$ the curve has the dependence $\Psi_1/\mu \sim (1/\mu - 1/\mu_c)^{1/2}$ as before. So we again have a second order phase transition at this point. The critical value $1/\mu_c = 0.89$.

We can now turn on A_x in this setting, and investigate the response of the system as we increase the chemical potential for the A_x field, S_x at various values of $1/\mu$. The results are shown in Fig 4.15. The story here is qualitatively similar to the $\Psi_1 = 0$ case: we again see the existence of a critical current above which there is no condensate. For small values of $1/\mu$ there is a first order phase transition as S_x is varied, as seen on the left hand side plot (Fig 4.15(a)). Here $1/\mu = 0.61$. For larger values of $1/\mu$ the nature of the transition changes to second order, as seen on the right hand side plot for $1/\mu = 0.813$ (Fig 4.15(b)). Note again that we are below the critical value $1/\mu_c = 0.89$ where the condensate ceases to exist for $A_x = 0$.

As in the $\Psi_1 = 0$ case, we can look at the behaviour of Ψ_1/μ as a function of $1/\mu$ and S_x/μ, shown in Fig 4.16. Below $1/\mu_{c'} \approx 0.6$, Ψ_1/μ is a non-monotonic function of S_x/μ and

[25]Note that for large values of the condensate Ψ_1 the gravity backreaction is important and our approximation is no longer valid.

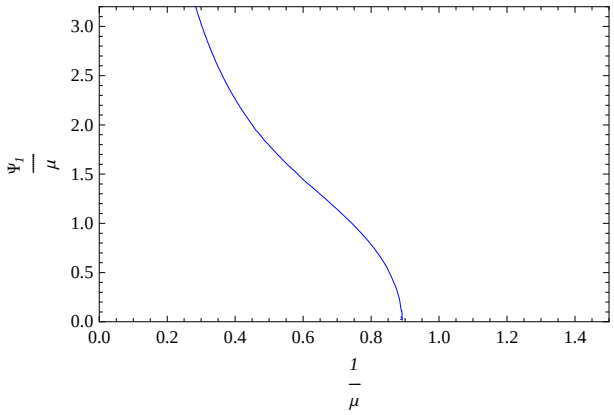

Figure 4.14: Plot of Ψ_1 as a function of $1/\mu$, for $A_x = 0$.

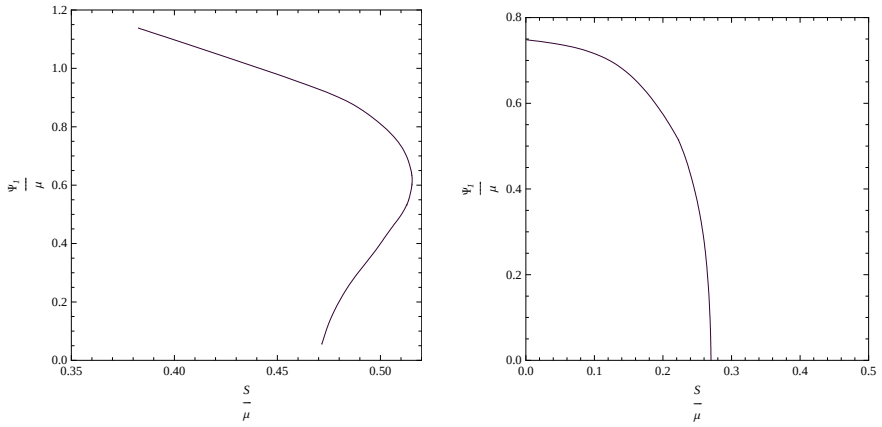

(a) $1/\mu = 0.61$ (b) $1/\mu = 0.813$

Figure 4.15: Plot of Ψ_1 as a function of $1/\mu$, for $A_x \neq 0$.

we have a first order transition at a critical value $S_{x.c}/\mu$. For $1/\mu > 1/\mu_{c'}$ the dependence becomes monotonic, and the transition becomes second order.

4.5 Connection to Superfluids

We note here that due to the global nature of the associated $U(1)$ symmetry, the condensation phenomenon we witness here is more similar to a superfluid. The phase structure we find can be interpreted by comparing with the known behaviour of superfluids [113]. Consider

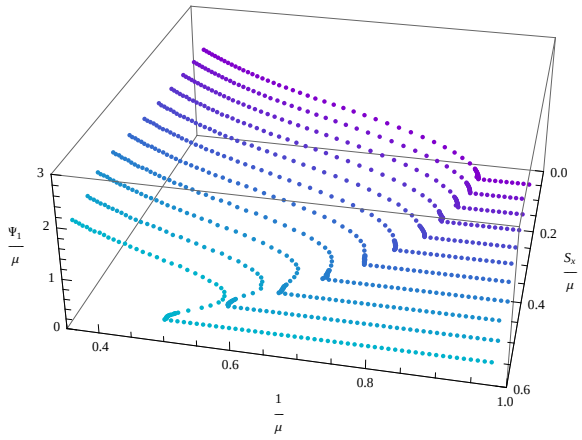

Figure 4.16: Plot of Ψ_1/μ as a function of $1/\mu$ and S_x/μ.

a charged superfluid confined to a thin film. The system can be described by a Landau-Ginzburg type theory with the following Lagrangian:

$$L = \alpha(T)|\psi|^2 + \frac{\beta}{2}|\psi|^4 + \frac{1}{2m}\left|(-i\nabla - \mathbf{A})\,\psi\right|^2, \tag{4.22}$$

where ψ is the condensate. The supercurrent can be defined in terms of $\psi(\mathbf{r}) = |\psi(\mathbf{r})|e^{i\varphi(\mathbf{r})}$ as

$$\mathbf{J} = \frac{|\psi|^2}{m}\left(\nabla\varphi - \mathbf{A}\right) \equiv |\psi|^2\mathbf{v}_s, \tag{4.23}$$

where $\mathbf{v}_s$ is the mechanical fluid velocity. We can think of $\mathbf{J}$ as being the response to the mechanical velocity $\mathbf{v}_s$. Note that in the field theory we get from our gravity picture, both the condensate ψ and the vector potential $\mathbf{A}$ are spatially homogeneous. Then $\mathbf{v}_s \propto \mathbf{A}$, i.e., a constant mechanical velocity is induced by a uniform vector potential[26].

At low temperatures the quasiparticle energies are shifted by an amount proportional to the fluid velocity $\mathbf{v}_s$, and this reduces the energy gap as $\mathbf{v}_s$ is increased. There exists a critical velocity where the gap goes to zero; at this point the system undergoes a first order transition to the normal state. Experimentally, it is known for superfluids at temperatures close to zero that as $\mathbf{v}_s$ is increased, the supercurrent $\mathbf{J}$ initially increases in proportion to $\mathbf{v}_s$. However, once $\mathbf{v}_s$ reaches a critical value $\mathbf{v}_{s,c}$, the current drops steeply to zero. This corresponds to the first order phase transition at the critical velocity.

[26]Note that since our system is homogeneous, we can make the direction along the vector potential periodic without any modifications. A constant vector potential cannot be gauged away and is thus physically meaningful. We thank Gary Horowitz for discussions on this point.

The situation is quite different near the critical temperature. There is still a phase transition, but it can be shown to be of second order. The current drops to zero smoothly at the critical velocity.

These observations agree qualitatively with our model if we identify the quantity S_x with the magnitude mechanical velocity of the fluid $\mathbf{v}_s$.

4.6 Gravity Backreaction

It is an important question that how the solutions change as we incorporate the gravity backreaction. Without the scalar condensation such a solution is just the standard RN black hole in AdS^{3+1} space. The metric of which is given by [128],

$$\begin{aligned} ds^2 &= \frac{L^2}{z^2}(-f(z)dt^2 + dx^2 + dy^2) + \frac{L^2 dz^2}{z^2 f(z)} \\ A_t &= \mu(1 - \frac{z}{z_0}) \\ f(z) &= 1 + q^2 z^4 - (1+q^2)z^3 \end{aligned} \tag{4.24}$$

The whole solution including the A_t can be given a Lorentz boost with velocity v in the x direction and the resulting solution has a A_x^{new} given by $A_x^{new} = \beta A_t$, where $\beta = \frac{v}{\sqrt{1-v^2}}$. As A_t has a non-trivial dependence on the radial coordinate z, A_x will also have the same non-trivial dependence. Dual of such a configuration is naturally interpreted as a boosted gauge theory plasma with charge. This solution may also be thought as the "backreacted" version of our constant A_x solution in a normal (non-superconducting) black hole background.

Now, let us assume the likely scenario that a superconducting black hole solution survives after considering gravity backreaction. Such a backreacted superconducting solution may also be given a Lorentz boost and the resulting solution will have a non-trivial dependence on A_x. Our supercurrent solution should *not* be confused with such a trivial boosted solution. Our solution should be interpreted as a solution where black hole horizon remains fixed (or is moving with a constant velocity) but the condensate has an arbitrary velocity with respect to the horizon. The supercurrent solution can not be generated by boosting, as it does not obey the constraint of a boosted solution, i.e. $A_x^{new} = \beta A_t$ and $g_{tx}^{new} = -\beta(g_{tt} + g_{xx})$. With a chemical potential S_x, it is likely that the dominant solution at low temperature will be a supercurrent type solution. Whether the structure of the phase diagram changes significantly after considering gravity backreaction is an open question.

4.7 Conclusions

In this paper we exhibit a static solution to the system with a charged scalar field coupled to the AdS black hole, which in the dual field theory corresponds to a static current flowing

in a superconducting fluid with no emf applied. We see an interesting phase structure, with a first order transition to the normal state at low temperatures as the fluid velocity is increased. At temperatures close to the critical value T_c, the transition becomes second order. As mentioned in the previous section, it would be nice to verify whether the phase diagram is modified in the fully back reacted geometry.

The model we have considered does not have any magnetic field in the boundary, as A_x does not depend on any of the field theory directions y. One can turn on a non-trivial magnetic field by incorporating a dependence on y in A_x, i.e., $A_x \equiv A_x(z, y)$. This can be used to study phenomena such as the Meissner effect. In particular, one can check the nature of the superconductor, i.e., whether it is Type I or Type II. In the andlatter case one can try to find vortex solutions. However, in this case the field equations become coupled nonlinear partial differential equations, which are harder to solve. It would also be interesting to study the modifications of these models to include impurity etc.

Embedding the superconducting gravity solutions into string / M theory is an important issue. Whether any probe brane configuration in some AdS like space gives rise to the type of Lagrangian we are discussing, would be an interesting avenue to explore.

As we have discussed, the $U(1)$ symmetry in our model is a realized globally in the boundary. It will be an interesting direction to setup some brane/gravity model where the symmetry breaking is local. That would be more akin to real life superconducting materials.

We have just begun to understand strongly coupled physics of condensed matter systems holographically. Exploring these modifications may allow us to extract new information about the universality classes and phase structures of strongly coupled systems.

Chapter 5

Conclusion and Outlook

In this thesis we discuss three examples of using the gauge/gravity duality to study strongly coupled phenomena in gravitation and field theories. To the very least these examples show that the gauge/gravity duality provides us with a new way of constructing effective theories that can be used to extract the essential physics governing these strongly coupled phenomena. Furthermore, constructing effective theories using different configurations of D branes or objects in M theory offers us an opportunity to study strongly coupled physics in theories differing in matter content and retaining different amount of supersymmetry in similar holographic setups. We can establish new universality classes suitable for analyzing these theories at strongly coupled regimes. Here we conclude by mentioning works that have already appeared in the literature and are related to the topics discussed in this thesis. We also point out possible future directions and extensions.

In Chapter two, we have seen that one can analyze the phase structure of weakly coupled gauge theory through an effective matrix model. When a pure gauge theory is placed on a small two sphere, we find through a three loop calculation that the deconfinement transition is second-order. The nature of the deconfinement transitions in $3+1$ and $1+1$ dimensions have been analyzed in a similar fashion[32, 33]. Through the gauge/gravity duality, the matrix model gives us a way to analyze the thermodynamics of gravitational theories when the curvature corrections are important. In particular, by carefully examine a matrix model similar to the one obtained in chapter two, the correspondence point [88] – the point where a small black hole is indistinguishable from a long fundamental string has been identified in the matrix model [79, 80]. One can also extend the analysis of the phase diagram to where the chemical potentials conjugate to the R charges are turned on. The extended phase diagram obtained through the corresponding matrix model can be compared to that of R charged black holes in ten dimensions or five dimensional rotating black holes whose angular momenta can be related to the R charges through dimensional reduction. Such analysis has been performed and demonstrated qualitative agreement between the phase structures of the two systems[84].

The effects of the baryon chemical potential can also be incorporated in the matrix model. Unfortunately it seems that at the large N limit the distinction between $SU(N)$ and $U(N)$ disappears and $1/N$ corrections would be required for such endeavor. Another interesting direction would be to analyze the effects of fundamental degrees of freedom on the deconfinement transition[81, 82]. It is well known that the deconfinement transition softens as the number of flavors to the number of colors ratio increases. Such softening has been seen explicitly in the matrix model computation[83]. Most recently, the black hole information

paradox has been rephrased in terms of the matrix quantum mechanics [86, 87, 89]. It would be interesting to study bulk dynamical problems in this setting.

Next, we use perturbative calculations in gravity to study the thermodynamics of strongly coupled gauge theories. Recent developments have given us new insights towards constructing gravity duals of more realistic models of QCD and their phase structures can be studied through perturbation theories in the quenched approximation. Using this setup, Sakai and Sugimoto constructed the gravity dual of a gauge theory with deconfinement transition and chiral symmetry restoration. We study this model at finite baryon chemical potential and zero temperature. We identify a first-order transition from vacuum to a phase with finite baryon density in the case of zero quark mass. In the finite density phase, the baryons form a condensate on the flavor branes and the condensate has a well defined edge in the holographic direction, which corresponds to an energy scale in the gauge theory. The condensate expands towards the UV as the chemical potential is raised. We propose that this is a bulk manifestation of the quark Fermi surface in the gauge theory. Similar transitions from vacuum to nuclear matter have also been found in other models of holographic gauge theory. It is found that when $D7$ branes are embedded in the Poincare patch of anti-de Sitter spacetime the condensate involves both fermions and bosons. It is interesting to study whether the Fermi surface would still form in these cases. However, at zero temperature, the distribution of the condensate is hidden behind the Poincare horizon. We have performed analysis to study the situation in the global coordinate where the distribution of the condensate has to be solved as part of the equations of motion. It turns out that the expansion of the condensate is present in this model as well as other holographic QCD constructions where the condensate involves a hypermultiplet [91]. It would be also interesting to see the case when the condensate involves only bosons [85]. Other signatures of a Fermi surface at strong coupling such as the appearance of a singularity in certain two point functions of quasi-particle excitation have also been studied in the holographic context [90]. The gravitational description of the Fermi surface and its instabilities will improve our understanding of the mechanisms behind the phase transitions of QCD.

Another important development in studying strongly coupled gauge theory with their gravity duals is that they provide a way to understand the hydrodynamics of strongly coupled quark gluon plasma [100, 103]. Dynamical properties such as various diffusion coefficients and viscosity can be extracted from Kubo type formula with the correlation functions computed in the dual gravity theory. There was previously no analytic methods to compute these quantities, and numerical techniques such as lattice gauge theory also face technical challenges due to their intrinsic Euclidean nature. Based on results from gauge/gravity duality, a universal bound for the viscosity to entropy density ratio is proposed [65].

$$\frac{\eta}{s} \geq \frac{1}{4\pi} \tag{5.1}$$

This bound is found to be saturated at leading large N_c and large 't Hooft coupling limit in most examples analyzed even when fundamental degrees of freedom are present [63].

Although systems violating the bound have also being discovered in cases when a certain set of higher curvature corrections are included[104]. The universality gives hope that results from gravity calculations may also be applied to real QCD and compared to experimental data at the Relativistic Heavy Ion Collider. These dynamical quantities have also been recently used to obtain the thermodynamics of large rotating charged black holes in anti-de Sitter space-times in various dimensions. It would be interesting to calculate these quantities at finite chemical potential. This will require taking into account of the back reaction of the embedding and the gauge fields of the flavor branes perturbatively. In particular, it will be interesting to see if the viscosity to entropy density ratio bound is still saturated.

It is also possible to consider extensions to the holographic models of gauge theories. It is known that the QCD phase diagram is sensitive to physical parameters such as the quark mass and the θ angle. It would be interesting to study these effects using gravity. Specifically, in the Sakai Sugimoto model, quark masses are turned on by including a bulk field corresponding to open strings stretched between the flavor branes [102], while a nonzero gauge theory θ angle corresponds to a Wilson loop for the RR one form around the compact direction in the geometry[105].

Thirdly, we use a bottom up approach to construct a holographic superconducting/superfluid system. We analyze the superfluid solution at zero frequency and mapped out the phase diagram as a function of temperature and the superfluid velocity. We find that interesting phase structure as the superconducting transition switches from second-order to first-order as the superfluid velocity is increased. This suggests that a critical point exists in the phase diagram and agrees qualitatively with the weak coupling analysis using the BCS theory.

Several interesting aspects of the holographic model for superconductor/superfluid have been revealed. Close to zero temperature, the conductivity develops resonance poles at finite frequency when the mass of the condensing scalar field is at the Breitenlohner-Freedman bound [129] . It is possible to consider the mass of the scalar field as a continuous parameter and find the critical mass where the resonance poles starts to appear. Our analysis suggests that the transition occurs near the conformal value. The resonance behavior is related to the formation of bound states of the scalar field from quasi-normal modes as poles in their correlation functions reach the real axis in the complex frequency plane. It will be interesting to study the effects of the backreaction of these superconducting bound states on the background geometry.

The construction above can be generalized to where the gauge fields are non-Abelian [93, 97, 98]. This also allows for embedding of the model into string theory. We place a pair of flavor $D7$ branes in the background generated by a stack of $D3$ branes. The dual gauge theory is a model for two flavor supersymmetric QCD at large N_c. The $U(2)$ gauge fields on the world volume of the flavor branes are mapped to the expectation values of mesonic operators in the dual fields theory. We find that certain mesonic operators condense when the critical iso-spin chemical potential is above a critical value. The condensates break the $U(1)$ iso-spin symmetry. The superfluid solution and the corresponding phase diagram is constructed, showing similar features as the Abelian case. The (pion) superfluid phase is

known to exist in QCD at large iso-spin chemical potential. Since the dual gauge theories is explicitly known, we can use such setup to study the microscopics of the holographic superconductor/superfluid. On the string theory side, other fields such as the transverse scalars on the flavor branes can also condense through the same mechanism. We can map out the pattern of condensation of these fields as the iso-spin chemical potential is raised and its field theory implications. It is also important to study whether the condensates modifies the embedding of the flavor branes. Most recently, another way to embed the holographic superconducting systems into string theory has been found in the context of Calabi Yau compactification of type IIA string theory. It has been used to analyze the stability of a landscape of these compactification solutions towards the formation of these superconducting states [94].

It is well known that superfluids possess unique hydrodynamic properties. It will be interesting to investigate these properties using the holographic setup. Hydrodynamic quantities such as various diffusion coefficients can be extracted from correlation functions computed in the dual gravity theory. We hope to compute the viscosity in the geometry where the backreaction of the condensate is taken into account[95]. The coefficients can also be extracted from long wavelength expansions of the gravitational equations of motion [101]. It will also be interesting to study the causal structure corresponding to these superconducting solutions. Such investigations have proven to be a valuable tool to obtain new information about relativistic hydrodynamics.

Bibliography

[1] Juan Martin Maldacena. The large N limit of superconformal field theories and supergravity. *Adv. Theor. Math. Phys.*, 2:231–252, 1998, hep-th/9711200.

[2] C. V. Johnson, "D-brane primer," arXiv:hep-th/0007170.
J. Polchinski, "String theory. Vol.1, 2," *Cambridge, UK: Univ. Pr. (1998) 531 p*

[3] E. Witten, "Anti-de Sitter space, thermal phase transition, and confinement in gauge theories," Adv. Theor. Math. Phys. **2**, 505 (1998) [arXiv:hep-th/9803131].

[4] G. 't Hooft, "A PLANAR DIAGRAM THEORY FOR STRONG INTERACTIONS," Nucl. Phys. B **72** (1974) 461.

[5] D. Youm, "Black holes and solitons in string theory," Phys. Rept. **316**, 1 (1999) [arXiv:hep-th/9710046].

[6] O. Aharony, S. S. Gubser, J. M. Maldacena, H. Ooguri and Y. Oz, "Large N field theories, string theory and gravity," Phys. Rept. **323**, 183 (2000) [arXiv:hep-th/9905111].

[7] E. Witten, "Anti-de Sitter space and holography," Adv. Theor. Math. Phys. **2**, 253 (1998) [arXiv:hep-th/9802150].

[8] I. R. Klebanov and E. Witten, "AdS/CFT correspondence and symmetry breaking," Nucl. Phys. B **556** (1999) 89 [arXiv:hep-th/9905104].

[9] D. Z. Freedman, S. D. Mathur, A. Matusis and L. Rastelli, "Correlation functions in the CFT(d)/AdS($d+1$) correspondence," Nucl. Phys. B **546**, 96 (1999) [arXiv:hep-th/9804058].

[10] J. L. Hovdebo, M. Kruczenski, D. Mateos, R. C. Myers and D. J. Winters, "Holographic mesons: Adding flavor to the AdS/CFT duality," Int. J. Mod. Phys. A **20**, 3428 (2005).

[11] B. A. Burrington, J. T. Liu, L. A. Pando Zayas and D. Vaman, "Holographic duals of flavored N = 1 super Yang-Mills: Beyond the probe approximation," JHEP **0502**, 022 (2005) [arXiv:hep-th/0406207].

[12] F. Canoura, P. Merlatti and A. V. Ramallo, "The supergravity dual of 3d supersymmetric gauge theories with unquenched flavors," JHEP **0805**, 011 (2008) [arXiv:0803.1475 [hep-th]].

[13] J. K. Erickson, G. W. Semenoff and K. Zarembo, "Wilson loops in N = 4 supersymmetric Yang-Mills theory," Nucl. Phys. B **582**, 155 (2000) [arXiv:hep-th/0003055].

[14] N. Itzhaki, J. M. Maldacena, J. Sonnenschein and S. Yankielowicz, "Supergravity and the large N limit of theories with sixteen supercharges," Phys. Rev. D **58**, 046004 (1998) [arXiv:hep-th/9802042].

[15] T. Banks, W. Fischler, S. H. Shenker and L. Susskind, "M theory as a matrix model: A conjecture," Phys. Rev. D **55**, 5112 (1997) [arXiv:hep-th/9610043].

[16] T. Banks, N. Seiberg and S. H. Shenker, "Branes from matrices," Nucl. Phys. B **490**, 91 (1997) [arXiv:hep-th/9612157].

[17] M. Berkooz, M. Rozali and N. Seiberg, "Matrix description of M theory on T**4 and T**5," Phys. Lett. B **408**, 105 (1997) [arXiv:hep-th/9704089].

[18] D. E. Berenstein, J. M. Maldacena and H. S. Nastase, "Strings in flat space and pp waves from N = 4 super Yang Mills," JHEP **0204**, 013 (2002) [arXiv:hep-th/0202021].

[19] F. Karsch, "Lattice QCD at high temperature and density," Lect. Notes Phys. **583**, 209 (2002) [arXiv:hep-lat/0106019].

[20] E. Keski-Vakkuri and P. Kraus, "Quantum Hall Effect in AdS/CFT," JHEP **0809**, 130 (2008) [arXiv:0805.4643 [hep-th]].

[21] J. L. Davis, P. Kraus and A. Shah, "Gravity Dual of a Quantum Hall Plateau Transition," JHEP **0811**, 020 (2008) [arXiv:0809.1876 [hep-th]].

[22] S. A. Hartnoll, P. K. Kovtun, M. Muller and S. Sachdev, Phys. Rev. B **76**, 144502 (2007) [arXiv:0706.3215 [cond-mat.str-el]].

[23] S. W. Hawking and G. T. Horowitz, "The Gravitational Hamiltonian, action, entropy and surface terms," Class. Quant. Grav. **13**, 1487 (1996) [arXiv:gr-qc/9501014].

[24] S. W. Hawking and D. N. Page, "Thermodynamics Of Black Holes In Anti-De Sitter Space," Commun. Math. Phys. **87** (1983) 577.

[25] O. Aharony, O. Bergman, D. L. Jafferis and J. Maldacena, "N=6 superconformal Chern-Simons-matter theories, M2-branes and their JHEP **0810**, 091 (2008) [arXiv:0806.1218 [hep-th]].

[26] R. Hagedorn, "Statistical thermodynamics of strong interactions at high energies. 3. Heavy-pair (quark) production rates," Nuovo Cim. Suppl. **6**, 311 (1968).

[27] J. J. Atick and E. Witten, "The Hagedorn Transition and the Number of Degrees of Freedom of String Theory," Nucl. Phys. B **310**, 291 (1988).

[28] J. M. Maldacena, "Wilson loops in large N field theories," Phys. Rev. Lett. **80**, 4859 (1998) [arXiv:hep-th/9803002].

[29] K. Rajagopal and F. Wilczek, "The condensed matter physics of QCD," arXiv:hep-ph/0011333.

[30] D. J. Gross and E. Witten, "Possible Third Order Phase Transition In The Large N Lattice Gauge Theory," Phys. Rev. D **21**, 446 (1980).

[31] M. Creutz, "On Invariant Integration Over SU(N)," J. Math. Phys. **19**, 2043 (1978).

[32] O. Aharony, J. Marsano, S. Minwalla, K. Papadodimas and M. Van Raamsdonk, "The Hagedorn / deconfinement phase transition in weakly coupled large N gauge theories," arXiv:hep-th/0310285.

[33] O. Aharony, J. Marsano, S. Minwalla, K. Papadodimas and M. Van Raamsdonk, "A first order deconfinement transition in large N Yang-Mills theory on a small S**3," Phys. Rev. D **71**, 125018 (2005) [arXiv:hep-th/0502149].

[34] B. Sundborg, "The Hagedorn transition, deconfinement and N = 4 SYM theory," Nucl. Phys. B **573**, 349 (2000) [arXiv:hep-th/9908001].

[35] M. Teper, "The Finite temperature phase transition of SU(2) gauge fields in (2+1)-dimensions," Phys. Lett. B **313**, 417 (1993).
J. Christensen, G. Thorleifsson, P. H. Damgaard and J. F. Wheater, "Thermodynamics of SU(3) lattice gauge theory in (2+1)-dimensions," Nucl. Phys. B **374**, 225 (1992).
Philippe de Forcrand, Oliver Jahn, " Deconfinement transition in 2+1-dimensional SU(4) lattice gauge theory," hep-lat/0309153
K. Holland, "Another weak first order deconfinement transition: three-dimensional SU(5) gauge theory," JHEP 0601 (2006) 023,
J. Liddle, M. Teper "The deconfining phase transition for SU(N) theories in 2+1 dimensions" arXiv:hep-th/0509082.

[36] This file is available at http://www.fas.harvard.edu/ papadod/3loop/3loop.html.

[37] B. Svetitsky, L. G. Yaffe , "Critical Behavior At Finite Temperature Confinement Transitions," Nucl. Phys. B210:423,1982 .

[38] M. R. Douglas and V. A. Kazakov, "Large N phase transition in continuum QCD in two-dimensions," Phys. Lett. B **319**, 219 (1993) [arXiv:hep-th/9305047].

[39] E. D'Hoker, "Perturbative Results On QCD In Three-Dimensions At Finite Temperature," Nucl. Phys. B **201**, 401 (1982).

[40] D. V. Boulatov, "Wilson loop on a sphere," Mod. Phys. Lett. A **9**, 365 (1994) [arXiv:hep-th/9310041].

[41] R. Narayanan and H. Neuberger, "Infinite N phase transitions in continuum Wilson loop operators," JHEP **0603**, 064 (2006) [arXiv:hep-th/0601210].
F. Bursa and M. Teper, "Strong to weak coupling transitions of SU(N) gauge theories in 2+1 dimensions," arXiv:hep-th/0511081.

[42] Edmonds, A. R. Angular momentum in quantum mechanics Princeton University Press, 1974.

[43] Jones, M. N. (Michael Norman), Spherical harmonics and tensors for classical field theory Published: Letchworth, Hertfordshire, England : Research Studies Press ; New York : Wiley, c1985.

[44] T. Schafer, "Phases of QCD," arXiv:hep-ph/0509068.

[45] M. A. Stephanov, "QCD phase diagram: An overview," PoS **LAT2006**, 024 (2006) [arXiv:hep-lat/0701002].

[46] D. T. Son and A. O. Starinets, "Viscosity, Black Holes, and Quantum Field Theory," arXiv:0704.0240 [hep-th].

[47] O. Aharony, S. S. Gubser, J. M. Maldacena, H. Ooguri and Y. Oz, "Large N field theories, string theory and gravity," Phys. Rept. **323**, 183 (2000) [arXiv:hep-th/9905111].

[48] A. Karch and E. Katz, "Adding flavor to AdS/CFT," JHEP **0206**, 043 (2002) [arXiv:hep-th/0205236].

[49] I. R. Klebanov and M. J. Strassler, "Supergravity and a confining gauge theory: Duality cascades and chiSB-resolution of naked singularities," JHEP **0008**, 052 (2000) [arXiv:hep-th/0007191].

[50] S. Kobayashi, D. Mateos, S. Matsuura, R. C. Myers and R. M. Thomson, "Holographic phase transitions at finite baryon density," JHEP **0702**, 016 (2007) [arXiv:hep-th/0611099].

[51] T. Sakai and S. Sugimoto, "Low energy hadron physics in holographic QCD," Prog. Theor. Phys. **113**, 843 (2005) [arXiv:hep-th/0412141].

[52] O. Bergman, G. Lifschytz and M. Lippert, "Holographic Nuclear Physics," arXiv:0708.0326 [hep-th].

[53] J. L. Davis, M. Gutperle, P. Kraus and I. Sachs, "Stringy NJL and Gross-Neveu models at finite density and temperature," arXiv:0708.0589 [hep-th].

[54] O. Aharony, J. Sonnenschein and S. Yankielowicz, "A holographic model of deconfinement and chiral symmetry restoration," Annals Phys. **322**, 1420 (2007) [arXiv:hep-th/0604161].

[55] K. Hashimoto, T. Hirayama and A. Miwa, "Holographic QCD and pion mass," JHEP **0706**, 020 (2007) [arXiv:hep-th/0703024].

[56] N. Evans and E. Threlfall, "Quark Mass in the Sakai-Sugimoto Model of Chiral Symmetry Breaking," arXiv:0706.3285 [hep-th].

[57] P. Basu, A. Mukherjee and H. H. Shieh, "Supercurrent: Vector Hair for an AdS Black Hole," arXiv:0809.4494 [hep-th].

[58] E. Witten, "Baryons In The 1/N Expansion," Nucl. Phys. B **160**, 57 (1979).

[59] E. Witten, "Baryons and branes in anti de Sitter space," JHEP **9807**, 006 (1998) [arXiv:hep-th/9805112].

[60] M. A. Halasz, A. D. Jackson, R. E. Shrock, M. A. Stephanov and J. J. M. Verbaarschot, "On the phase diagram of QCD," Phys. Rev. D **58**, 096007 (1998) [arXiv:hep-ph/9804290].

[61] H. Hata, T. Sakai, S. Sugimoto and S. Yamato, "Baryons from instantons in holographic QCD," arXiv:hep-th/0701280.

[62] D. K. Hong, M. Rho, H. U. Yee and P. Yi, "Dynamics of Baryons from String Theory and Vector Dominance," arXiv:0705.2632 [hep-th].
D. K. Hong, M. Rho, H. U. Yee and P. Yi, "Chiral dynamics of baryons from string theory," arXiv:hep-th/0701276.

[63] D. Mateos, R. C. Myers and R. M. Thomson, "Holographic viscosity of fundamental matter," Phys. Rev. Lett. **98**, 101601 (2007) [arXiv:hep-th/0610184].

[64] D. V. Deryagin, D. Y. Grigoriev and V. A. Rubakov, "Standing wave ground state in high density, zero temperature QCD at large Int. J. Mod. Phys. A **7**, 659 (1992).

[65] P. Kovtun, D. T. Son and A. O. Starinets, "Viscosity in strongly interacting quantum field theories from black hole physics," Phys. Rev. Lett. **94**, 111601 (2005) [arXiv:hep-th/0405231].

[66] E. Shuster and D. T. Son, "On finite-density QCD at large N(c)," Nucl. Phys. B **573**, 434 (2000) [arXiv:hep-ph/9905448].

[67] K. Nawa, H. Suganuma and T. Kojo, Too "Brane-induced Skyrmions: Baryons in holographic QCD," arXiv:hep-th/0701007.

[68] K. Nawa, H. Suganuma and T. Kojo, "Baryons in Holographic QCD," Phys. Rev. D **75**, 086003 (2007) [arXiv:hep-th/0612187].

[69] K. Y. Kim, S. J. Sin and I. Zahed, "Dense hadronic matter in holographic QCD," arXiv:hep-th/0608046.

[70] N. Horigome and Y. Tanii, "Holographic chiral phase transition with chemical potential," JHEP **0701**, 072 (2007) [arXiv:hep-th/0608198].

[71] S. J. Sin, "Gravity Back-reaction to the Baryon Density for Bulk Filling Branes," arXiv:0707.2719 [hep-th].

[72] D. Yamada, "Sakai-Sugimoto Model at High Density," arXiv:0707.0101 [hep-th].

[73] S. K. Domokos and J. A. Harvey, "Baryon number-induced Chern-Simons couplings of vector and axial-vector mesons in holographic QCD," arXiv:0704.1604 [hep-ph].

[74] Y. Kim, B. H. Lee, S. Nam, C. Park and S. J. Sin, "Deconfinement phase transition in holographic QCD with matter," arXiv:0706.2525 [hep-ph].

[75] Y. Kim, C. H. Lee and H. U. Yee, "Holographic Nuclear Matter in AdS/QCD," arXiv:0707.2637 [hep-ph].

[76] E. Antonyan, J. A. Harvey, S. Jensen and D. Kutasov, "NJL and QCD from string theory," arXiv:hep-th/0604017.

[77] A. Parnachev and D. A. Sahakyan, "Chiral phase transition from string theory," Phys. Rev. Lett. **97**, 111601 (2006) [arXiv:hep-th/0604173].

[78] A. Parnachev and D. A. Sahakyan, "Photoemission with chemical potential from QCD gravity dual," Nucl. Phys. B **768**, 177 (2007) [arXiv:hep-th/0610247].

[79] L. Alvarez-Gaume, C. Gomez, H. Liu and S. Wadia, "Finite temperature effective action, AdS(5) black holes, and 1/N expansion," Phys. Rev. D **71**, 124023 (2005) [arXiv:hep-th/0502227].

[80] L. Alvarez-Gaume, P. Basu, M. Marino and S. R. Wadia, "Blackhole / string transition for the small Schwarzschild blackhole of AdS(5) x S**5 and critical unitary matrix models," Eur. Phys. J. C **48**, 647 (2006) [arXiv:hep-th/0605041].

[81] H. J. Schnitzer, "Confinement / deconfinement transition of large N gauge theories in perturbation theory with N(f) fundamentals: N(f)/N finite," arXiv:hep-th/0612099.

[82] H. J. Schnitzer, "Confinement / deconfinement transition of large N gauge theories with N(f) fundamentals: N(f)/N finite," Nucl. Phys. B **695**, 267 (2004) [arXiv:hep-th/0402219].

[83] P. Basu and A. Mukherjee, "Dissolved deconfinement: Phase Structure of large N gauge theories with fundamental matter," Phys. Rev. D **78**, 045012 (2008) [arXiv:0803.1880 [hep-th]].

[84] P. Basu and S. R. Wadia, "R-charged AdS(5) black holes and large N unitary matrix models," Phys. Rev. D **73**, 045022 (2006) [arXiv:hep-th/0506203].

[85] M. Van Raamsdok and K. Whyte, To appear.

[86] N. Iizuka and J. Polchinski, "A Matrix Model for Black Hole Thermalization," JHEP **0810**, 028 (2008) [arXiv:0801.3657 [hep-th]].

[87] N. Iizuka, T. Okuda and J. Polchinski, "Matrix Models for the Black Hole Information Paradox," arXiv:0808.0530 [hep-th].

[88] G. T. Horowitz and J. Polchinski, "A correspondence principle for black holes and strings," Phys. Rev. D **55**, 6189 (1997) [arXiv:hep-th/9612146].

[89] G. Festuccia and H. Liu, "Excursions beyond the horizon: Black hole singularities in Yang-Mills theories. I," JHEP **0604**, 044 (2006) [arXiv:hep-th/0506202].

[90] M. Kulaxizi and A. Parnachev, "Holographic Responses of Fermion Matter," arXiv:0811.2262 [hep-th].

[91] H. H. Shieh and G. van Anders, "Comments on Holographic Fermi Surfaces," arXiv:0810.1661 [hep-th].

[92] Sean A. Hartnoll, Christopher P. Herzog, and Gary T. Horowitz. Building an AdS/CFT superconductor. 2008, 0803.3295.

[93] P. Basu, J. He, A. Mukherjee and H. H. Shieh, "Superconductivity from D3/D7: Holographic Pion Superfluid," arXiv:0810.3970 [hep-th].

[94] F. Denef and S. A. Hartnoll, "Landscape of superconducting membranes," arXiv:0901.1160 [hep-th].

[95] S. A. Hartnoll, C. P. Herzog and G. T. Horowitz, "Holographic Superconductors," JHEP **0812**, 015 (2008) [arXiv:0810.1563 [hep-th].

[96] C. P. Herzog, P. K. Kovtun and D. T. Son, "Holographic model of superfluidity," arXiv:0809.4870 [hep-th].

[97] M. Ammon, J. Erdmenger, M. Kaminski and P. Kerner, "Flavor Superconductivity from Gauge/Gravity Duality," arXiv:0903.1864 [hep-th].

[98] M. Ammon, J. Erdmenger, M. Kaminski and P. Kerner, "Superconductivity from gauge/gravity duality with flavor," arXiv:0810.2316 [hep-th].

[99] Tadakatsu Sakai and Shigeki Sugimoto. Low energy hadron physics in holographic QCD. *Prog. Theor. Phys.*, 113:843–882, 2005, hep-th/0412141.

[100] Dam T. Son and Andrei O. Starinets. Viscosity, Black Holes, and Quantum Field Theory. *Ann. Rev. Nucl. Part. Sci.*, 57:95–118, 2007, 0704.0240.

[101] S. Bhattacharyya *et al.*, "Local Fluid Dynamical Entropy from Gravity," JHEP **0806**, 055 (2008) [arXiv:0803.2526 [hep-th]].

[102] O. Bergman, S. Seki and J. Sonnenschein, "Quark mass and condensate in HQCD," JHEP **0712**, 037 (2007) [arXiv:0708.2839 [hep-th]].

[103] D. Mateos, "String Theory and Quantum Chromodynamics," Class. Quant. Grav. **24**, S713 (2007) [arXiv:0709.1523 [hep-th]].

[104] M. Brigante, H. Liu, R. C. Myers, S. Shenker and S. Yaida, "Viscosity Bound Violation in Higher Derivative Gravity," Phys. Rev. D **77**, 126006 (2008) [arXiv:0712.0805 [hep-th]].

[105] E. Witten, "Theta dependence in the large N limit of four-dimensional gauge theories," Phys. Rev. Lett. **81**, 2862 (1998) [arXiv:hep-th/9807109].

[106] Christopher P. Herzog, Pavel Kovtun, Subir Sachdev, and Dam Thanh Son. Quantum critical transport, duality, and M-theory. *Phys. Rev.*, D75:085020, 2007, hep-th/0701036.

[107] Koushik Balasubramanian and John McGreevy. Gravity duals for non-relativistic CFTs. *Phys. Rev. Lett.*, 101:061601, 2008, 0804.4053.

[108] Allan Adams, Koushik Balasubramanian, and John McGreevy. Hot Spacetimes for Cold Atoms. 2008, 0807.1111.

[109] Juan Maldacena, Dario Martelli, and Yuji Tachikawa. Comments on string theory backgrounds with non- relativistic conformal symmetry. 2008, 0807.1100.

[110] Shamit Kachru, Xiao Liu, and Michael Mulligan. Gravity Duals of Lifshitz-like Fixed Points. 2008, 0808.1725.

[111] Christopher P. Herzog, Mukund Rangamani, and Simon F. Ross. Heating up Galilean holography. 2008, 0807.1099.

[112] Sean A. Hartnoll and Christopher P. Herzog. Impure AdS/CFT. *Phys. Rev.*, D77:106009, 2008, 0801.1693.

[113] Michael Tinkham. *Introduction to Superconductivity*. McGraw-Hill, Inc., 1996.

[114] Steven S. Gubser. Breaking an Abelian gauge symmetry near a black hole horizon. 2008, 0801.2977.

[115] R. Bartnik and J. Mckinnon. Particle - Like Solutions of the Einstein Yang-Mills Equations. *Phys. Rev. Lett.*, 61:141–144, 1988.

[116] P. Bizon. Colored black holes. *Phys. Rev. Lett.*, 64:2844–2847, 1990.

[117] N. E. Mavromatos. Eluding the no-hair conjecture for black holes. 1995, gr-qc/9606008.

[118] Mikhail S. Volkov and Dmitri V. Gal'tsov. Gravitating non-Abelian solitons and black holes with Yang-Mills fields. *Phys. Rept.*, 319:1–83, 1999, hep-th/9810070.

[119] Steven S. Gubser. Colorful horizons with charge in anti-de Sitter space. 2008, 0803.3483.

[120] Steven S. Gubser and Fabio D. Rocha. The gravity dual to a quantum critical point with spontaneous symmetry breaking. 2008, 0807.1737.

[121] Matthew M. Roberts and Sean A. Hartnoll. Pseudogap and time reversal breaking in a holographic superconductor. *JHEP*, 08:035, 2008, 0805.3898.

[122] Steven S. Gubser and Silviu S. Pufu. The gravity dual of a p-wave superconductor. 2008, 0805.2960.

[123] Wen-Yu Wen. Inhomogeneous magnetic field in AdS/CFT superconductor. 2008, 0805.1550.

[124] Tameem Albash and Clifford V. Johnson. A Holographic Superconductor in an External Magnetic Field. 2008, 0804.3466.

[125] Kengo Maeda and Takashi Okamura. Characteristic length of an AdS/CFT superconductor. 2008, 0809.3079.

[126] Jacob D. Bekenstein. Black hole hair: Twenty-five years after. 1996, gr-qc/9605059.

[127] Peter Breitenlohner and Daniel Z. Freedman. Stability in Gauged Extended Supergravity. *Ann. Phys.*, 144:249, 1982.

[128] L. J. Romans. Supersymmetric, cold and lukewarm black holes in cosmological Einstein-Maxwell theory. *Nucl. Phys.*, B383:395–415, 1992, hep-th/9203018.

[129] G. T. Horowitz and M. M. Roberts, Phys. Rev. D **78**, 126008 (2008) [arXiv:0810.1077 [hep-th]].

Appendix A

Appendix to Chapter 2

A.1 Spherical Harmonics

In this section we set up our conventions for the vector spherical harmonics [42, 43]. The definition of a vector spherical harmonics is:

$$\bar{V}_{JlM} = \sum_q V^q_{JlM} \widehat{e}_q = \sum_{m,q} Y_{lm} \widehat{e}_q (l\, m\, 1\, q |\, J\, M) \tag{A.1}$$

where the $\widehat{e}_q$ are in the spherical tensor basis:

$$\begin{aligned} \widehat{e}_+ &= -\frac{\widehat{e}_x + i\widehat{e}_y}{2^{1/2}} \\ \widehat{e}_- &= \frac{\widehat{e}_x - i\widehat{e}_y}{2^{1/2}} \\ \widehat{e}_0 &= \widehat{e}_z. \end{aligned} \tag{A.2}$$

The raising and lowering of the vector index q is given by:

$$V_{JlM,q} = (-1)^q V^{-q}_{JlM} \tag{A.3}$$

and

$$\bar{V}^*_{JlM} = (-1)^{M+J-l+1} \bar{V}_{Jl-M}. \tag{A.4}$$

The vector spherical harmonics can be used to expand any well behaved vector fields in R^3 and they can be categorized into the following orthonormal basis [43]:

$$\begin{aligned} \bar{P}_{JM} &= \frac{1}{(2J+1)^{1/2}} [-(J+1)^{1/2} \bar{V}_{JJ+1M} + J^{1/2} \bar{V}_{JJ-1M}] = \bar{r} Y_{JM} \\ \bar{B}_{JM} &= \frac{1}{(2J+1)^{1/2}} [J \frac{(J+1)^{1/2}}{r} \bar{V}_{JJ+1M} + (J+1) \frac{J^{1/2}}{r} \bar{V}_{JJ-1M}] = \nabla Y_{JM} \\ \bar{C}_{JM} &= -\bar{r} \times \frac{r}{(J(J+1))^{1/2}} \bar{B}_{JM} = -i \bar{V}_{JJM}. \end{aligned} \tag{A.5}$$

The first of the above does not live in the tangent space of the two sphere, while the second do not contribute to the effective action by gauge fixing. We have the following useful expression for $\bar{V}_{JJM}$ following from the last of the above identities:

$$V_{JJM,q} = \frac{L_q}{(J(J+1))^{1/2}} Y_{JM+q} \tag{A.6}$$

$$
\begin{aligned}
L_+ &= \frac{-1}{2^{1/2}}((J-M)(J+M+1))^{1/2} = -\frac{(-1)^{J-M}}{2}((2J+2)(2J+1)(2J))^{1/2}\begin{pmatrix} J & J & 1 \\ M & -M-1 & 1 \end{pmatrix} \\
L_- &= \frac{1}{2^{1/2}}((J+M)(J-M+1))^{1/2} = \frac{(-1)^{J+M}}{2}((2J+2)(2J+1)(2J))^{1/2}\begin{pmatrix} J & J & 1 \\ -M & M-1 & 1 \end{pmatrix} \\
L_0 &= M = \frac{(-1)^{J-M}}{2}((2J+2)(2J+1)(2J))^{1/2}\begin{pmatrix} J & J & 1 \\ M & -M & 0 \end{pmatrix}. \qquad \text{(A.7)}
\end{aligned}
$$

A.2 Effective Vertices

As we have seen in section 3, when expended in terms of scalar and vector spherical harmonics, the Lagrangian for pure Yang-Mills theory on $S^2 \times S^1$ contains effective vertices that are integrals of products of spherical harmonics. Here we explicitly compute effective vertices. We will write the results with 3-j symbols:

$$
\begin{pmatrix} j_1 & j_2 & j_3 \\ m_1 & m_2 & m_3 \end{pmatrix} = (-1)^{j_1-j_2-m_3}(2j_3+1)^{-1/2}(j_1\, m_1\, j_2\, m_2 | j_3\, -m_3). \qquad \text{(A.8)}
$$

A useful formula for sum of products of three 3-j symbols:

$$
\begin{aligned}
\sum_{\mu_1\mu_2\mu_3} \quad & (-1)^{l_1+l_2+l_3+\mu_1+\mu_2+\mu_3}\begin{pmatrix} j_1 & l_2 & l_3 \\ m_1 & \mu_2 & -\mu_3 \end{pmatrix}\begin{pmatrix} l_1 & j_2 & l_3 \\ -\mu_1 & m_2 & \mu_3 \end{pmatrix} \\
\times \quad & \begin{pmatrix} l_1 & l_2 & j_3 \\ \mu_1 & -\mu_2 & m_3 \end{pmatrix} = \begin{pmatrix} j_1 & j_2 & j_3 \\ m_1 & m_2 & m_3 \end{pmatrix}\begin{Bmatrix} j_1 & j_2 & j_3 \\ l_1 & l_2 & l_3 \end{Bmatrix}. \qquad \text{(A.9)}
\end{aligned}
$$

• SSS (given by Gaunt's formula for associated Legendre polynomials)[43]:

$$
\begin{aligned}
\int_{S^2} Y_{l_1m_1}Y_{l_2m_2}Y_{l_3m_3} &= (\frac{(2l_1+1)(2l_2+1)(2l_3+1)}{4\pi})^{1/2}\begin{pmatrix} l_1 & l_2 & l_3 \\ 0 & 0 & 0 \end{pmatrix}\begin{pmatrix} l_1 & l_2 & l_3 \\ m_1 & m_2 & m_3 \end{pmatrix} \\
&= I_{l_1l_2l_3}\begin{pmatrix} l_1 & l_2 & l_3 \\ m_1 & m_2 & m_3 \end{pmatrix} \qquad \text{(A.10)}
\end{aligned}
$$

• VSV, The D vertex

$$
\begin{aligned}
D^{\alpha_1\alpha_2\alpha_3} = \int_{S^2} \bar{V}_{l_1l_1m_1}\bar{V}_{l_2l_2m_2} \qquad & Y_{l_3m_3} = \\
(\frac{(2l_1+1)(2l_2+1)(2l_3+1)}{4\pi})^{1/2} \qquad & \frac{l_3(l_3+1)-l_1(l_1+1)-l_2(l_2+1)}{2(l_1(l_1+1)l_2(l_2+1))^{1/2}} \\
\begin{pmatrix} l_1 & l_2 & l_3 \\ 0 & 0 & 0 \end{pmatrix}\begin{pmatrix} l_1 & l_2 & l_3 \\ m_1 & m_2 & m_3 \end{pmatrix} &= R_1^{1/2}(l_1,l_2,l_3)\begin{pmatrix} l_1 & l_2 & l_3 \\ m_1 & m_2 & m_3 \end{pmatrix}. \qquad \text{(A.11)}
\end{aligned}
$$

Note $l_1+l_2+l_3$ has to be even for nonzero amplitudes.

• SVS, The C vertex

$$
C^{\alpha_3\alpha_2\alpha_1} = \int_{S^2} (\nabla Y_{l_1m_1})\bar{V}_{l_2l_2m_2}Y_{l_3m_3}
$$

$$= \frac{1}{2r}\left(\frac{(2l_1+1)(2l_2+1)(2l_3+1)}{4\pi}\right)^{1/2}\left(\frac{(J+1)(J-2l_3)(J-2l_2)(J-2l_1+1)}{l_2(l_2+1)}\right)^{1/2}$$
$$\begin{pmatrix} l_1-1 & l_2 & l_3 \\ 0 & 0 & 0 \end{pmatrix}\begin{pmatrix} l_1 & l_2 & l_3 \\ m_1 & m_2 & m_3 \end{pmatrix} = A_{l_1 l_2 l_3}\begin{pmatrix} l_1 & l_2 & l_3 \\ m_1 & m_2 & m_3 \end{pmatrix}. \tag{A.12}$$

where $J = l_1 + l_2 + l_3$ and it has to be odd for non-zero amplitudes.

• (curlV·r)(V×V·r), The E vertex

$$\begin{aligned} E^{\alpha_3\alpha_1\alpha_2} &= \int_{S^2}(\nabla \times V_{J_3J_3M_3}\cdot\widehat{r})(V_{J_1J_1M_1}\times V_{J_2J_2M_2}\cdot\widehat{r}) \\ &= -\left(\frac{J_3(J_3+1)}{J_1(J_1+1)}\right)^{1/2} A_{J_1J_2J_3}\begin{pmatrix} J_1 & J_2 & J_3 \\ M_1 & M_2 & M_3 \end{pmatrix} \\ &= \widetilde{A}_{J_1J_2J_3}\begin{pmatrix} J_1 & J_2 & J_3 \\ M_1 & M_2 & M_3 \end{pmatrix}. \end{aligned} \tag{A.13}$$

Note since $J = J_1+J_2+J_3$ has to be odd in order for $A_{J_1J_2J_3}$ to be nonzero, $\begin{pmatrix} J_1 & J_2 & J_3 \\ M_1 & M_2 & M_3 \end{pmatrix}$ will pick up a negative sign upon interchanging J_1, J_2. This suggests $\widetilde{A}_{J_1J_2J_3}$ needs to be symmetric in J_1, J_2, which can be checked to be true in our expression.

A.3 Summation Formulas

The following identities are useful in computing the two loop diagrams.

$$\sum_{m's} D^{\alpha\beta\gamma}D^{\bar{\alpha}\bar{\beta}\bar{\gamma}} = R_1(j_\alpha, j_\beta, j_\gamma) \tag{A.14}$$

$$\sum_{m's,j_\gamma} D^{\alpha\beta\gamma}D^{\bar{\alpha}\bar{\beta}\bar{\gamma}} = \frac{(2j_\alpha+1)(2j_\beta+1)}{8\pi} \tag{A.15}$$

$$\sum_{m's,j_\gamma} D^{\alpha\bar{\alpha}\gamma}D^{\beta\bar{\beta}\bar{\gamma}} = \frac{(2j_\alpha+1)(2j_\beta+1)}{4\pi} \tag{A.16}$$

where

$$\begin{aligned} R_1(l_1,l_2,l_3) &= \left(\frac{(2l_1+1)(2l_2+1)(2l_3+1)}{4\pi}\right)\frac{(l_3(l_3+1)-l_1(l_1+1)-l_2(l_2+1))^2}{4l_1(l_1+1)l_2(l_2+1)} \\ &\quad \begin{pmatrix} l_1 & l_2 & l_3 \\ 0 & 0 & 0 \end{pmatrix}^2 \end{aligned} \tag{A.17}$$

$$\sum_{m's} E^{\alpha\beta\gamma}E^{\bar{\alpha}\bar{\beta}\bar{\gamma}} = +\widetilde{A}^2(j_\beta, j_\gamma, j_\alpha)\sigma(J_\alpha, J_\beta, J_\gamma) \tag{A.18}$$

$$\sum_{m's} E^{\alpha\beta\gamma} E^{\bar{\beta}\bar{\alpha}\bar{\gamma}} = (-1)\widetilde{A}(j_\beta, j_\gamma, j_\alpha)\widetilde{A}(j_\alpha, j_\gamma, j_\beta)\sigma(J_\alpha, J_\beta, J_\gamma) \tag{A.19}$$

where $\widetilde{A}(l_1, l_2, l_3)$ is defined as above. and $\sigma(J_\alpha, J_\beta, J_\gamma)$, is 1 if its arguments satisfies the triangle inequality, and is zero otherwise. The presence of $\sigma(J_\alpha, J_\beta, J_\gamma)$ is just a reminder that we need to impose the triangle inequality on $J_\alpha, J_\beta, J_\gamma$ at each vertex which is obvious from the left hand side but is somewhat obscured by the summation.

The following identities are useful in computing the three loop diagrams. Again, a hat over the indicies means summing over their cyclic permutations.

$$\sum_{m} D^{\alpha\overline{\alpha}\lambda} = -(-1)^{J_\alpha} R_1^{1/2}(J_\alpha, J_\alpha, 0)(2J_\alpha+1)^{1/2}\delta_{J_\lambda,0}\delta_{m_\lambda,0} \tag{A.20}$$

$$\sum_{m's} D^{\alpha\beta\gamma} D^{\overline{\alpha\beta}\tau} = (-1)^{J_\gamma}\frac{1}{(2J_\gamma+1)}\delta_{J_\gamma,J_\tau} R_1(\alpha,\beta,\gamma) \tag{A.21}$$

$$\sum_{m's} D^{\alpha\gamma\tau} D^{\beta\overline{\gamma\tau}} = (-1)^{J_\alpha+1}\frac{1}{(2J_\alpha+1)}\delta_{J_\alpha,J_\beta} R_1(\alpha,\gamma,\tau) \tag{A.22}$$

$$\sum_{m's} C^{\alpha\epsilon\gamma} C^{\overline{\gamma\epsilon}\beta} = (-1)^{J_\alpha+1}\frac{1}{(2J_\alpha+1)}\delta_{J_\alpha,J_\beta} A(\gamma\epsilon\alpha)A(\alpha\epsilon\gamma) \tag{A.23}$$

$$\sum_{m's} E^{\alpha\gamma\epsilon} E^{\overline{\epsilon\gamma}\beta} = (-1)^{J_\alpha}\frac{1}{(2J_\alpha+1)}\delta_{J_\alpha,J_\beta} \widetilde{A}(\gamma\epsilon\alpha)\widetilde{A}(\gamma\alpha\epsilon) \tag{A.24}$$

$$\sum_{m's} D^{\gamma\tau\alpha} E^{\overline{\tau\gamma}\beta} = 0 \tag{A.25}$$

$$\sum_{m's} C^{\alpha\gamma\tau} D^{\overline{\gamma}\beta\overline{\tau}} = 0 \tag{A.26}$$

$$\begin{aligned}\sum_{m's,J_\lambda,J_\tau} D^{\alpha\overline{\alpha}\lambda} \qquad & D^{\gamma\epsilon\overline{\lambda}} D^{\overline{\gamma\epsilon}\tau} D^{\beta\overline{\beta}\tau} \\ &= (-1)^{J_\alpha+J_\beta}\delta_{J_\gamma,J_\epsilon}(2J_\alpha+1)^{1/2}(2J_\beta+1)^{1/2} R_1^{1/2}(\alpha,\alpha,0) R_1^{1/2}(\beta,\beta,0) R_1(\gamma,\gamma,0) \\ &= \delta_{J_\gamma,J_\epsilon}\frac{1}{16\pi^2}(2J_\alpha+1)(2J_\gamma+1)(2J_\beta+1)\end{aligned} \tag{A.27}$$

$$\sum_{m's,J_\lambda} D^{\alpha\overline{\alpha}\lambda} D^{\gamma\epsilon\overline{\lambda}} D^{\beta\overline{\gamma}\tau} D^{\overline{\beta\epsilon\tau}} = (-1)^{J_\alpha+J_\gamma}\delta_{J_\gamma,J_\epsilon}\frac{(2J_\alpha+1)^{1/2}}{(2J_\gamma+1)^{1/2}} R_1^{1/2}(\alpha,\alpha,0) R_1^{1/2}(\gamma,\gamma,0) R_1(\beta,\gamma,\tau) \tag{A.28}$$

$$\sum_{m's} D^{\alpha\gamma\lambda} D^{\overline{\alpha}\epsilon\overline{\lambda}} D^{\beta\overline{\epsilon}\tau} D^{\overline{\beta\gamma\tau}} = \delta_{J_\gamma,J_\epsilon}\frac{1}{(2J_\gamma+1)} R_1(\alpha,\gamma,\lambda) R_1(\beta,\gamma,\tau) \tag{A.29}$$

$$\sum_{m's} D^{\alpha\gamma\lambda} D^{\overline{\alpha\gamma}\tau} D^{\epsilon\beta\overline{\lambda}} D^{\overline{\epsilon\beta\tau}} = \delta_{J_\lambda, J_\tau} \frac{1}{(2J_\lambda + 1)} R_1(\alpha, \gamma, \lambda) R_1(\epsilon, \beta, \lambda) \tag{A.30}$$

$$\sum_{m's} D^{\alpha\beta\lambda} D^{\gamma\epsilon\overline{\lambda}} \quad D^{\overline{\beta}\epsilon\tau} D^{\overline{\alpha\gamma\tau}} = -1^{\sum_{j's}} R_1^{1/2}(\alpha, \beta, \lambda) R_1^{1/2}(\gamma, \epsilon, \lambda) R_1^{1/2}(\beta, \epsilon, \tau) R_1^{1/2}(\alpha, \gamma, \tau) \begin{Bmatrix} J_\gamma & J_\alpha & J_\tau \\ J_\beta & J_\epsilon & J_\lambda \end{Bmatrix} \tag{A.31}$$

$$\sum_{m's, J_\lambda} D^{\rho\overline{\rho}\lambda} D^{\alpha\beta\overline{\lambda}} \widehat{E}^{\overline{\alpha}\tau\sigma} \widehat{E}^{\overline{\beta\sigma\tau}} = -(-1)^{J_\alpha + J_\rho} \delta_{J_\alpha, J_\beta} \frac{(2J_\rho + 1)^{1/2}}{(2J_\alpha + 1)^{1/2}} R_1^{1/2}(\alpha, \alpha, 0) R_1^{1/2}(\rho, \rho, 0) \widetilde{A}_{\widehat{\tau\sigma\alpha}} \widetilde{A}_{\widehat{\sigma\tau\alpha}} \tag{A.32}$$

$$\sum_{m's} C^{\sigma\gamma\rho} C^{\overline{\rho\gamma\tau}} D^{\alpha\beta\overline{\sigma}} D^{\overline{\alpha\beta}\tau} = \delta_{J_\alpha, J_\tau} \frac{-1}{(2J_\tau + 1)} A_{\rho\gamma\tau} A_{\tau\gamma\rho} R_1(\alpha, \beta, \tau) \tag{A.33}$$

$$\sum_{m's} D^{\alpha\beta\lambda} D^{\overline{\alpha}\gamma\overline{\lambda}} \widehat{E}^{\overline{\beta}\epsilon\rho} \widehat{E}^{\overline{\epsilon\gamma\rho}} = -\delta_{J_\gamma, J_\beta} \frac{1}{(2J_\gamma + 1)} \widetilde{A}_{\widehat{\epsilon\rho\beta}} \widetilde{A}_{\widehat{\epsilon\gamma\rho}} R_1(\alpha, \gamma, \lambda) \tag{A.34}$$

$$\sum_{m's} \widehat{E}^{\gamma\alpha\rho} \widehat{E}^{\overline{\rho\alpha\epsilon}} \widehat{E}^{\overline{\gamma}\tau\beta} \widehat{E}^{\overline{\beta\tau}\epsilon} = \delta_{J_\gamma, J_\epsilon} \frac{1}{(2J_\gamma + 1)} \widetilde{A}_{\widehat{\alpha\rho\gamma}} \widetilde{A}_{\widehat{\alpha\epsilon\rho}} \widetilde{A}_{\widehat{\tau\beta\gamma}} \widetilde{A}_{\widehat{\tau\epsilon\beta}} \tag{A.35}$$

$$\sum_{m's} D^{\alpha\gamma\rho} D^{\beta\epsilon\overline{\rho}} \widehat{E}^{\overline{\alpha\beta}\tau} \widehat{E}^{\overline{\epsilon\gamma\tau}} = -(-1)^{\sum_{j's}} R_1^{1/2}(\alpha, \gamma, \rho) R_1^{1/2}(\beta, \epsilon, \rho) \widetilde{A}_{\widehat{\beta\tau\alpha}} \widetilde{A}_{\widehat{\gamma\tau\epsilon}} \begin{Bmatrix} J_\alpha & J_\gamma & J_\rho \\ J_\epsilon & J_\beta & J_\tau \end{Bmatrix} \tag{A.36}$$

$$\sum_{m's} \widehat{E}^{\rho\sigma\tau} \widehat{E}^{\overline{\alpha}\beta\overline{\tau}} \widehat{E}^{\overline{\beta}\gamma\overline{\rho}} \widehat{E}^{\overline{\gamma}\alpha\overline{\sigma}} = -1^{\sum_{j's}} \widetilde{A}_{\widehat{\sigma\tau\rho}} \widetilde{A}_{\widehat{\beta\tau\alpha}} \widetilde{A}_{\widehat{\gamma\rho\beta}} \widetilde{A}_{\widehat{\alpha\sigma\gamma}} \begin{Bmatrix} J_\rho & J_\sigma & J_\tau \\ J_\alpha & J_\beta & J_\gamma \end{Bmatrix} \tag{A.37}$$

$$\sum_{m's} D^{\alpha\gamma\rho} D^{\beta\overline{\gamma}\sigma} C^{\overline{\rho\beta}\tau} C^{\overline{\tau\alpha\sigma}} = -1^{\sum_{j's}} R_1^{1/2}(\alpha, \gamma, \rho) R_1^{1/2}(\beta, \gamma, \sigma) A_{\tau\beta\rho} A_{\sigma\alpha\tau} \begin{Bmatrix} J_\alpha & J_\gamma & J_\rho \\ J_\beta & J_\tau & J_\sigma \end{Bmatrix} \tag{A.38}$$

$$\sum_{m's} \widehat{E}^{\alpha\beta\gamma} C^{\rho\overline{\gamma}\sigma} D^{\overline{\beta}\tau\overline{\sigma}} D^{\overline{\alpha\tau\rho}} = -(-1)^{\sum_{j's}} \widetilde{A}_{\widehat{\beta\gamma\alpha}} A_{\sigma\gamma\rho} R_1^{1/2}(\beta, \tau, \sigma) R_1^{1/2}(\alpha, \tau, \rho) \begin{Bmatrix} J_\beta & J_\gamma & J_\alpha \\ J_\rho & J_\tau & J_\sigma \end{Bmatrix} \tag{A.39}$$

expressions that are zero :
in 3h:

$$\sum_{m's} D^{\alpha\gamma\lambda} D^{\beta\epsilon\bar{\lambda}} \widehat{E}^{\overline{\alpha\gamma}\rho} \widehat{E}^{\bar{\epsilon}\beta\bar{\rho}} = \delta_{J_\lambda, J_\rho} \frac{1}{(2J_\lambda + 1)} R_1^{1/2}(\alpha, \gamma, \lambda) R_1^{1/2}(\beta, \epsilon, \lambda) \widetilde{A}_{\widehat{\gamma\lambda\alpha}} \widetilde{A}_{\widehat{\beta\lambda\epsilon}} = 0 \quad \text{(A.40)}$$

in 3m, 3g:

$$\sum_{m's} D^{\alpha\beta\lambda} C^{\overline{\lambda\alpha}\rho} D^{\gamma\epsilon\bar{\rho}} \widehat{E}^{\overline{\beta\gamma\epsilon}} = \delta_{J_\beta, J_\rho} \frac{1}{(2J_\rho + 1)} R_1^{1/2}(\alpha, \rho, \lambda) R_1^{1/2}(\gamma, \epsilon, \rho) A_{\rho\alpha\lambda} \widetilde{A}_{\widehat{\gamma\epsilon\rho}} = 0 \quad \text{(A.41)}$$

We can use the following to simplify the above expressions:

$$\sum_{l_3} R_1(l_1, l_2, l_3) = \frac{(2l_1 + 1)(2l_2 + 1)}{8\pi} \quad \text{(A.42)}$$

$$R_1^{1/2}(l_1, l_1, 0) = (-1)^{l_1+1} \frac{(2l_1 + 1)^{1/2}}{2\pi^{1/2}} \quad \text{(A.43)}$$

Appendix B

Appendix to Chapter 3: Holographic Dictionary

Consider a configuration (before decoupling) with a D4-brane in the 01234 directions (with x_4 noncompact) and a D8-brane in the 012356789 directions, but bent in a U shape so as to intersect the D4-brane at two places along x_4. Locally, one of these intersections is a D8 and the other is a $\bar{\text{D8}}$. Now, we are interested in the coupling between the D8-brane gauge field and the operators

$$B_L = \psi_L^\dagger \psi_L$$

at the one intersection and

$$B_R = \psi_R^\dagger \psi_R$$

at the other intersection. We define $\psi_L^\dagger$ and $\psi_R^\dagger$ such that they create particles with positive charge on the D4-brane, or physically, such that a test charge on the D4-brane is repelled from both of these particles. In this case, the baryon number operator is

$$B = 1/N_c(\psi_L^\dagger \psi_L + \psi_R^\dagger \psi_R)$$

and we have a coupling $a_0 B$ in the effective action where a_0 is the time component of the D4-brane gauge field.

We would now like to understand how the two operators B_L and B_R couple to the D8 brane gauge field. To do this, we note that if we perform a rotation by π in the 1-4 directions, centered at the point on the D4-brane between the two D8-branes, we get back to precisely the same configuration, since the D4-brane does not change orientation, while the D8 and $\bar{\text{D8}}$ branes will switch orientation but also switch position.

Now, suppose we have a configuration with one $\psi_L^\dagger$ particle at the D8 intersection. This repels a test charge on the D4-brane, so after the rotation it is still a particle that repels a test charge, but now it is a particle at the D8-bar intersection. It must therefore be a $\psi_R^\dagger$ particle. Thus, a $\psi_L^\dagger$ particle is mapped to $\psi_R^\dagger$ particle. Now, suppose that we have a test charge on the D8-brane that is repelled by the particle in the initial configuration. In the rotated configuration, this test charge will still be repelled (by the $\psi_R^\dagger$ particle). Also, the test charge in the new configuration will have the same sign as in the old configuration, since we have simply performed a rotation. This means that if we describe the entire U-shaped D8-brane using a single patch, both $\psi_L^\dagger$ and $\psi_R^\dagger$ particle will source electric fields pointing away from the D4-brane (or both towards the D4-brane, depending on our convention).

This implies further that if we use a single field A_0 over the entire D8-brane configuration, then the coupling of A_0 to B_L at the D8 intersection will have the same sign as the coupling of A_0 to B_R at the D8-bar intersection. For the Sakai-Sugimoto setup, this implies that if we want to turn on a chemical potential for baryon number (i.e. turn on the operator B), we want to choose A_0 to have the same sign at $\sigma = \infty$ as at $\sigma = -\infty$ (if we use the same gauge field over the whole brane configuration).

Appendix C

Appendix to Chapter 4: A Note on Dimensions

Lets start with the metric

$$ds^2 = -f(r)dt^2 + \frac{dr^2}{f(r)} + r^2(dx^2 + dy^2) \tag{C.1}$$

Here ds^2 is dimensionless, hence if we scale the boundary coordinates x, y, t by a constant α, then r needs to be scaled by α^{-1}. Thus $f(r)$ should scale as α^{-2}. From the equation for A_t

$$A_t'' + \frac{2}{r}A_t' - \frac{2\Psi^2}{f}A_t = 0 \tag{C.2}$$

we see that ψ does not need to scaled. Also, from the equation for ψ

$$\psi'' + \left(\frac{f'}{f} + \frac{2}{r}\right) + \frac{A_t^2}{f^2}\psi + \frac{2}{L^2 f}\psi = 0 \tag{C.3}$$

we see that ψ'' and $\frac{A_t^2}{f^2}\psi$ must scale the same way, so A_t scales like r (since $f(r)$ scales like r^2). Now we know the boundary coordinates x, y, t have mass dimension -1. From the scaling behaviour, we can now determine the dimensions of all other operators:

$$\begin{aligned} [\psi] &= 0 \\ [r] = [A] = [\mu] = [\Psi_1] &= 1 \\ [\rho] = [\Psi_2] &= 2 \end{aligned} \tag{C.4}$$